AD NUMBER

AD849798

NEW LIMITATION CHANGE

TO

Approved for public release, distribution unlimited

FROM

Distribution authorized to U.S. Gov't. agencies and their contractors; Critical Technology; FEB 1969. Other requests shall be referred to US Air Force Systems Command, Attn: Rome Air Development Center, Griffiss AFB, NY 13441.

AUTHORITY

RADC, USAF ltr, 17 Sep 1971

RADC-TR-68-397
Final Technical Report
February 1969

HF ANTENNA OPTIMIZATION STUDY

Virgil R. Arens
Claes T. Elfving
Ursel R. Embry
Donald L. Johnstone
Sylvania Electronic Systems - Western Division

Rome Air Development Center
Air Force Systems Command
Griffiss Air Force Base, New York

When US Government drawings, specifications, or other data are used for any purpose other than a definitely related government procurement operation, the government thereby incurs no responsibility nor any obligation whatsoever; and the fact that the government may have formulated, furnished, or in any way supplied the said drawings, specifications, or other data is not to be regarded, by implication or otherwise, as in any manner licensing the holder or any other person or corporation, or conveying any rights or permission to manufacture, use, or sell any patented invention that may in any way be related thereto.

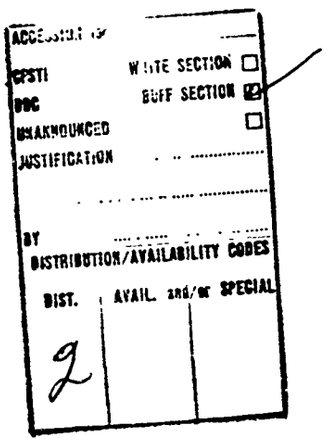

Do not return this copy. Retain or destroy.

HF ANTENNA OPTIMIZATION STUDY

Virgil R. Arens
Claes T. Elfving
Ursel R. Embry
Donald L. Johnstone
Sylvania Electronic Systems - Western Division

AFLC, GAFB, N.Y., 21 Mar 69-155

FOREWORD

This final technical report was prepared by the Sylvania Electronics Systems, Mountain View, California 94040 under contract F30602-67-C-0045, project 5582, task 558202. The project engineer was Carmen S. Malagisi, Rome Air Development Center, EMATA, Griffiss Air Force Base, NY 13440.

The authors wish to express their appreciation to Mr. Kenneth K. Mei of the University of California, Berkeley, California, for his assistance in this study.

Distribution of this report is limited for the protection of technical know-how relating to critical products and other technology restricted by U.S. Mutual Security Acts.

This technical report has been reviewed and is approved.

Carmen S Malagisi

Approved: CARMEN S. MALAGISI
Project Engineer

Approved: LEO W. SULLIVAN
Colonel USAF
Chief, Surveillance and
Control Division

FOR THE COMMANDER:

IRVING J. GABELMAN
Chief, Advanced Studies Group

ABSTRACT

This report presents a summation of the work performed under the Antenna HF Optimization Study, a study to determine the optimum log periodic dipole array design for a high gain, low coverage HF antenna over real and/or ground screen covered earth. The major problem encountered is one of determining antenna electrical characteristics accurately in free space and in a real earth environment. The present state of the art in analytical antenna design does not allow the engineer to predict log periodic antenna electrical characteristics, especially over real earth, with sufficient accuracy to be valuable for strict system requirements. To solve this problem, a mathematical model of a log periodic antenna is set up and solved with the use of high speed digital computers. The model used allows one to obtain the current distribution on the antenna knowing only its physical dimensions and something about the conductivity of the material used in its construction. The theoretical model, which treats the antenna as a boundary value problem, automatically includes all the interactions or mutual coupling between elements. From the computed values of the currents on the antenna all electrical characteristics of the antenna, such as radiation patterns, absolute gain, and input impedance are calculated. Theoretical and measured UHF radiation patterns and gains are compared for evaluation of the technique. Free space and real earth calculations are presented and an optimum antenna design is chosen from this information.

TABLE OF CONTENTS

LIST OF ILLUSTRATIONS

LIST OF ILLUSTRATIONS -- Continued

LIST OF ILLUSTRATIONS -- Continued

EVALUATION

1. The objective of this effort was to investigate antenna techniques applicable to arrays of HF dipole log periodic elements to provide gains of 17 dbi and radiation coverage with a minimum of 14 dbi from two (2) through 16 degrees in elevation and plus and minus 8 degrees in azimuth over the 3 - 30 MH_z frequency range with minimum real estate.

2. The approach taken by Sylvania was to investigate H-Plane arrays of log periodic elements of the DuHamel and Mei configurations. The original approach was to perform both an analytical and experimental effort to determine the advantages of the Mei array approach over the conventional DuHamel array configuration. After the effort had been initiated, it was redirected to put full emphasis on developing a computer program which would have the capability of computing the performance characteristics of dipole log periodic elements and arrays of log periodic elements in both the DuHamel and Mei configurations. This computer program was written for the RADC GE 635/645 Computer in order that RADC antenna engineers could make efficient use of the computer program using RADC's computer facilities. RADC used its computer facilities with the Sylvania antenna program to obtain the performance characteristics of log periodic arrays as presented in this report. It was determined by the many computer runs performed by RADC, that the computer program developed by Sylvania has a limitation of only being able to handle log periodic structures with bandwidths less than an octave. The results from analyzing log periodic structures larger than an octave bandwidth did not correlate very well with experimental results.

3. The results of this effort have shown that the following parameters have a significant effect on the performance of dipole log periodic elements:

a. Dipole diameter

b. Characteristic impedance of feed line

c. Tau factor

d. Alpha factor

e. Number of dipole elements on structure

f. Bandwidth of the structure

This computer program will enable the antenna engineer to determine optimum antenna parameters for arrays of dipole log periodic elements before an extensive experimental effort is undertaken. It is hoped that the limitations of this program can be overcome and can be made to satisfactorily handle greater bandwidth structures.

4. With the use of the RADC GE 635/645 Computer Facilities and the computer program developed under this effort, the Air Force will be able to analytically determine the performance characteristics of large HF log periodic dipole arrays for future radar systems. This capability will also be advantageous for analyzing in more detail the performance characteristics of dipole log periodic structures.

Carmen S. Malagisi

CARMEN S. MALAGISI
Project Engineer
RADC/EMATA
Griffiss AFB, NY

I INTRODUCTION

Insufficient information on the electrical characteristics of antennas is and has been a continuous problem to the systems engineer. Whenever he attempts to predict the receiver signal level a lack of detailed gain characteristics becomes significant. The amount of information available varies greatly from one type of antenna to another. The antenna we wish to consider in this study is the log-periodic antenna.

There are may different forms of log-periodic antennas; however, only one may be considered as useful at the present time for the operating frequencies many for long-range purposes -- the log-periodic dipole antenna (LPDA). Figure I-1 is an example of a VHF log-periodic dipole antenna, the absolute gain of which is too low for long-range systems. These antennas may of course be arrayed to increase the gain to the required level. Arraying may be accomplished such that the resulting array has the same frequency-independent characteristics as the fundamental antenna. This technique has a theoretical maximum gain. Figure I-2 is an artists concept of such an array in the HF region. One may also array the antennas to give broad-band characteristics that change with frequency, but have no theoretical limit on maximum gain; however, at the present time we are concerned only with the frequency-independent array.

The determination of the electrical characteristics of a LPDA, when the antenna is a close-spaced array on a homogeneous earth covered by a ground screen of finite length, is not an easy task. The first step in the complete

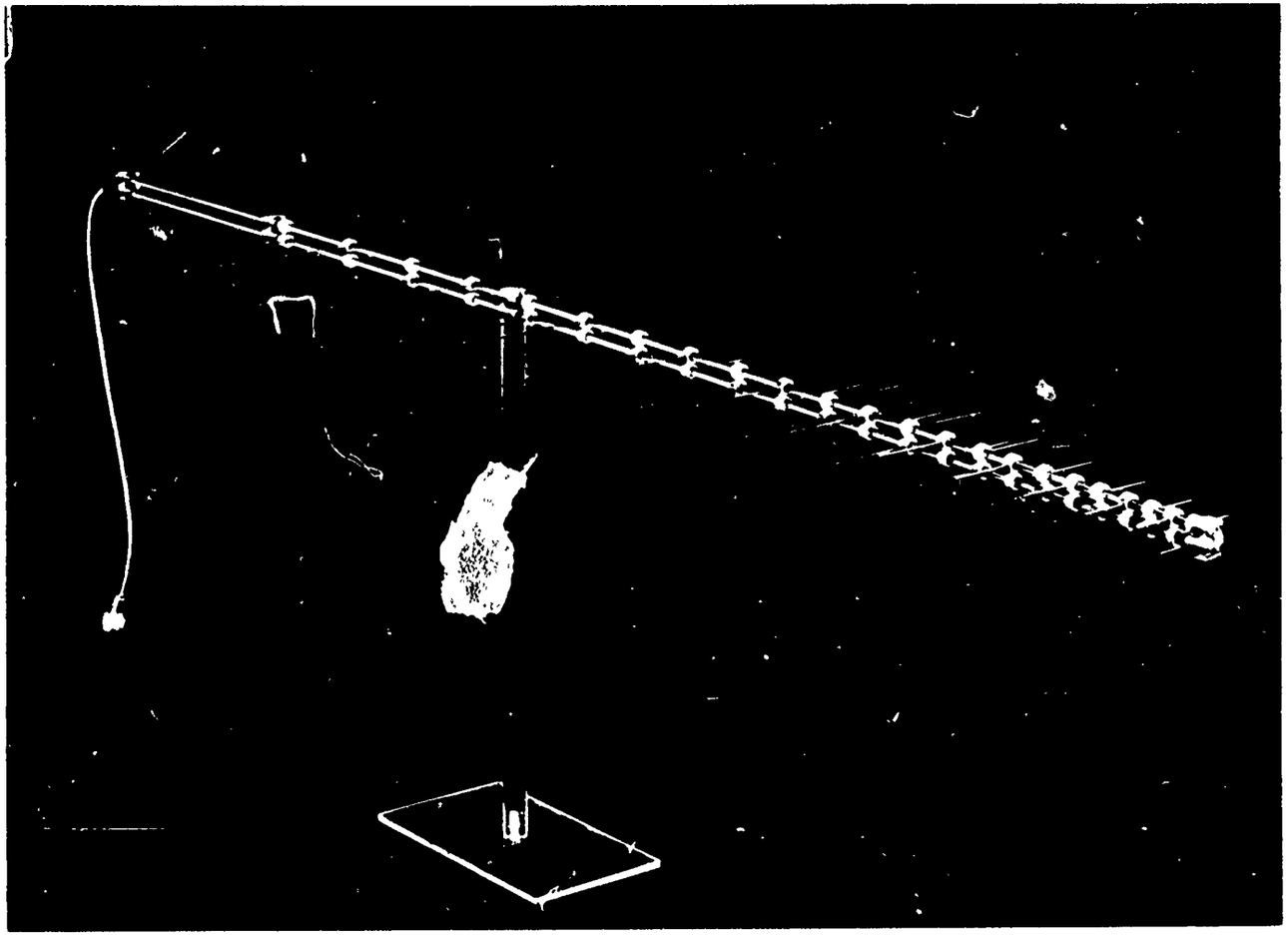

Figure I-1. VHF Log-Periodic Dipole Antenna.

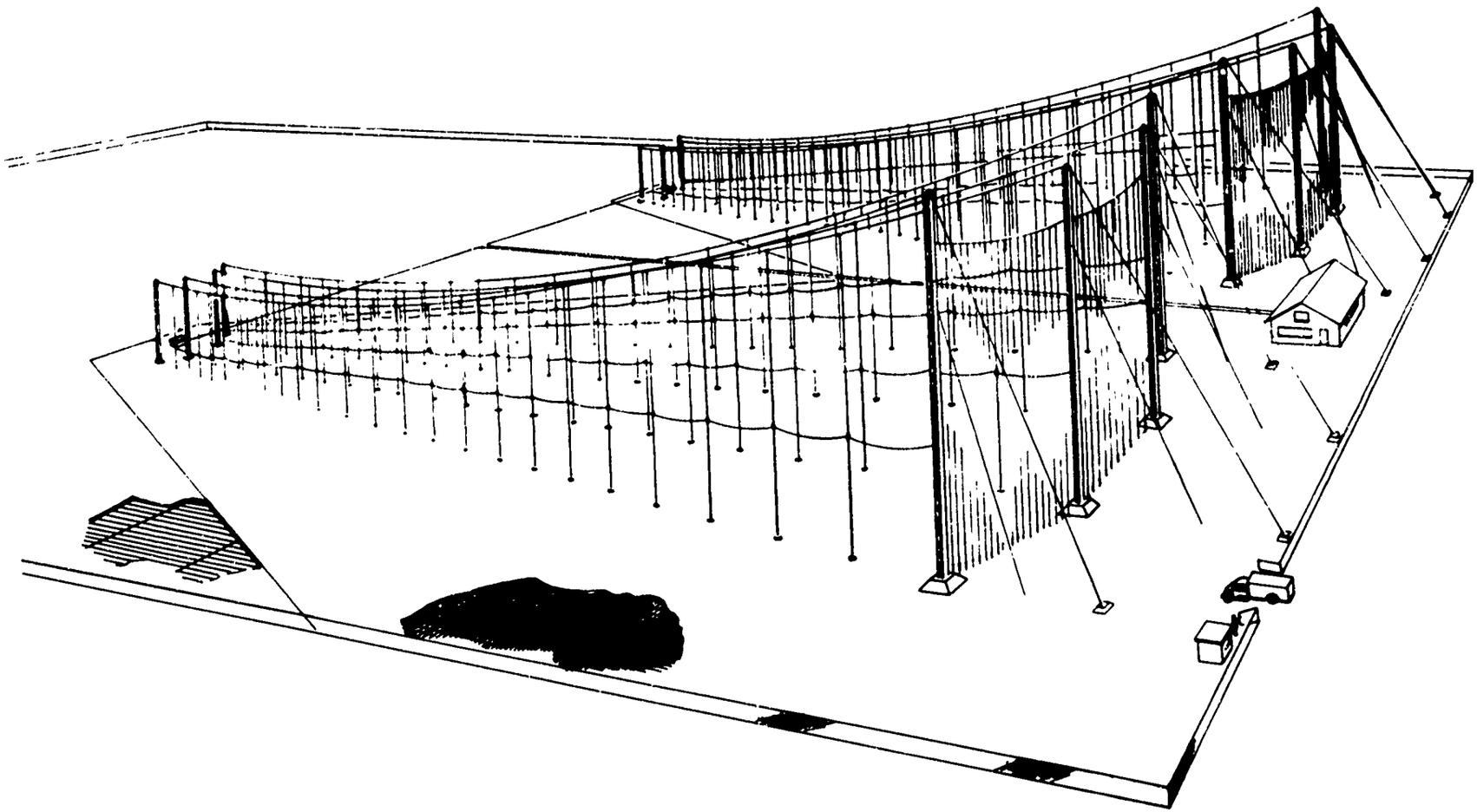

Figure I-2. Artist's Concept of Arrayed HF Log-Periodic Antennas

solution of this problem is the determination of the theoretical characteristics of such an antenna in free space. This report is addressed primarily to this problem. The mathematical techniques to be developed must, of course, be of a form that is applicable when the complete antenna is composed of arrays of LPDA's.

The LPDA is in a class of antennas that to the present day do not have suitable approximate mathematical solutions. Attempts to compensate for the mutual coupling between the non-equal-length close-spaced dipole elements using the usual arraying theory have been unsatisfactory. The present state of the art in analytical antenna design does not allow the engineer to truly predict the performance of log-periodic dipole antennas.

The assumptions of the form of the current distribution on the dipole elements and consideration of the interaction between pairs of dipoles, neglecting the effects of neighboring dipoles, has given useful but limited results.

The techniques used in obtaining solutions of the LPDA go beyond the usual analytical methods and make maximum use of advanced numerical analysis and high-speed digital computers. Many "solutions" to antenna problems in the past have made assumptions on the current distribution on the elements and have used this assumed current distribution to determine radiation patterns, etc. In other words, an answer has been assumed for a major portion of the problem and only the minor problem of determining the far-field pattern (given the current distribution) has been solved. In this report no assumptions on the distribution of current are made; the antenna is treated as a boundary-value problem for which a solution can be obtained by numerical analysis and the aid of a digital computer.

I. (Continued)

Thus only those parameters that define the antenna physically and the operating frequency are the input parameters to the digital computer program. The computer program, in turn, determines the current distribution on the antenna based on these physical parameters. From these derived values of the currents on the antenna, all electrical characteristics of the antenna, such as radiation patterns, maximum absolute gain, and input impedance are calculated.

As shown in Section III the boundary-value problem, which mathematically represents the antenna, can be represented by a Fredholm integral equation. (A Fredholm integral equation is one where the unknown is under the integral sign.) It can be shown that such an integral equation can be considered as the limit of a set of n algebraic equations where the accuracy of the solution is a function of n. Use is made of this fact by writing the n algebraic equations and solving the n equations using matrix techniques. These equations are, of course, complex in the mathematical sense.

The next section of this report presents the theory behind the mathematical model of an n element log-periodic dipole antenna in free space. The third section presents some of the numerical results obtained from the computer program which utilized the mentioned mathematical model.

II THEORY

A. INTRODUCTION

The primary objective of this section is to present the theory behind the mathematical model of an n element log-periodic antenna in free space. The analysis of this mathematical model by numerical techniques will be discussed simultaneously to enable the reader to understand the capabilities and limitations of the computer programs utilizing this particular model. This section does not provide a documentation of the program that has been written using the model to be discussed, but merely provides the theory and methods used to write such a program.

The next part of this section provides a brief outline of the basic theory involved in the mathematical modeling of a wire antenna beginning with a simple dipole and then extending this concept to include a log-periodic antenna. The remainder of this section provides a detailed analysis of how the model is derived from the theory and what numerical techniques are used to implement this theory on a digital computer.

B. OUTLINE

To find an expression for the current on a dipole in terms of the applied voltage it is convenient to first derive an equation relating the voltage to the vector potential, and then find an expression for the vector potential in terms of the current.

The electric field at any point outside a dipole can be expressed as

$$\vec{E} = -\nabla\phi - j\omega\vec{A} \quad . \tag{1}$$

Now, defining $\nabla \cdot \vec{A}$ as

$$\nabla\cdot\vec{A} = -j\omega\mu\epsilon\,\phi \quad , \tag{2}$$

we get

$$\vec{E} = \frac{1}{j\omega\mu\epsilon}\left[\nabla(\nabla\cdot\vec{A} + \omega^2\mu\epsilon\vec{A})\right] \quad . \tag{3}$$

Assuming the dipole parallel to the z-axis, Equation (3) reduces to

$$E_z = -j\frac{\omega}{k^2}\left(\frac{d^2A_z}{dz^2} + k^2A_z\right) \quad , \tag{4}$$

where

$$k^2 = \omega^2\mu\epsilon \quad .$$

For a perfect conductor the tangential electric field is zero on the boundary. Equation (4) then becomes

$$\frac{d^2A_z}{dz^2} + k^2A_z = 0 \quad . \tag{5}$$

B. (Continued)

The general solution of this differential equation is

$$A_z = C_1 \cos kz + C_2 \sin kz \quad . \tag{6}$$

With a slice generator of voltage V applied at the center of the dipole, as derived by Hallén,[5] Equation (6) becomes

$$A_z = C_1 \cos kz + \frac{V}{2} \sin k|z| \quad . \tag{7}$$

This is the vector potential-voltage relationship that we set out to find.

To relate the voltage to the current flowing on the dipole, we can now use the known relationship between the vector potential, A_z, and the dipole current,

$$A_z = \frac{\mu}{4\pi} \int_{-\ell}^{\ell} I'_z \frac{e^{-jkR}}{R} \, dz' \, , \tag{8}$$

where R is the distance between the point in space and the point on the dipole where current I'_z is flowing.

Combining Equations (7) and (8) we obtain the desired current-voltage relationship,

$$\int_{-\ell}^{\ell} I'_z \frac{e^{-jkR}}{R} \, dz' = B \cos kz + j \frac{V}{2\eta} \sin k|z| \quad . \tag{9}$$

In order to solve this integral, we approximate the integral by a finite sum of currents along the dipole. Each term in this sum contains an unknown value of current. To solve for these unknown current values, we need the same number of equations as we have increments of currents along the dipole. By specifying the value of z to a specific increment along the dipole, one equation can be written for each current segment. With the dipole divided into N segments, we now have N number of independent equations. A typical equation for the i-th segment is

B. (Continued)

$$\sum_{n=1}^{N} I'_{z_n} \frac{e^{-jkR_n}}{R_n} \Delta z_n = B \cos kz_i + j\frac{V}{2\eta} \sin k\left|z_i\right| \quad , \tag{10}$$

where n covers all dipole segments, including the i-th segment. In addition to the N number of unknown currents, the integration constant B is unknown.

An additional independent equation is obtained from the boundary condition that the current at the tip of the dipole is zero;

$$I\Big|_{z=\ell} = 0 \quad . \tag{11}$$

With N+1 independent equations, the N+1 unknowns can now be determined.

The same theory can be applied to a series of dipoles, as in the case of a log-periodic dipole array. For a log-periodic array with M number of dipoles, Equation (10) becomes

$$\sum_{m=1}^{M} \sum_{n=1}^{N} I'_{z_n} \frac{e^{-jkR_n}}{R_n} \Delta z_{mn} = B_j \cos kz_{ji} + j\frac{V_j}{2\eta} \sin k\left|z_{ji}\right| \quad , \tag{12}$$

where m covers all dipoles, including the j-th dipole.

The unknown voltage, V_j, at the base of the j-th dipole in the array is related to the applied voltage, V, at the input terminal of the array by a series of tranmission line equations.

The currents on the dipoles of a log-periodic antenna, calculated by using the approach described above, are by definition the actual currents, including all mutual interactions between the dipoles.

From these values of currents on the structure all electrical characteristics of the antenna, such as far-field patterns, the absolute gain and input impedance can be calculated.

C. THE DIPOLE ANTENNA

The cylindrical, center-driven antenna has been analyzed as a boundary value problem by many workers. Basically, two methods of attacking the problem of determining the distribution of current along the center-driven antenna have been used. In the first of these,[6] which is not a boundary value treatment, one uses the apparent similarity between the antenna and an open-end parallel-wire transmission line. Thus, by suitably correcting existing transmission line theory, a satisfactory approximation for the antenna can be determined.

The second method proceeds from the point of view that the antenna is

C. (Continued)

a boundary-value problem which can be formulated in general terms and the resulting equations solved by the use of the numerical methods and high-speed digital computers. Thus, to solve this problem, equations are needed in terms of parameters such as the radius and length that characterize the dipole antenna, rather than in terms of characteristic impedance, terminal impedance, etc., which are basically foreign to the antenna.

The dipole antenna has been investigated from the point of view of a boundary value problem by many workers such as R.W.P. King,[1] Hallén,[5] L.V. King,[8] Brillouin,[9] and Aharoni.[10] In nearly all of these papers, different but comparable methods were used. Some are analytically complicated in determining the equations, and all are complicated in their attempts to solve the resulting integral equation. Actually, the problem can be set up formally,[11] and this will lead to the integral equation first obtained by Hallén as shown below.

1. The Differential Equation

Since we are concerned with antennas that will be used at high frequencies, we will assume the antennas to be thin. By this it is meant that the ratio of radius r_o of the cross section to length 2ℓ of the antenna is negligible. It is not permissible to regard r_o as zero, for the quantity

$$\Omega = 2\ell n\left(\frac{2\ell}{r_o}\right) \tag{13}$$

cannot be neglected. Thus, while errors of the order r_o/ℓ can be tolerated, the antenna cannot be regarded as infinitely thin. A lower bound on Ω has been given by Brillouin[9] of $\Omega > 14$ or $\ell/r_o > 1000$. For the purposes of this presentation this is not a significant restriction. This restriction allows us to ignore the ends of the antenna, which greatly simplifies the problem but does not decrease the useful accuracy.

The analytical problem of determining the distribution of current on an antenna which we will assume to be cylindrical (triangular or other shapes can be represented by a suitably selected cylinder), of half length ℓ, and radius r_o, may be formulated in terms of the general boundary condition which requires continuity of the tangential component of the electric field across any boundary surface between two media. For this analysis it is convenient to use a cylindrical coordinate system with the z axis lying along the axis of the

C.1 (Continued)

dipole, and $z = 0$ at the center of the dipole. We thus have (assuming the antenna to be a solid wire for purposes of discussion) the following boundary conditions.

a. E_z as one approaches the surface of the wire from inside the wire must be equal to E_z as one approaches the surface of the wire at the same point from outside the wire.

b. E_r as one approaches the end of the wire from inside the wire must be equal to E_r as one approaches the same end of the wire at the same point from outside the wire.

Since the ends of the wire are required to be small by the restriction on Ω as defined in (a) above, the average electric field, E_r, on the ends must be less than the average field along the wire. This follows since the radial current must vanish at $r = 0$ and $r = r_o$ and it cannot reach a large amplitude in this extremely short distance relative to a wavelength. Accordingly, nothing of significance is neglected as far as the antenna as a whole is concerned if no account is taken of the end faces of the wire, and hence, E_r. We will thus assume the current to vanish at $z = \pm\ell$ without flowing radially inward on the end faces.

While at this time conductors with finite conductivity have not been considered in the computer programs, it is planned in the future to consider conductors with finite conductivity. Thus, in the formulation of the differential equation here, we will assume that the wire has a finite internal impedance per unit length of Z_i and that the cross sectional distribution of current in the wire is essentially the same as in an infinitely long wire. In other words, for the purposes of this analysis it will be taken for granted that the cross sectional and axial distributions of current are mutually independent. This is always true to a very high degree of approximation in a good conductor.

Accordingly we have

$$E_z\Big|_{r=r_o} = Z_i I_z \quad , \tag{14}$$

where E_z is the value from the internal approach to the surface and I_z is the total current in the wire at point z.

C.1 (Continued)

At any point in space outside the wire the electric field is

$$\vec{E} = -\nabla\phi - j\omega\vec{A} \quad , \tag{15}$$

where ϕ and A are the scalar and vector potentials, respectively, and ω is the angular frequency. Now the relationship between ϕ and A is

$$\nabla \cdot \vec{A} = -j\omega\mu\epsilon = j\left(\frac{\omega}{c^2}\right)\phi \quad , \tag{16}$$

where μ is the permeability, which for free space has the value $4\pi \times 10^{-7}$ henries per meter; ϵ is the permittivity, which for free space has the value 8.85×10^{-12} farads per meter; and c is the velocity of light.

By substituting Equation (16) in Equation (15) we have

$$\vec{E} = -\nabla\left(\frac{\nabla \cdot \vec{A}}{-j\omega\mu\epsilon}\right) - j\omega\vec{A} \tag{17}$$

or

$$\vec{E} = \frac{1}{j\omega\mu\epsilon}\left[\nabla\left(\nabla \cdot \vec{A} + \omega^2\mu\epsilon\vec{A}\right)\right] . \tag{18}$$

Define

$$k^2 = \omega^2\mu\epsilon = \frac{\omega^2}{c^2} = \left(\frac{2\pi}{\lambda}\right)^2 \quad , \tag{19}$$

where λ = wavelength.

Since the wire antenna carries only a z component of current, the vector potential will have only a z component. Thus, Equation (18) will become, with the definition given in Equation (19),

$$E_z = -j\frac{\omega}{k^2}\left(\frac{d^2A_z}{dz^2} + k^2A_z\right) \quad . \tag{20}$$

C.1 (Continued)

If we now impose the boundary condition, Equations (14) and (20) will give the following differential equation in the vector potential:

$$Z_i I_z = -j \frac{\omega}{k} \left(\frac{d^2 A_z}{dz^2} + k^2 A_z \right) \tag{21}$$

or

$$\frac{d^2 A_z}{dz^2} + k^2 A_z = \frac{jk^2}{\omega} Z_i I_z \quad . \tag{22}$$

From this last equation we see that the vector potential can be represented by a one-dimensional wave equation which would be homogeneous for the perfect conductor ($Z_i = 0$). It is readily verified that the scalar potential can be represented by a similar equation.

The differential equation given by (22) is a nonhomogeneous equation and can possibly be rewritten in the form of an ordinary differential equation and solved by numerical methods on a digital computer. In contrast to initial value problems, which are characterized by the fact that the information given concerns all the conditions at a given point, a boundary-value problem such as defined by Equation (22) is one which gives the conditions at two or more distinct points. In this equation we are seeking we must find a relationship between the vector potential and the z coordinate at all points on the wire. This type of problem is often called a "jury problem". In contrast, the initial value problem is to find the relationship at another point given its value at a given point; i.e., as the independent variable is increased by a small increment. This process is sometimes referred to as a "marching problem". The numerical solution of marching problems are much simpler than those of jury problems; in fact, all good computer centers will have many subprograms to handle the marching problem, while all jury problems must be set up and programmed separately.

There are, of course, other ways in which one may solve the boundary value differential equation as shown in Equation (22). One approach that can be used and will be used here is to restate the problem as an integral equation.

C.2 The Integral Equation

Since Equation (22) is a nonhomogeneous equation, the general solution must consist of a complementary function and a particular integral. The complementary function may be written in the form

$$A_z^c = \frac{-j}{c} \left[C_1 \cos kz + C_2 \sin kz \right] , \tag{23}$$

where C_1 and C_2 are arbitrary constants of integration. A particular integral has been obtained and is

$$A_z^p = \frac{jZ_i}{c} \int_0^z I(z') \sin (z-z') \, dz' . \tag{24}$$

One may verify that (24) does satisfy (22) by substituting (24) in (22).

This equation is valid everywhere including the surface of the antenna, but will not be valid at $z = 0$ since the scalar potential will have a discontinuity due to the driving voltage at that point. This voltage source can be inserted using King's[1] slice generator. To allow for this additional condition, the differential equation must be rewritten as two equations as follows:

$$A_z = \frac{-j}{c} \left[C_1 \cos kz + C_2 \sin kz - Z_i \int_0^z I(z') \sin k(z-z') \, dz' \right] \quad \text{for } z > 0 \tag{26}$$

and

$$A_z = \frac{-j}{c} \left[C_3 \cos kz + C_4 \sin kz - Z_i \int_0^z I(z') \sin k(z-z') \, dz' \right] \quad \text{for } z < 0 . \tag{27}$$

Now the boundary conditions will determine the constants C_1, C_2, C_3, and C_4.

C.2 (Continued)

Now from Equations (15) and (16) at $r = r_o$ the scalar potential is

$$\phi_z = -\frac{j\omega}{c^2} \frac{\partial A_z}{\partial z}\bigg|_{r=r_o} . \tag{28}$$

Inspection of Equations (26) and (27) in view of (28) indicates that if A_z is an even function, ϕ_z must be an odd function, and vice versa. If we let that thickness of the slice generator be 2δ, then

$$\phi_\delta = \frac{V}{2} \tag{29}$$

and

$$\phi_{-\delta} = \frac{V}{2} \tag{30}$$

where V is the applied voltage, then the function ϕ_z is odd. Thus, A_z must be even. These conditions are represented in equation form by

$$\phi_z = \phi_{-z} \tag{31}$$

and

$$A_z = A_{-z} . \tag{32}$$

In order that (26) and (27) may satisfy (31) and (32) for all values, the following relation must hold:

$$C_3 = C_1 \quad \text{and} \quad C_4 = C_2 . \tag{33}$$

C.2 (Continued)

We can then combine Equations (26) and (27) into the following form:

$$A_z = -\frac{j}{c}\left[C_1 \cos kz + C_2 \sin k|z| - Z_i \int_0^z I(z') \sin k(z-z')\, dz'\right] . \tag{34}$$

It is readily shown that (34) is unchanged if $-z$ is everywhere written for z. In the integral one must replace the variable z' by $-z'$.

The boundary condition on the scalar potential is

$$V = \lim_{\delta \to 0} \left[\phi_\delta - \phi_{-\delta}\right] \tag{35}$$

as we allow the slice generator thickness to approach zero. From Equation (33) we may write

$$\left.\frac{\partial A_z}{\partial z}\right|_{z=\delta} = \frac{-j\omega}{c^2}\,\phi_\delta \tag{36}$$

and

$$\left.\frac{\partial A_z}{\partial z}\right|_{z=-\delta} = \frac{-j\omega}{c^2}\,\phi_{-\delta} , \tag{37}$$

so that

$$\phi_\delta = -\phi_{-\delta} = \frac{j c^2}{\omega}\left.\frac{\partial A_z}{\partial z}\right|_{z=-\delta} \tag{38}$$

and

$$V = 2 \lim_{\delta \to 0} \phi_\delta = \frac{2jc^2}{\omega} \lim_{\delta \to 0} \left.\frac{\partial A_z}{\partial a}\right|_{z=\delta} . \tag{39}$$

C.2 (Continued)

Upon differentiating Equation (34) with respect to z and setting z equal to δ and allowing δ to approach zero, we have

$$\lim_{\delta \to 0} \left. \frac{\partial A_z}{\partial z} \right|_{z=\delta} = \frac{-jkC_2}{c} \quad , \tag{40}$$

so that with $k = \omega/c$ we then have

$$C_2 = \frac{1}{2} V \quad . \tag{41}$$

The equation for the vector potential then may be written

$$A_z = \frac{-j}{c} \left[C_1 \cos kz + \frac{V}{2} \sin k|z| - Z_i \int_0^z I(z') \sin k(z-z')\, dz' \right] \quad . \tag{42}$$

Figuratively speaking, let us for the moment sit back and see what Equation (42) is saying, and what it is that we desire. First, it is an equation for the vector potential on or outside the dipole. Secondly, it has two unknown constants, C_1 and Z_i. Z_i is no concern at the moment since we know it is the internal impedance per unit length of wire that can be determined when we so desire.

C_1 is an integration constant and therefore related to a boundary condition. The only boundary condition that has not been used is the condition at the tip of the dipole. We know that the current must be zero at the tip. That is, C_1 can be determined by the equation

$$I \Big|_{z=\ell} = 0 \quad . \tag{43}$$

But this is an equation for the current while Equation (42) includes C_1 in the equation for the vector potential. Therefore, it appears we must obtain a relationship between the vector potential and the current. Then, when we have the equation relating the vector potential to the current and substituting Equation (42), we can determine C_1 by the use of Equation (43). To obtain the relationship between the current and the vector potential, we must use the Helmholtz equation which relates the vector potential and the current.

C.2 (Continued)

The amplitude of the vector potential defined by Equations (15) and (16) must satisfy the Helmholtz equation

$$\nabla^2 \vec{A} + k^2 \vec{A} = \mu \vec{i} \quad , \tag{44}$$

where $\vec{i}$ is the volume density of current flowing in the antenna. The Helmholtz integral, by substituting in Equation (44), can be shown to satisfy this equation. This integral is

$$\vec{A} = \frac{\mu}{4\pi} \int_v \frac{\vec{i}_1'}{r_1} e^{-jkr_1} \, dv' \quad , \tag{45}$$

where v is the volume of the antenna, dv' is an element of v, $\vec{i}'_1$ is the current density at dv', and r_1 is the distance between the point whose cylindrical coordinates are (r, θ, z) where $\vec{A}$ is to be computed and the element dv' is at (r', θ', z'). There are no radial components to $\vec{A}$, since we have assumed no radial components of current flow. The z component is

$$A_z = \frac{\mu}{4\pi} \int_v \frac{i_z'}{r_1} e^{-jkr_1} \, dv' \quad . \tag{46}$$

It has been shown by King and Harrison[11] that $A_{z'}$ evaluated from

$$A_z = \frac{\mu}{4\pi} \int_{-\ell}^{\ell} \frac{I_z' e^{-jkR}}{R} \, dz' \tag{47}$$

where

$$R = \sqrt{(z-z')^2 + r^2}$$

on the surface of the antenna differs by a negligible amount from A_z computed by the exact equation given by (44) and (45). Here R is the distance from the point (r, θ, z)

C.2 (Continued)

outside the conductor where A_z is to be calculated to the center of the element dz' at z' on the axis.

Finally, by using Equation (47) in Equation (42) we have

$$\frac{jc\mu}{4\pi} \int_{-\ell}^{\ell} I'_z \frac{e^{-jkR}}{R} \, dz' = C_1 \cos kz + \frac{V}{2} \sin k|z| - Z_i \int_0^z I'_z \sin k(z-z') \, dz' \quad . \quad (48)$$

The solution of this equation or the same equation where Z_i has been set to zero can be done by at least two methods. The method we will not use consists of expanding the integral on the left into two integrals by the use of integration by parts. This results in one integral which is integrable in closed form and another integral which is not integrable in closed form. If one performs this integration and substitutes back in the original equation, a first order solution is derived. If Equation (43) is then applied and C_1 determined, one has the expression that was originally derived by Hallén. His derivation, of course, was not the same as given here. It is this approach which gives rise to the expression for Ω as used in (13). The other method is numerical, and since it is the method used, the solution will be given in detail in the next subsection.

D. NUMERICAL SOLUTION OF THE INTEGRAL EQUATION

At this time we have not considered conductors with finite conductivity; therefore, in this subsection we will assume that the internal impedance per unit length is zero. We may then rewrite Equation (48) as follows:

$$\int_{-\ell}^{\ell} I'_z \frac{e^{-jkR}}{R} dz' - B \cos kz + \frac{jV}{2\eta} \sin k|z| = 0, \tag{49}$$

where

$$B = \frac{4\pi C_2}{jc\mu}$$

and

η = impedance of free space $\cong 120\pi$.

Further,

$$\frac{e^{-jkR}}{R} = G'(z, z'), \tag{50}$$

which is the free-space Green's function.

We may then write (49) as follows:

$$\int_{-\ell}^{\ell} I'_z \, G'(z, z') \, dz' - B \cos z + \frac{jV}{2\eta} \sin k|z| = 0. \tag{51}$$

Equation (51) is an equation of the form

$$\alpha(x) \, y(x) = F(x) + D \int_a^b K(x, \xi) \, y(\xi) \, d\xi, \tag{52}$$

where α, F, and K are given functions and D, a, and b are constant. This equation is known as a Fredholm integral equation. The function y(x) is to be determined.

When $\alpha \neq 0$, the above equation involves the unknown function both inside and outside the integral. In the special case when $\alpha \equiv 0$, the unknown function appears only under the integral sign, and the equation is known as an integral of the first kind; in the case where

D. (Continued)

$\alpha = 1$, the equation is said to be of the second kind. It would appear at first glance that Equation (51) is of the first kind, but it is in fact of the second kind. The reason for this is that the integration constant B is a function of the current - specifically, the current at the tip of the dipole.

It can be shown[12] that a Fredhom integral equation can be considered as the limit of a set of n algebraic equations, as the number of equations increases without limit. Use can be made of this fact to obtain approximate solutions to such integral equations. Therefore, we must determine a method whereby Equation (52) can be expressed as a set of n algebraic equations.

In elementary integral calculus an integral of the form

$$y = \int_a^b F(x)\, dx \tag{53}$$

is defined as the limit of an equation of the form

$$y = \lim_{n \to \infty} \sum_{k=1}^{n} \Delta x_k \, F(x_k), \tag{54}$$

where the interval (a,b) is divided into n subintervals of lengths Δx_1, $\Delta x_2, \ldots . \Delta x_n$, and x_k is the point in the k-th subinterval. An approximate value of y can be obtained by not proceeding to the limit, and hence by expressing y approximately as the weighted sum of the ordinates $F(x_k)$ at n chosen points $x_1, x_2, \ldots . x_n$ of the interval (a,b):

$$y \cong h \sum_{k=1}^{n} W_k \, F(x_k), \tag{55}$$

where h is the length of all intervals and W_k is a "weighting" coefficient associated with the x_k point. In its simplest form, we let the point x_k be at the center of the k-th interval and give the value unity to all the weighting coefficients. The resulting formula is known as the trapezoidal rule. The accuracy of the approximation can of course be increased by increasing n or changing the weighting coefficient or functions. An example of the latter is Simpson's rule, which is applicable only if n is odd, is where the weighting coefficients are of the form

$$\left\{W_1, W_2, W_3, \ldots . W_{n-2}, W_{n-1}, Wn\right\} = 1/3 \left\{1, 4, 2, 4, \ldots . 2, 4, 1\right\} \tag{56}$$

D. (Continued)

when n is greater than five. More elaborate formulas can be found in the literature[13,14,15] where this technique is often called Gaussian quadrature.

Thus, Equation (52) by the use of Equation (55) can be approximated in the form when it is the second kind where D = 1. Let y(x) not under the integral be B(x):

$$B(x) + F(x) + h \sum_{k=1}^{n} W_k K(x,x_k)\, y(x_k) = 0 \tag{57}$$

where the points x_k are spaced a distance h apart with the first and last points being h/2 from the points a and b. If we now require that equation be written at each of n chosen points where the points are the x_k points, we obtain n linear equations

$$B(x_i) + F(x_i) + h \sum_{k=1}^{n} W_k\, K(x_i,x_k)\, y(x_k) = 0 \qquad i = 1, 2, \ldots . n \tag{58}$$

in the unknowns $y(x_1), y(x_2), \ldots . y(x_n)$ which specify approximate values of the unknown function y(x) at the n points. Introducing the following abbreviations,

$$F_i = F(x_i),\ K_{ij} = K(x_i, x_j),\ B_i = B(x_i),$$

where K_{ij} is the value of $K(x,\xi)$ when $x = x_i$ and $\xi = x_j$, the set of equations given by (58) can be written in the form

$$h \sum_{k=1}^{n} K_{ik}\, y_k + F_i + B_i = 0. \tag{59}$$

Thus, if we consider the numbers F_i, B_i, and y_k as components of the vectors $\vec{F}$, $\vec{B}$, and $\vec{y}$, and define the matrix $\widetilde{K} = [K_{ij}]$, the set of equations (59) can be written concisely in the form

$$h\, \widetilde{K}\, [y] + [\vec{F}] + [\vec{B}] = 0 \tag{60}$$

or

$$[\vec{y}] = 1/h\, \widetilde{K}^{-1} \left\{ [\vec{F}] + [\vec{B}] \right\} = 0, \tag{61}$$

D. (Continued)

where $\tilde{K}^{-1}$ = inverse of the matrix $\tilde{K}$, thus obtaining the value of y at n uniformly spaced points.

Using the method outlined in the above paragraphs, we may rewrite Equation (51) as a set of linear algebraic equations

$$h \sum_{k=1}^{2n} W_k G'(z_i, z_k) I_k - B \cos kz_i + \frac{jV}{2\eta} \sin k \left| z_i \right| \quad i = 1,2,\ldots n, \tag{62}$$

where I_k is the current on the dipole at the k-th point. Investigation of this set of n equations will show that we have n equations and n+2 unknowns; the unknowns being B and V. We must find two additional equations before we can solve the set of equations given in (62). The applied voltage which is represented by V presents no problem. We may let the applied voltage be unity giving the following equation:

$$V - 1 = 0. \tag{63}$$

To determine B we must write an equation that expresses the current at the tip. This can be accomplished in two ways. The first method we used was to write a Taylor series expansion of the current at the points k = 1, 2, 3,....m that is in terms of I_1, I_2, I_3,.... I_m, where m < n, since there are only n points on the half dipole. The k = 1 point is h/2 from the tip, k = 2 point is 3h/2 from the tip, k = 3 point is 5h/2 from the tip, and the k = m point is (2m + 1)h/2 from the tip. While the resulting equation does not involve B, it is the additional expression required to give the required square matrix. Since we are no longer using the Taylor series expression, the lengthy derivation will not be given, only the final equation which is as follows:

$$I_1 - \frac{\binom{m}{1}}{3} I_2 + \frac{\binom{m}{2}}{5} I_3 + \ldots \frac{\binom{m}{m} I_m}{2m+1} = 0, \tag{64}$$

where $\binom{m}{j}$ is the binominal coefficient given by

$$\binom{m}{j} = \frac{m!}{j!\,(n-j)!}. \tag{65}$$

D. (Continued)

The second method is to extrapolate the currents I_1, I_2, and I_3 which are unknowns and require that the current at the tip be zero. The equation will be of the form

$$f(\ell - h/2) I_1 + g(\ell - \frac{3h}{2}) I_2 + h\,\ell\left(-\frac{5h}{2}\right) I_3 = 0. \tag{66}$$

The form of f, g, and h will be determined later. If the set of equations represented by Equation (62) are applied over both halves of the dipole, as is inferred, there are two things in error. First, with numerical integration represented by (62) as with analytical integration, one cannot integrate over a discontinuity. As shown in Equation (35), there is a discontinuity in the scalar potential at the slice generator in the center of the dipole. Secondly, since the current distribution on the dipole is an even function and Equation (62) is identical for z and -z, the resulting matrix will be singular. These two things can be corrected quite simply, while at the same time decreasing the number of terms in the matrix (62) by two, by taking note of the symmetry of the Green's function which is

$$G(z_i, z_j) = G(z_j, z_i). \tag{67}$$

First we reduce the number of points from 2n to n: that is, we integrate only over one half of the dipole. At the same time we replace the free-space Green's function with a modified Green's function which includes the effects of the point $-z_i$. That is, let

$$G(z_i, z_k) = G'(z_i, z_k) + G'(-z_i, z_k). \tag{68}$$

Thus, by writing the set of equations represented by Equation (62) using the modification given by Equation (68), Equation (63), and Equation (64), or Equation (66), we have a set of algebraic equations that relates the current on a dipole to the length of the dipole, the radius of the dipole, and the applied voltage.

E. SINUSOIDAL APPROXIMATION FOR THE NUMERICAL SOLUTION

In subsection D it was indicated that more elaborate formulas for the weighting coefficients can be found in the literature. Most of these methods are written assuming one has no knowledge of the behavior of the unknown function under the integral sign. Dr. Mei has pointed out that we do have knowledge of the behavior of the current on the dipole. We know that we must be able to represent it by a Fourier Series of finite length. Further, we should be able to represent the current in a region $\pm h/2$ about a point quite accurately

E. (Continued)

by only the first three terms in a Fourier series. Thus, we may approximate the current i(z) near the k-th segment as

$$I(z) = A_k + B_k \sin k(z-z_k) + C_k \cos k(z-z_k), \tag{69}$$

or by applying at the k-th point and the points on either side and writing I_k for $I(z_k)$, we have

$$I_{k-1} = A_k - B_k \sin kh + C_k \cos kh \tag{70}$$

$$I_k = A_k + C_k \tag{71}$$

$$I_{k+1} = A_k + B_k \sin kh + C_k \cos kh \tag{72}$$

Solving this set of simultaneous equations for A_k, B_k, C_k in terms of I_{k-1}, I_k, I_{k+1}, we have

$$\Delta_k = 2 \sin kh \cos kh - 2 \sin kh - 2 \sin kh (\cos kh - 1) \tag{73}$$

$$A_k = \frac{1}{\Delta k} \left[-\sin kh\, I_{k-1} + 2 \sin kh \cos kh\, I_k - \sin kh\, I_{k+1} \right] \tag{74}$$

$$B_k = \frac{1}{\Delta k} \left[(1-\cos kh)\, I_{k-1} + (\cos kh - \cos kh)\, I_k + (\cos kh - 1)\, I_{k+1} \right] \tag{75}$$

$$C_k = \frac{1}{\Delta k} \left[\sin kh\, I_{k-1} - 2 \sin kh\, I_k + \sin kh\, I_{k+1} \right] . \tag{76}$$

This gives for I(z)

$$\begin{aligned} I(z) = \frac{1}{\Delta k} \Big\{ & I_{k-1} \left[-\sin kh + (1-\cos kh) \sin k(z-z_k) + \cos k(z-z_k) \sin kh \right] \\ & + I_k \left[2 \sin kh + \cos kh - 2 \sin kh \cos k(z-z_k) \right] \\ & + I_{k+1} \left[-\sin kh + (\cos kh - 1) \sin k(z-z_k) - \sin kh \cos k(z-z_k) \right] \Big\} . \end{aligned} \tag{77}$$

E. (Continued)

Writing Equation (77) in a more compact form

$$I(z) = X(z)\, I_{k-1} + Y(z)\, I_k + Z(z)\, I_{k+1} \tag{78}$$

where the coefficients are given by

$$X(z) = \frac{1}{\Delta k}\left[-\sin kh + (1-\cos kh)\sin k(z-z_k) + \sin kh \cos k(z-z_k)\right] \tag{79}$$

$$Y(z) = \frac{1}{\Delta k}\left[2 \sin kh \cos kh - 2 \sin kh \cos k(z-z_k)\right] \tag{80}$$

$$Z(z) = \frac{1}{\Delta k}\left[-\sin kh + (\cos kh - 1)\sin k(z-z_k) + \sin kh \cos k(z-z_k)\right] . \tag{81}$$

Equation (78) states that the current in a given segment is a function of the current at the center of that segment and the current at the center of the segments on either side. Thus, as it stands (78) cannot be used for the point $k = 1$ located $h/2$ from the tip, or the point $k = n$ located $h/2$ from the center, since these points do not have points on either side. Therefore, we must determine a special set of coefficients for each of these points using the next two points moving away from the boundaries. Consider the tip point first. The expression for $I(z)$ in the tip segment is:

$$I(z) = A_1 + B_1 \sin k(z-z_1) + C_1 \cos k(z-z_1) \tag{82}$$

$$I_1 = A_1 + C_1 \tag{83}$$

$$I_2 = A_1 + B_1 \sin kh + C_1 \cos kh \tag{84}$$

$$I_3 = A_1 + B_1 \sin 2kh + C_1 \cos 2kh. \tag{85}$$

Solving this set of simultaneous equations we have

$$\Delta_1 = \Delta_k \tag{86}$$

$$A_1 = \frac{1}{\Delta_1}\left[-\sin kh\, I_1 + \sin 2kh\, I_2 - \sin kh\, I_3\right] \tag{87}$$

E. (Continued)

$$B_1 = \frac{1}{\Delta_1}\left[(\cos kh - \cos 2kh)\, I_1 + (\cos 2kh - 1)\, I_2 + (1 - \cos kh)\, I_3\right] \tag{88}$$

$$C_1 = \frac{1}{\Delta_1}\left[(\sin 2kh - \sin kh)\, I_1 - \sin 2kh\, I_2 + \sin kh\, I_3\right] . \tag{89}$$

Thus,

$$I(z) = X_1 I_1 + Y_1 I_2 + Z_1 I_3 \tag{90}$$

for the tip segment where

$$X_1 = \frac{1}{\Delta_1}\left[-\sin kh + (\cos kh - \cos 2kh) \sin k(z-z_1) + (\sin 2kh - \sin kh) \cos(z-z_1)\right] \tag{91}$$

$$Y_1 = \frac{1}{\Delta_1}\left[\sin 2kh - (1-\cos 2kh) \sin k(z-z_1) - \sin 2\,kh \cos k(z-z_1)\right] \tag{92}$$

$$Z_1 = \frac{1}{\Delta_1}\left[-\sin kh + (1 - \cos kh) \sin k(z-z_1) + \sin kh \cos k(z-z_1)\right] \tag{93}$$

The expression for the n-th segment is

$$I(z) = A_n + B_n \sin k(z-z_n) + C_n \cos k(z-z_n) , \tag{94}$$

which gives using the above method

$$I(z) = X_n I_n + Y_n I_{n-1} + Z_n I_{n-2}, \tag{95}$$

where

$$X_n = \frac{1}{\Delta_n}\left[-\sin kh + (\cos 2kh - \cos kh) \sin k(z-z_n) + (\sin 2kh - \sin kh) \cos k(z-z_n)\right] \tag{96}$$

E. (Continued)

$$Y_n = \frac{i}{\Delta_n}\left[\sin 2kh + (1 - \cos 2kh)\sin k(z-z_n) - \sin 2kh \cos k(z-z_n)\right] \quad (97)$$

$$Z_n = \frac{1}{\Delta_n}\left[-\sin kh + (\cos kh - 1)\sin k(z-z_n) + \sin kh \cos k(z-z_n)\right] . \quad (98)$$

In Equation (55) it is assumed that the function was constant over the segment, thus the area was represented by the product of $f(x_k)$ and h. Now, however, I(z) is not constant and to obtain the area we must perform an integration over the distance h. Further, each element of that part of the matrix which represents the integral will consist of terms involving the currents on either side excluding the special cases near the boundaries. These terms of the matrix will be

$$A(i,k) = \int_{a_k}^{b_k} (X_k I_{k-1} + Y_k I_k + Z_k I_{k+1})\, G(z_i, z')\, dz' , \quad (99)$$

where

$$a_k = z_k - h/2$$

$$b_k = z_k + h/2$$

and for the tip point

$$A(i, 1) = \int_{a_1}^{b_1} (X_1 I_1 + Y I_2 + Z I_3)\, G(z_i, z')\, dz' , \quad (100)$$

where

$$a_1 = z_1 - h/2 = \ell - \frac{3h}{2}$$

$$b_1 = z_1 + h/2 = \ell ,$$

and for the base point

$$A(i, n) = \int_{a_n}^{b_n} (X_n I_n + Y_n I_{n-1} + Z_n I_{n-2})\, G(z_i, z')\, dz' \quad (101)$$

E. (Continued)

where

$$a_n = z_n - h/2 = 0$$

$$b_n = z_n + h/2 = \frac{3h}{2} .$$

Since the unknown currents I_{k-1}, I_k, and I_{k+1} are under the integral sign, one might ask if replacing one integral equation by m integral equations do we represent the integrals in (82) to (84) by a m point sum. This is not true since the current I_{k-1}, I_k, and I_{k+1} are not variables in the integrals - they are constants. The type of integral we are concerned with here is of the form

$$\int_a^b X(z', z_k)\, G(z_i, z')\, dz' \tag{102}$$

where b-a = h. When given z', z_k and z_i we can calculate the product XG

One of the more accurate methods of numerical integration is using Lagrangian integration coefficients,[16] where

$$\int_a^b f(x)\, dx \doteq \alpha_0 y_0 + \alpha_1 y_1 + \ldots . \alpha_n y_n, \tag{103}$$

where the α's are the coefficients and y's are the values of f(x) at the n points. Accuracy increases with the number of points, but the computer time also increases. The use of 10 intervals which is 11 points seems to be a good compromise. The value of the Lagrangian integration coefficients for n = 10 are given in Table III-1. Thus, by evaluating the product $X_i G_i \alpha_i$ at each of the i points in the interval (a,b) and summing and multiplying by h/10, the integral represented by Equation (102) can be evaluated and inserted in Equation (99)-(101).

Table III-1. Lagrangian Integration Coefficients

i	α_i
0	0.268341483
1	1.775359414
2	-0.810435705
3	4.549462882
4	-4.351551226
5	7.137646304
6	-4.351551226
7	4.549462882
8	-0.810435705
9	1.775359414
10	0.268341483

E. (Continued)

With this sinusoidal approximation we can decrease the number of points on the dipole for a given accuracy. Also we need no longer do a Taylor series expansion for the boundary condition but can use Equation (90) with $z = \ell$.

$$I(\ell) = X_1(\ell) I_1 + Y_1(\ell) I_2 + Z_1(\ell) I_3 = 0 \tag{104}$$

and the current at the feed point is given by

$$I(0) = X_n(0) I_n + Y_n(0) I_{n-1} + Z_n(0) I_{n-2} . \tag{105}$$

F. SIMULTANEOUS LINEAR EQUATIONS

Finally, one note on the solution of the n + 2 simultaneous linear equations. Most computing centers have subroutines that can solve a set of complex simultaneous linear equations using various methods. While the computer we have available is sufficiently large to handle a single dipole, it was felt that when one had antennas with more than five dipoles there would be insufficient core. Thus, a subroutine was developed that does not require more than two rows of the argumented matrix in the core at one time by the use of magnetic tape units for storage. The method used was the Gauss-Jordan elimination method with normalization.[17] This method allows us, if desired, to solve up to 500 simultaneous linear equations without overflow. By properly filling the matrix we have not experienced any difficulty with round-off errors so far (130 equations).

G. EQUATION FORMULATION FOR A LOG-PERIODIC DIPOLE ANTENNA

After one has formulated the equations for a single dipole, what changes or additions must be made to give the set of simultaneous linear equations that will describe a log-periodic antenna? There is one change to be made and one addition to be made. We must change Equation (62) so that the interaction between the different dipoles of the antenna are properly handled. We must also add additional equations to represent the transmission lines that tie the dipoles of log-periodic elements together.

The approach used below to determine the changes is based on the separate work of one of the authors.[18]

The vector potential on a dipole antenna in the presence of N-1 other dipoles, which need not be of the same length, can be represented by an equation which is based on Equation (47) using the symbology given in Equation (50). The vector potential will, if all the dipoles are parallel to the z-axis with their centers being in the $z = 0$ plane, have only a z component. Thus, we have at point P

$$A_z(P) = \sum_{m=1}^{nd} \int_0^{\ell_m} I_m(z')\, G(z', z_p)\, dz' , \tag{106}$$

where $A_z(P)$ is the vector potential at any point which is outside the dipoles, nd is the number of dipoles, ℓ_m is the length of one half of dipole m, $I_m(z')$ is the current flowing in dipole m at the point z', and $G(z', z_p)$ is a modified Green's function of the form given by Equation (68) and with r of Equation (47) replaced by d, the horizontal distance between the dipole m and point P.

The scalar potential at point P can be found from the following relationship

$$\phi = \int_v \frac{\rho\, e^{-jkR}}{4\pi \epsilon R}\, dv, \tag{107}$$

where ρ is the charge density and v is the volume. We may rewrite Equation (107) for our antenna as follows:

$$\phi(P) = -\frac{1}{jw\epsilon} \sum_{m=1}^{nd} \int_0^{\ell_m} \frac{\partial I_m(z')}{\partial z'}\, G(z', z_p)\, dz' , \tag{108}$$

G. (Continued)

which after integration by part and using the quantity

$$-\frac{\partial G}{\partial z'} = \frac{\partial G}{\partial z_p} \tag{109}$$

we have

$$\phi(P) = -\frac{1}{jw\epsilon} \sum_{m=1}^{nd} \int_{o}^{\ell_m} I_m(z') \frac{\partial}{\partial z_p} G(z', z_p)\, dz' \ . \tag{110}$$

The tangential electric field on any antenna produced by the currents on the other antennas is

$$E_z = -\nabla\phi - jw\mu A_z = \frac{-\partial\phi(P)}{\partial z_p} - jw\mu A_z(P), \tag{111}$$

where the point P is on the surface of the dipole but

$$\phi(P) = -\frac{1}{jw\epsilon} \frac{\partial A_z(P)}{\partial z_p} \ . \tag{112}$$

Therefore,

$$E_z = \frac{1}{jw\epsilon} \frac{\partial^2 A_z(P)}{\partial z_p} - j\omega\mu A_z(P) \tag{113}$$

or

$$j\omega E_z = \left[\frac{\partial}{\partial z_p} + k^2\right] A_z(P) \ . \tag{114}$$

For the tangential electric field to vanish on the surface of the dipoles, we have for dipole m

$$E_z(P)_m - E_z(P)_m \text{ (incident)} = -V_m \delta(\ell_m) \tag{115}$$

or

$$A_{zp} = C_1 \sin k \left| z_p \right| + C_2 \cos k z_p \ . \tag{116}$$

G. (Continued)

This last equation can now be represented by a set of algebraic equations in the form given by Equation (62), etc.,

$$\sum_{i=1}^{nd} \left\{ h \sum_{m=1}^{n} W_m I_{im} G(z_{im}, z_j) \right\} - B_j \cos kz_j + \frac{2V_j}{2\eta_o} \sin k\left|z_j\right| = 0 \qquad (117)$$

$$j = 1, 2, \ldots . n.$$

Here we now have a boundary condition for each dipole, which is the reason that the B's are subscripted, and each dipole has its own driving voltage. Also, while Equation (117) cannot show, as it is written, the use of the sinusoidal approximation is used as outlined in subsection E. The equations for the boundary conditions on the tips of the dipoles are written using the form given by Equation (104).

H. TRANSMISSION LINE EQUATIONS

Equation (63) which is the single equation for the driving voltage on a single dipole will become the driving voltage of the transmission line which feeds the log-periodic dipole elements. To relate this voltage to the base of each dipole, an additional set of equations in terms of the current at the base of each dipole, flowing into the dipole and down the transmission line must be determined. These equations are based on the assumption that the transmission line has no ohmic or radiation losses.

There is no need to derive one single equation that gives the relationship between the input voltage or current and the voltage or current at the most distant dipole. We need only derive the relationship between the n and n+1 dipole and repeat this relationship between the n+1 and the n+2 dipoles until all sections of the transmission line have been covered. Figure III-1 shows the geometry involved.

The equations for an ideal transmission line are given by[19]

$$V_n = Ve^{-jS_n} + V'e^{jS_n} \qquad (118)$$

$$Z_o I_n = Ve^{-jS_n} - V'e^{jS_n} \qquad (119)$$

where S_n is the distance to a reference point on the left in radians from point n, V is the amplitude of the direct wave, V' is the amplitude of the reflected wave, V_n is the voltage

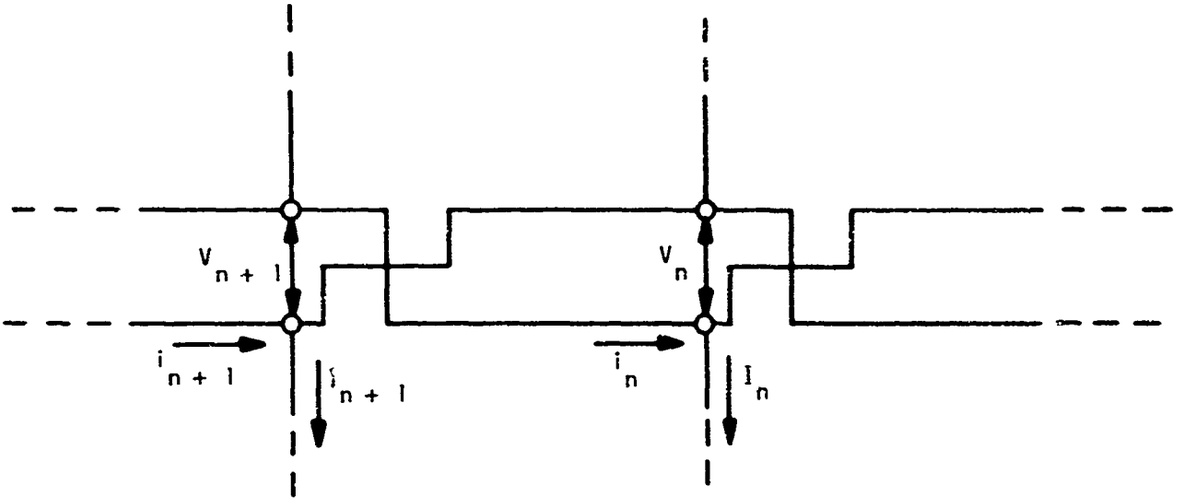

Figure II-1. Transmission Line Geometry

H. (Continued)

across element n, i_n is the current flowing into the junction of the transmission line and the n element, while Z_o is the surge impedance of the line. The determinant of these two equations is

$$D = \begin{vmatrix} e^{-js_n} & e^{js_n} \\ e^{-js_n} & -e^{js_n} \end{vmatrix} = -2 \tag{120}$$

while

$$V' = \frac{\begin{vmatrix} e^{-js_n} & V_n \\ e^{-js_n} & Z_o i_n \end{vmatrix}}{2} = \frac{e^{-js_n}}{2} (V_n - Z_o i_n) \ . \tag{121}$$

and

$$V = \frac{\begin{vmatrix} V_n & e^{js_n} \\ Z_o i_n & -e^{js_n} \end{vmatrix}}{2} = \frac{-e^{js_n}}{-2} (V_n + Z_o i_n). \tag{122}$$

Now let us consider the equations at the n+1 dipole with reference to the n dipole. If the spacing between the dipoles were sufficiently short so that the effects of the transmission line were zero, we need only consi er the transposition of the wires. Thus,

$$V_{n+1} = -V_n \quad \text{or} \quad -V_{n+1} = V_n \tag{123}$$

$$Z_o i_{n+1} = -Z_o i_n \quad \text{or} \quad -Z_o i_{n+1} = Z_o i_n \tag{124}$$

or rewriting (118) and (119) for the n+1 dipole we have

$$-V_{n+1} = Ve^{-js_{n+1}} + V'e^{js_{n+1}} \tag{125}$$

$$-Z_o i'_{n+1} = Ve^{-js_{n+1}} - V'e^{js_{n+1}} \ . \tag{126}$$

H. (Continued)

Substituting Equations (121) and (122) in (125), we have after reduction

$$-V_{n+1} = V_n \left[\frac{e^{j\sigma_n} + e^{-j\sigma_n}}{2} \right] + jZ_o i_n \left[\frac{e^{j\sigma_n} - e^{-j\sigma_n}}{2j} \right] , \tag{127}$$

where

$$\sigma_n = s_n - s_{n+1},$$

which gives

$$-V_{n+1} = V_n \cos \sigma_n + jZ_o i_n \sin \sigma_n \tag{128}$$

or

$$V_{n+1} + V_n \cos \sigma_n + jZ_o i_n \sin \sigma_n = 0 . \tag{129}$$

In a similar manner, we have

$$i'_{n+1} + \frac{jV_n}{Z_o} \sin \sigma_n + ji_n \cos \sigma_r = 0 . \tag{130}$$

The expression for the current i'_{n+1} is for the current to the right of dipole n+1, while the equation needed is for the current just to the left of dipole n+1. The voltage across the transmission line as one moves toward the generator and passes the feed point of the n+1 dipole must be continuous so Equation (129) is correct as it stands. However, the current must increase by the amount flowing into the dipole. Therefore, we must rewrite Equation (130) to include the current I_{n+1}, the current flowing into the n+1 dipole. The current on the left must be

$$I_L = (i_{n+1})_L + I_{n+1}, \tag{131}$$

while the current on the right is

$$I_R = i'_{n+1} . \tag{132}$$

H. (Continued)

Therefore, we have

$$i_{n+1} - I_{n+1} + \frac{jV_n}{Z_o} \sin\sigma_n + i_n \cos\sigma_n = 0 \quad , \tag{133}$$

where I_{n+1} is determined by Equation (95) as applied to the n+1 dipole.

To demonstrate how we apply these equations and consider the ends of the transmission lines, consider the 5-element dipole shown in Figure III-2. The current flowing in an antenna at the base of the antenna is, using Equation (45),

$$I_j = X_j I_{j'n} + Y_{j'} I_{J'n-1} + Z_k I_{j'n-2} \tag{134}$$

where the single subscript on I indicates the current flowing in to the base of the j dipole. The equations for the voltages will be

$$V_1 + \frac{V_2}{\cos\sigma_1} + j i_1 \frac{\sin\sigma_1}{\cos\sigma_1} Z_o = 0 \tag{135}$$

$$V_2 + \frac{V_3}{\cos\sigma_2} + j i_2 \frac{\sin\sigma_2}{\cos\sigma_2} Z_o = 0 \tag{136}$$

$$V_3 + \frac{V_4}{\cos\sigma_3} + j i_3 \frac{\sin\sigma_3}{\cos\sigma_3} Z_o = 0 \tag{137}$$

$$V_4 + \frac{V_5}{\cos\sigma_4} + j i_4 \frac{\sin\sigma_4}{\cos\sigma_4} Z_o = 0 \tag{138}$$

$$V_5 + \frac{V_o}{\cos\sigma_5} + j i_5 \frac{\sin\sigma_5}{\cos\sigma_5} Z_o = 0 \tag{139}$$

$$V_o = 1.0 \quad . \tag{140}$$

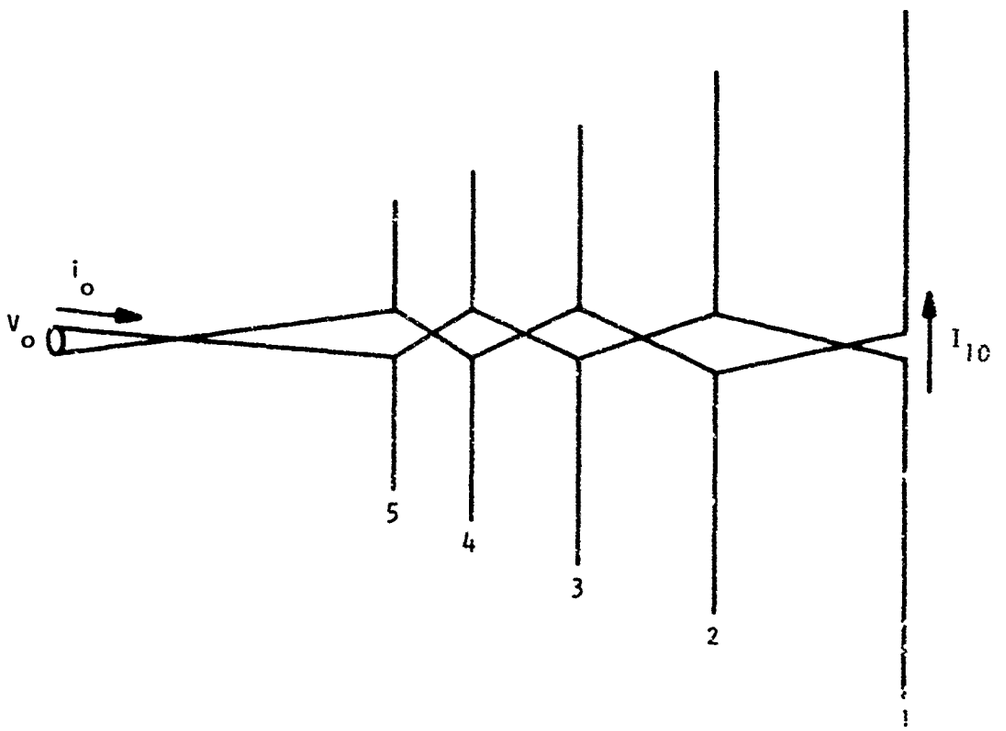

Figure II-2 Log-Periodic Antenna

H. (Continued)

For the currents we have, where i's represent transmission line currents and I's represent dipole currents,

$$i_1 - I_1 = 0 \tag{141}$$

$$i_2 - I_2 + \frac{jV_1}{Z_o} \sin\sigma_1 + i_1 \cos\sigma_1 = 0 \tag{142}$$

$$i_3 - I_3 + \frac{jV_1}{Z_o} \sin\sigma_2 + i_2 \cos\sigma_2 = 0 \tag{143}$$

$$i_4 - I_4 + \frac{jV_3}{Z_o} \sin\sigma_3 + i_3 \cos\sigma_3 = 0 \tag{144}$$

$$i_5 - I_5 + \frac{jV_4}{Z_o} \sin\sigma_4 + i_4 \cos\sigma_4 = 0 \tag{145}$$

$$i_0 + \frac{jV_5}{Z_o} \sin\sigma_5 + i_5 \cos\sigma_5 = 0 \ . \tag{146}$$

It is, of course, not realistic to have the long transmission line in front of the antenna, but this has been left on to make it easier to write the equations. It can be removed by subtracting σ_5 from all σ's.

I. FAR FIELD, INPUT IMPEDANCE, AND GAIN

The relationship between the current on a short dipole and the far field is given by [20]

$$E_\theta = \frac{j\,60\pi\, I\ell \sin\theta}{s\lambda} \tag{147}$$

where I is the current, θ is the polar angle, s is the distance from dipole to distant point where E_θ is to be determined, λ is the wavelength in meters, and ℓ is the length of the dipole. It is required, of course, that $\ell << \lambda$ and that the current be constant over ℓ or I represents its average value. The log-periodic antenna as we have represented it does not consist of a single short dipole, but arrays of short dipoles. Thus, the current shown in

I. (Continued)

Equation (147) is only representative of all the currents represented in Equation (117). We need then some relationship that will give the total E_θ in the far field.

If we assume that the distance to the point P where E_θ is to be determined is sufficiently far that the lines from P to all of the current elements on the antenna can be considered parallel; that is, we are in the Fraunhofer region and we can rewrite Equation (147) as follows

$$E_\theta = \sum_{m=1}^{ND} \sum_{i=1}^{NP} \frac{j\,60\pi\, I_{im} \sin\theta\, e^{-jk\,(s_{im} - s_o)}}{s_o \lambda} \tag{148}$$

where s_o is the distance to a reference point, for example, the apex of the log periodic and s_i is the distance to the current element i. NP is the number of points on the m-th dipole and ND is the number of dipoles in the array

Let y_{im} represent the distance from the center of the j dipole to the i-th point in radians. As before, θ_m represents the distance from apex of the log-periodic to the m dipole in radians. Then, by the use of a little trigonometry, we have

$$k\,(s_{im} - s_o) = -y_{im} \cos\theta + \sigma_m \sin\theta \cos\phi, \tag{149}$$

where θ is the polar angle and ϕ is the azimuthal angle in a spherical coordinate system. Thus, the far field E_θ at point P at a distance s_o, polar angle θ, and azimuthal angle ϕ, is expressed by

$$E_\theta = \sum_{m=1}^{ND} \sum_{i=1}^{NP} \frac{j\,60\pi\, I_{im} \sin\theta}{s_o \lambda} \exp\left\{-j(-y_{im} \cos\theta + \sigma_m \sin\theta \cos\phi)\right\} \tag{150}$$

If the applied voltage to the antenna is one volt, then the real part of the inverse of the input current is the radiation resistance while the imaginary part is the radiation reactance. The input current is shown in Figure III-2 as i_o. The transmission line between the shortest dipole and the apex is not a part of the antenna, it is assumed that the technique given after Equation (146) is used which makes this section of line of zero length.

Gain as it will be used on this project is defined as the gain relative to a lossless isotropic antenna in free space. It will be expressed in decibels--i.e -- dbi The

I. (Continued)

mathematical definition of gain then is, which is in agreement with the IEEE definition of power gain in a given direction,

$$G_{dbi} = 10 \log \left[\frac{4\pi \times \text{the radiation intensity in that direction}}{\text{total power accepted by the antenna}} \right], \tag{151}$$

where the radiation intensity, P, is the power radiated in the given direction per unit solid angle. That is

$$P = \frac{E_\theta^{\,2}\, r^2}{120\pi}. \tag{152}$$

J. CONCLUSION

This completes the derivation and description of the expressions that relate the physical parameters of a log-periodic antenna to the currents on the elements of the antenna, the input impedance, and gain where the solution was obtained assuming that we have a boundary value problem. Also the solution was obtained knowing that the best numerical techniques and digital computers were to be used.

III NUMERICAL RESULTS

A. INTRODUCTION

During the study covered by this report a step-by-step procedure was used to obtain a computer program for a log-periodic antenna in free space and over real earth. At first the theory presented in Section II of this report was programmed to calculate the current distribution on just a single dipole. When the validity of the results of this simple program had been verified, the more complicated case of two identical dipoles in free space was mathematically modeled and programmed. This procedure of applying the theory to problems of ever-increasing complexity and verifying the calculations at each stage of the process was followed throughout.

The following subsections present the numerical results of some of the most interesting stages in the development of the present computer program. At each step the computer results are compared with data previously published or to data obtained experimentally wherever practical.

B. SINGLE DIPOLE

As stated above, the theory was first applied to a single dipole in free space. The dipole was divided into 2N sections and the current computed for each of the individual sections. At first the current was assumed to be constant on each section of the dipole, but later it was found that the number of dipole divisions needed to obtain an accurate current distribution on the dipole could be reduced by assuming a more complex current form for each dipole section. The desirability of using a minimum number of dipole divisions is two-fold. The most obvious reason being a reduction in the computer time

B. --Continued

required for a given degree of accuracy. Although a savings in this quantity is not particularly important for the single dipole solution, it is essential if a multielement structure is to be analyzed. The second reason for requiring a minimum number of dipole divisions, although less obvious than the first, is equally important. In reducing the theoretical solution presented in Section II to form a suitable form for computer use, some approximations were made that require the length of each dipole division to be much greater than the diameter of the dipole; therefore, there is a maximum number of dipole divisions that can be used and still maintain a high degree of accuracy in the solution. For thin dipoles, of course, the problem does not arise since an accurate solution can be obtained by using a number of dipole divisions far below the maximum allowed.

B. --Continued

Figures III-1 and III-2 illustrate the current distribution on the half-wave dipole for different values of N and for both the constant current model on each division and the sinusoidal current model on each division. For comparison, the dipole current distribution calculated by R. W. P. King[1] is also shown on each graph. The advantage of using the sinusoidal current model for each segment of the dipole is seen by comparing the two figures. With the sinusoidal current form, the resulting current distributions approach that obtained by King with fewer dipole divisions and remain nearer King's distribution over a wider range of N than do the distributions obtained by using the constant current form for each division. It is also interesting to note that the maximum current is not at the center of the dipole as would be expected. This is explained by the fact that the particular dipole used is relatively thick and thus appears electrically longer than half a wavelength. Current distributions have been calculated for much thinner dipoles and the current maximum does appear at the center of the dipole as expected. (See Figure III-3)

The gain of this antenna was calculated using the method described in the section on theory and was 2.15 db, the value predicted by Jordan.[2]

C. TWO DIPOLES

Having verified that the theory was correctly applied to a single dipole, the next step was to try solving the current distributions on two dipoles connected by a transmission line.

Several cases of two dipoles in an array have been programmed and current distributions found. In many instances much useful information such as variations in input impedance with changing dipole spacings and lengths was found, but for the most part these results only served as a check on the theory and programming procedure and were not investigated further.

There is one particular case of general interest, however, which should suffice as a representative example of the many two-dipole arrays which have been programmed. The example in mind is an array of two half-wave dipoles separated by one-half wavelength and fed in phase to give a broadside radiating structure. The currents on both dipoles are identical. The dipoles are fed by a single voltage generator at the base of one dipole, with a section of transmission line one-half wavelength long connecting the remaining dipole. To obtain "in phase" voltages at the base of each dipole, the transmission line was switched so that there was an additional 180-degree phase shift at the second dipole besides

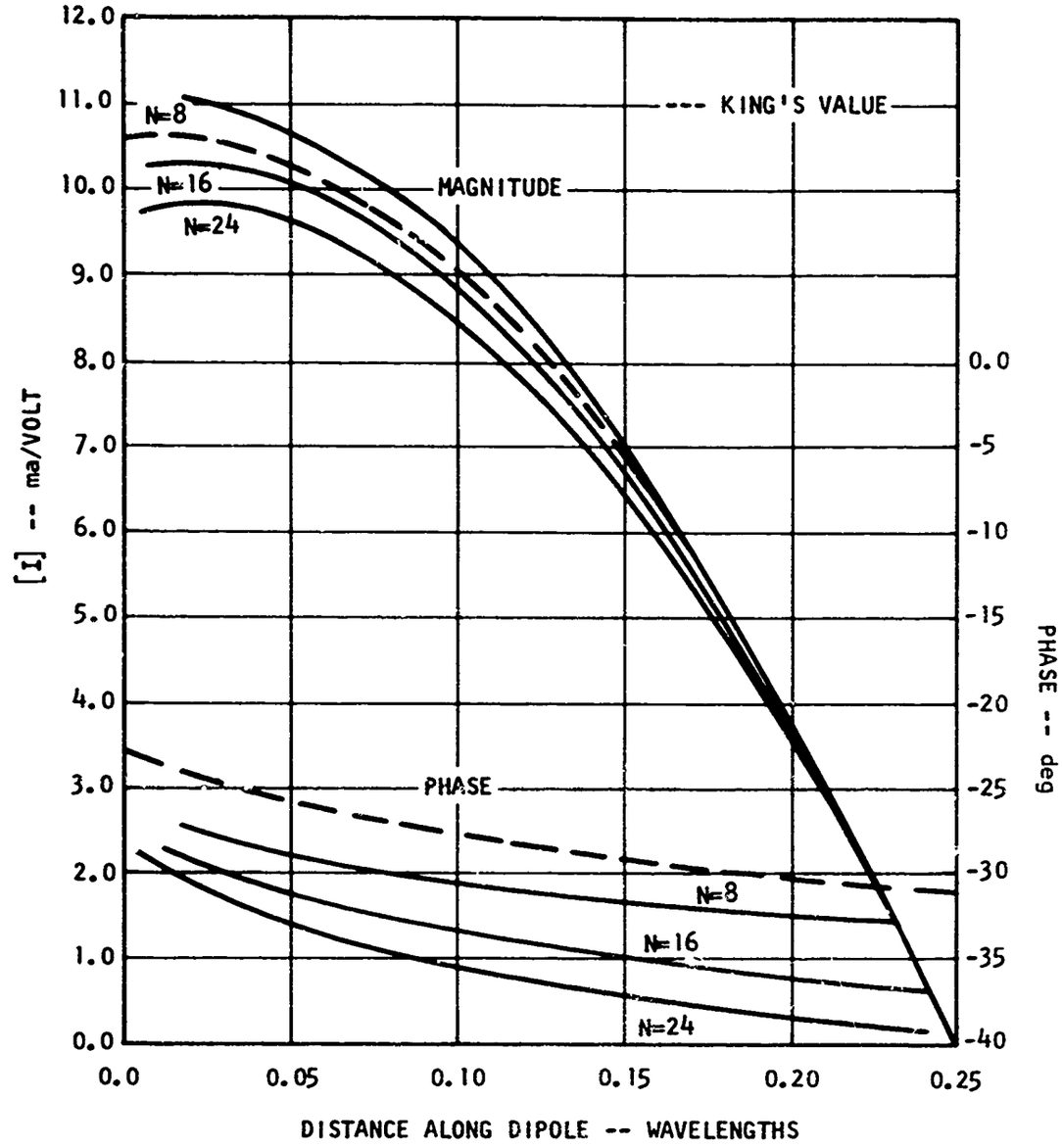

Figure III-1. Dipole Current Distribution, Constant Current Model

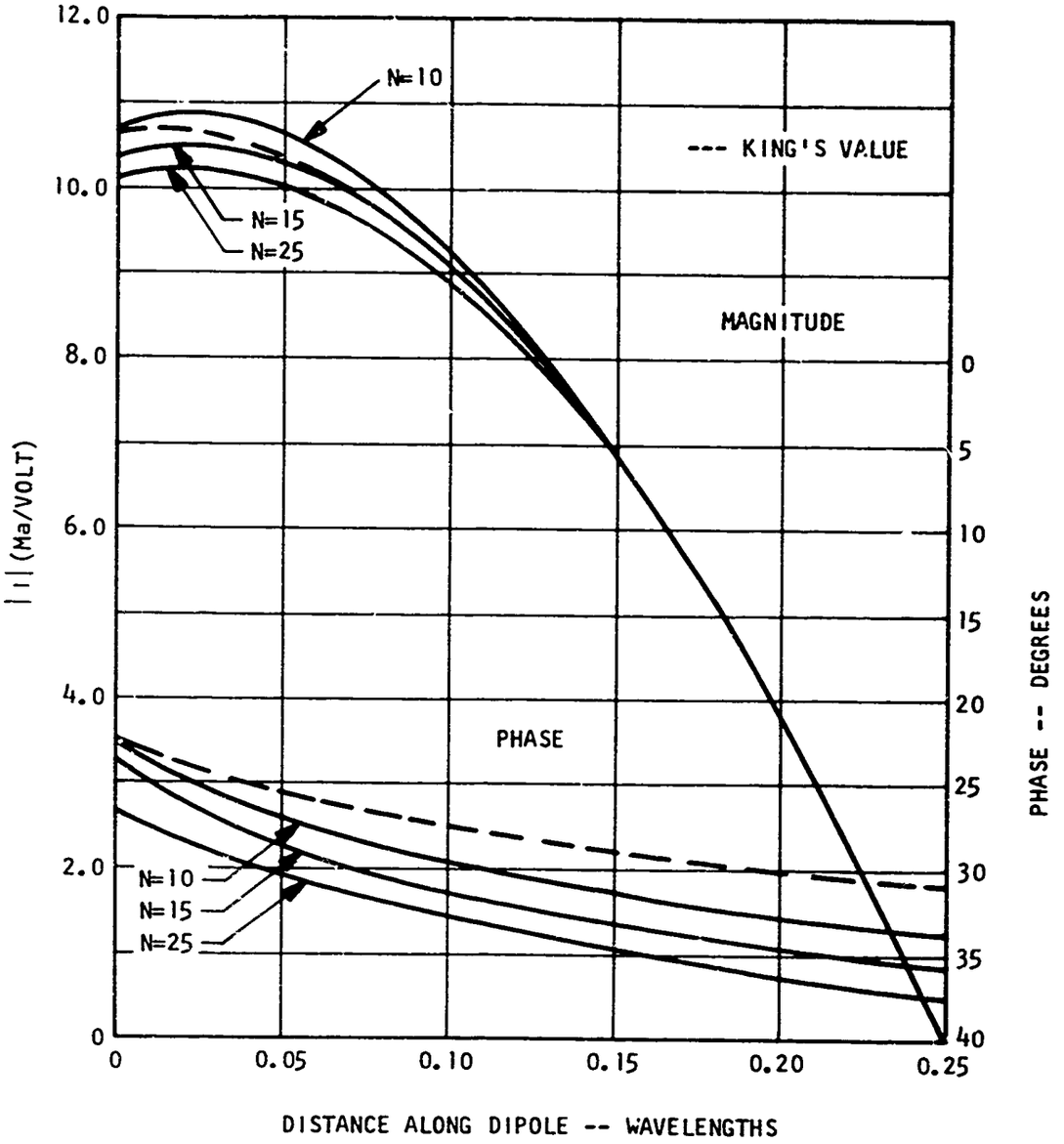

Figure III-2. Dipole Current Distribution, Sinusoidal Current Model

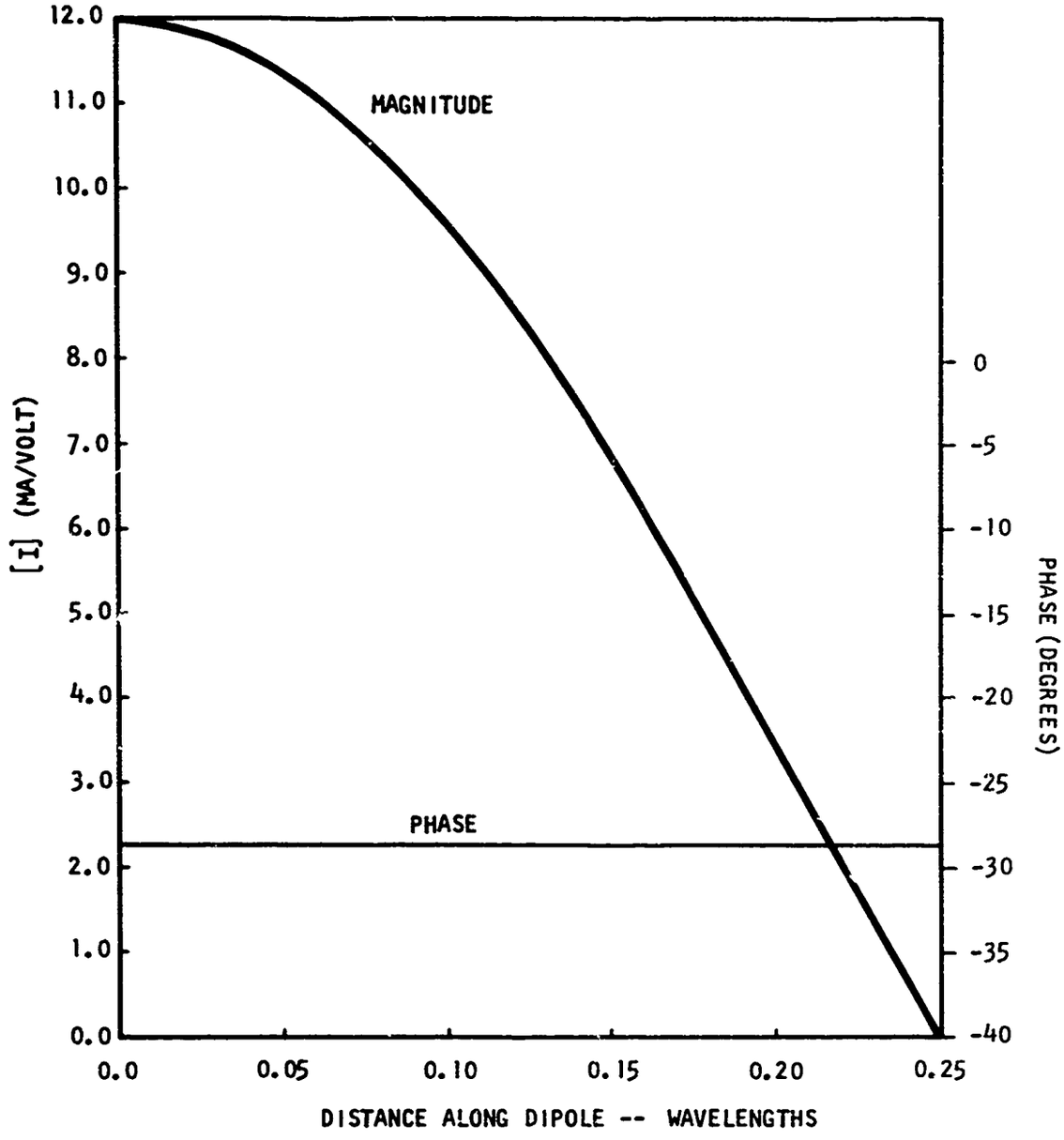

Figure III-3. Dipole Current Distribution (Thin dipole - Ω = 20)

C. (Continued)

the 180-degree phase shift introduced by the length of transmission line. The gain for this array is 6.029 db and is consistent with values found by using other methods.[3] The input impedance to each dipole is 62 + J6.3 ohms and is comparable to the value of 60 + j4 obtained by Kraus.

D. LOG-PERIODIC ANTENNA

In this section probably the most important results of the study are presented. These are the computed values of current distribution and radiated power for an entire log-periodic antenna. After many trial computer runs, a satisfactory program was finally achieved for the LP antenna and the results of this program were compared to data measured from existing antenna models.

The model that was analyzed on the computer was a 10-element switched-phase log-periodic antenna (bandwidth 250-500 MHz) with $\alpha = 45^{\circ}$ and $\tau = 0.853$. The antenna feed structure was a 137-ohm two-wire line. Two computer runs were made for two different frequencies. Figures III-4 and III-5 show the current distribution at frequencies of 300 MHz and 450 MHz, respectively. The currents are nearly as would be expected by antenna engineers. The highest currents appear on the elements near resonance and on the next smaller elements; i.e., the active region includes the resonant element plus the next several smaller elements. The phase progression from one element to the next is also in agreement with measurements made previously.[4]

Figures III-6 through III-9 show a comparison between measured and calculated radiation patterns at frequencies of 300 MHz and 450 MHz for this log-periodic dipole array.

Figures III-10 through III-14 show the current distribution and far-field patterns (measured and calculated) of a 6-element log-periodic at operating frequencies of 650 and 850 MHz. The design band limits are 550 and 1000 MHz.

Figures III-15 through III-19 show the current distribution and far-field patterns for a 10-element version of the antenna given above. In comparing the currents shown in Figures III-10 and III-15 one must note the difference in maximum values. The major reason is that both antennas theoretically were fed with ideal 1-volt sources, thus allowing the antenna with the lower input impedance to draw more current. In the calculation of absolute gain as described in Section II, this effect is accounted for automatically.

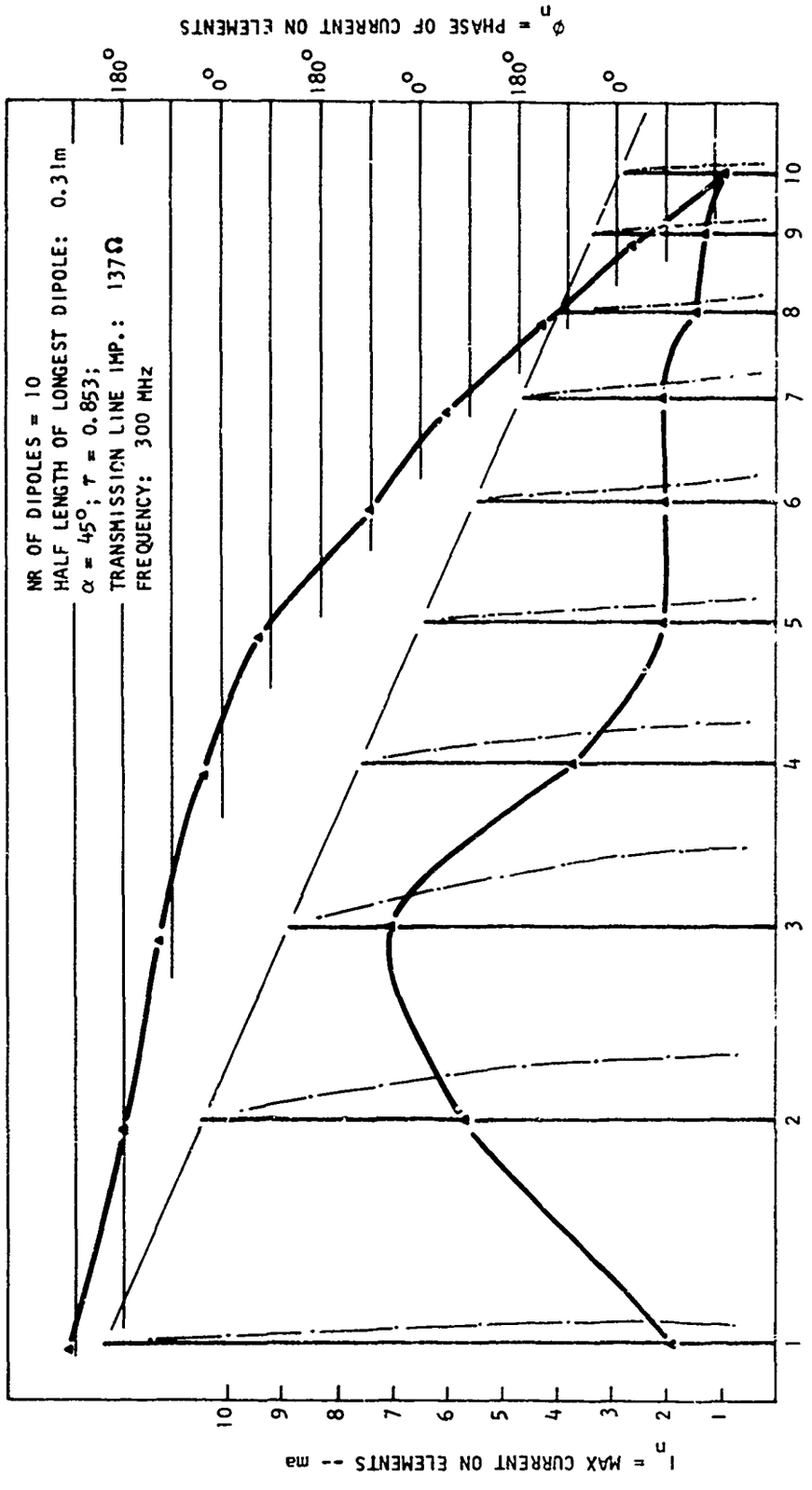

Figure III-4. Log-Periodic Current Distribution - 300 MHz

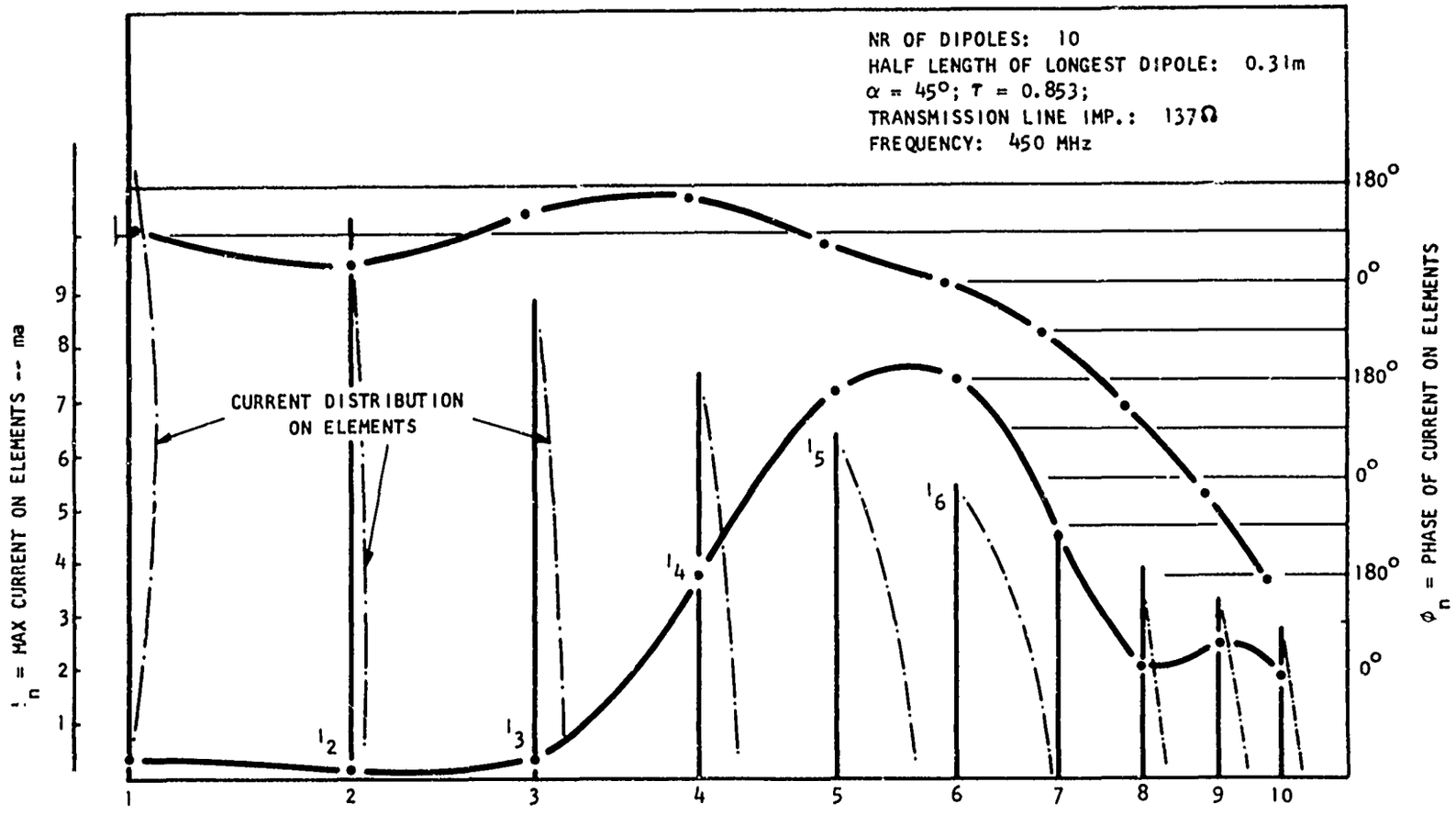

Figure III-5. Log-Periodic Current Distribution - 450 MHz

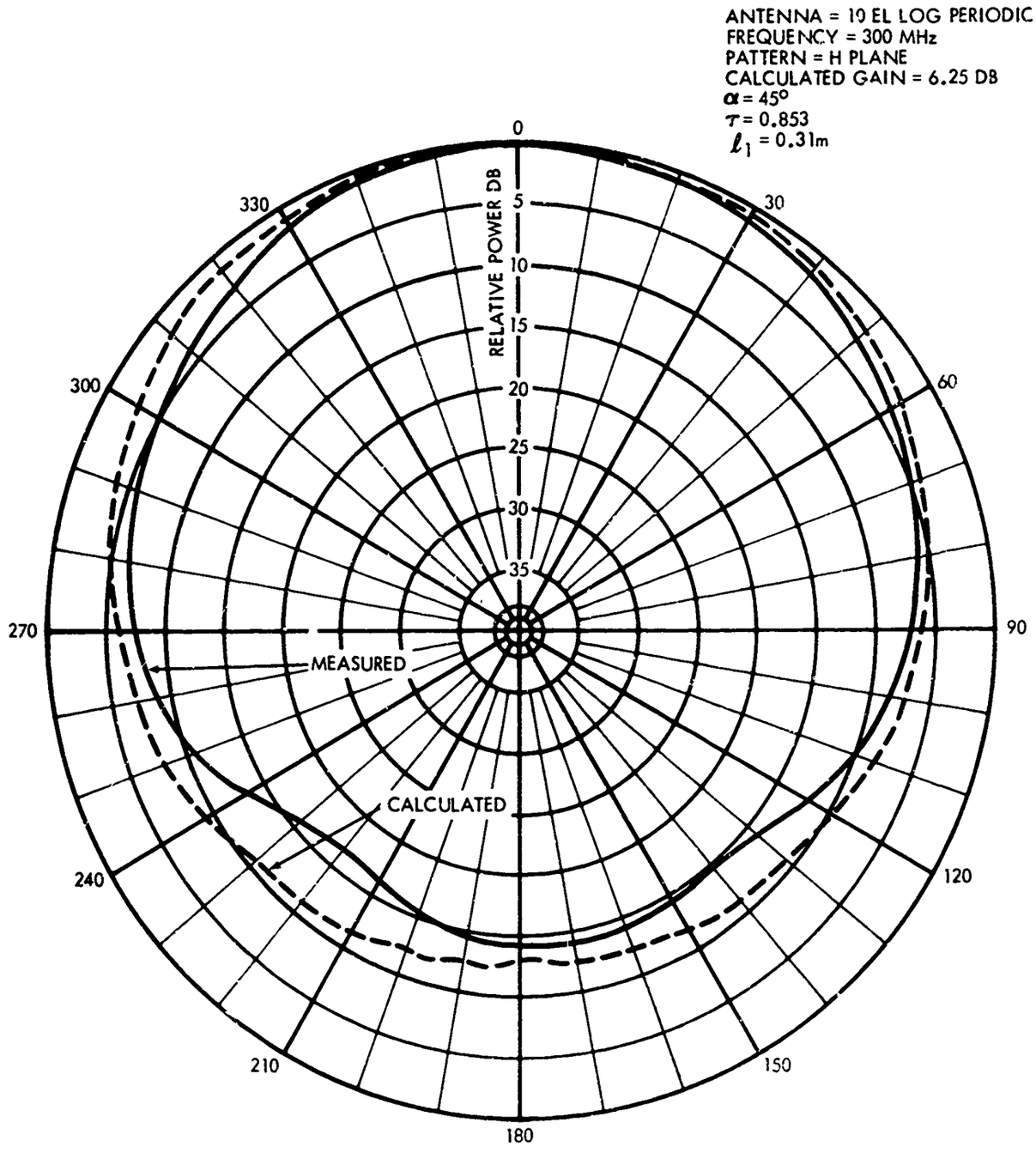

Figure III-6. Log-Periodic Azimuth Pattern - 300 MHz

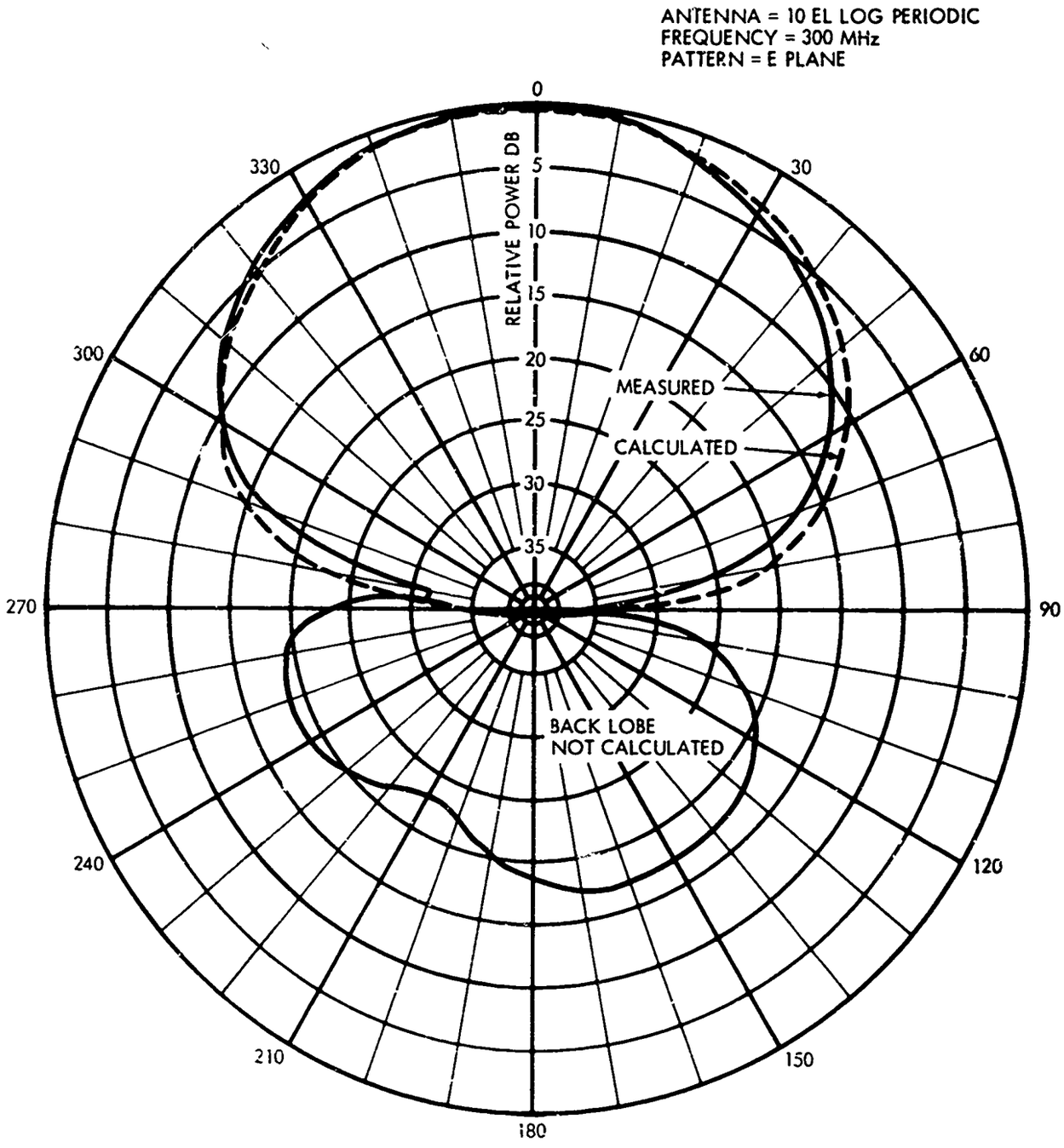

Figure III-7. Log-Periodic Elevation Pattern - 300 MHz

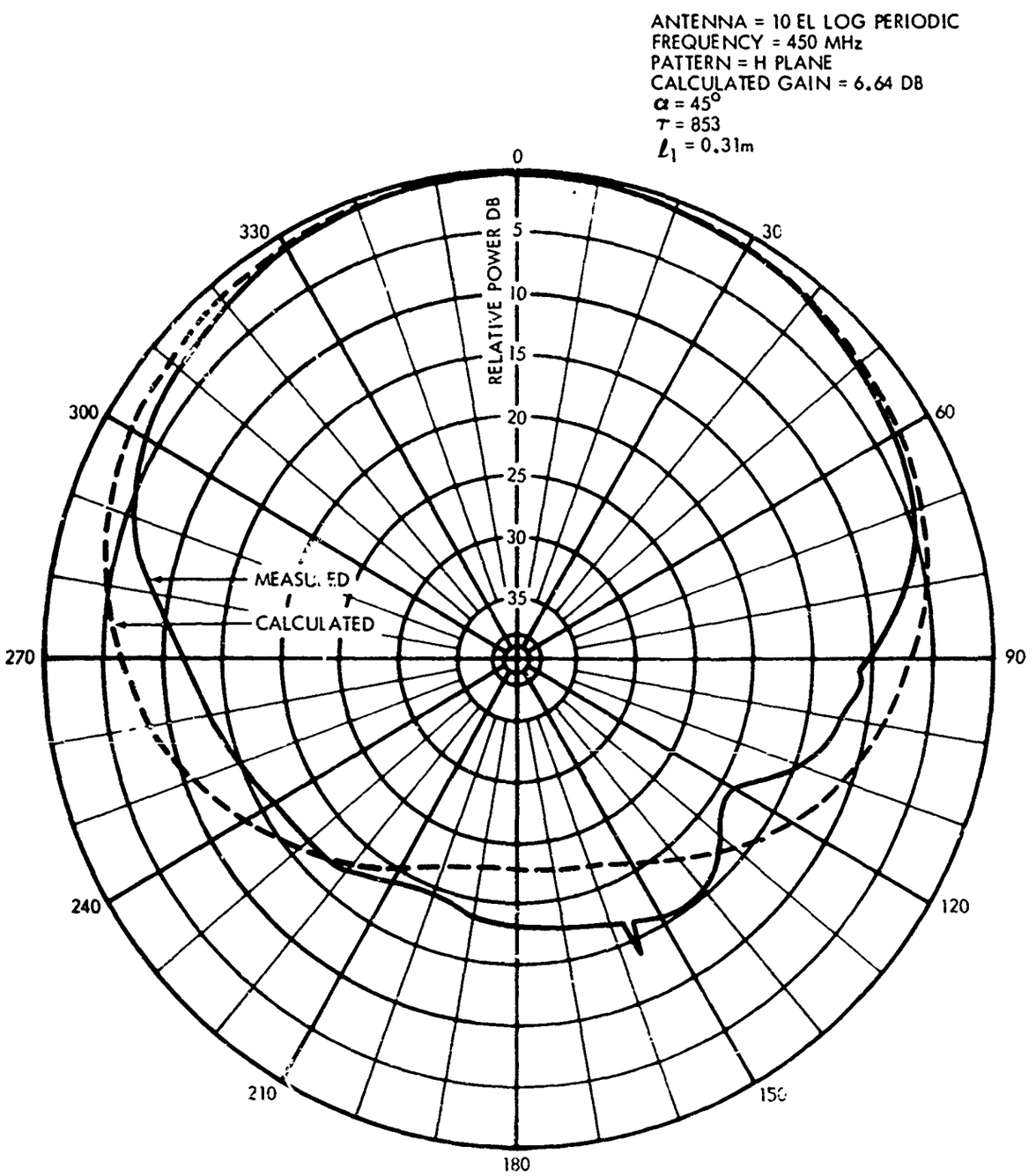

Figure III-8. Log-Periodic Azimuth Pattern - 450 MHz

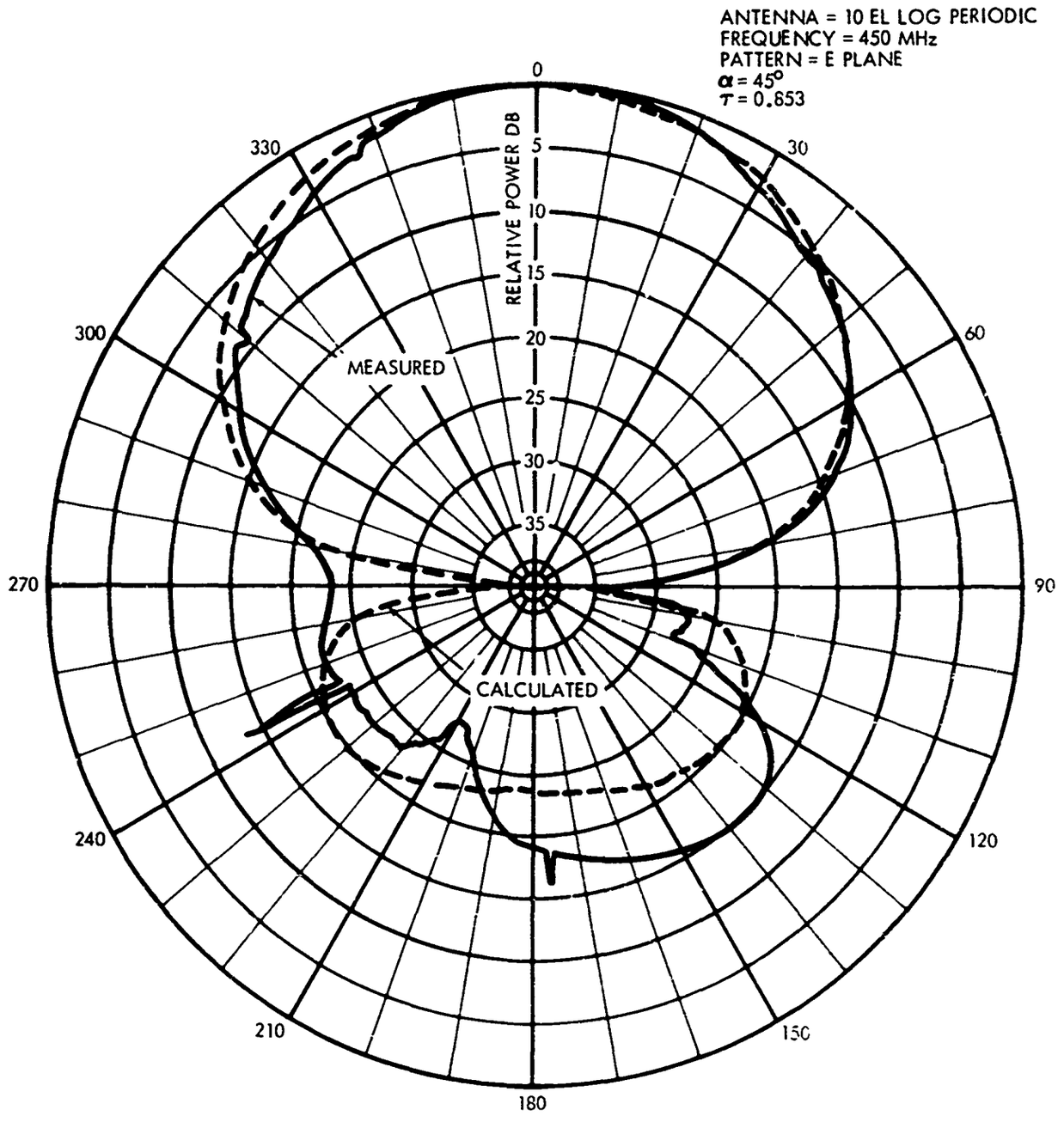

Figure III-9. Log-Periodic Elevation Pattern - 450 MHz

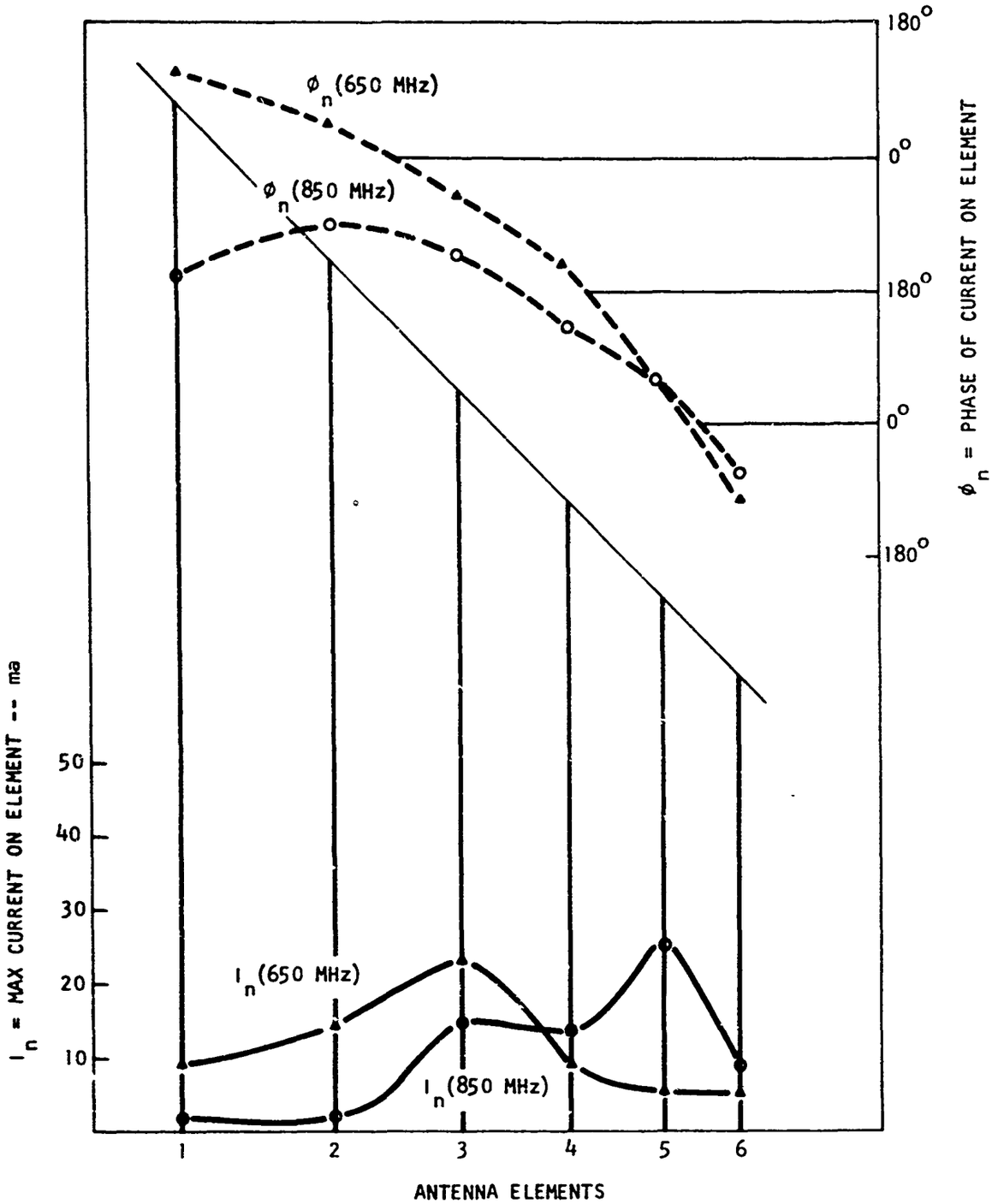

Figure III-10. Current Amplitude and Phase Distribution 6-element Log Periodic. $\tau = 0.85$, $\alpha = 90°$

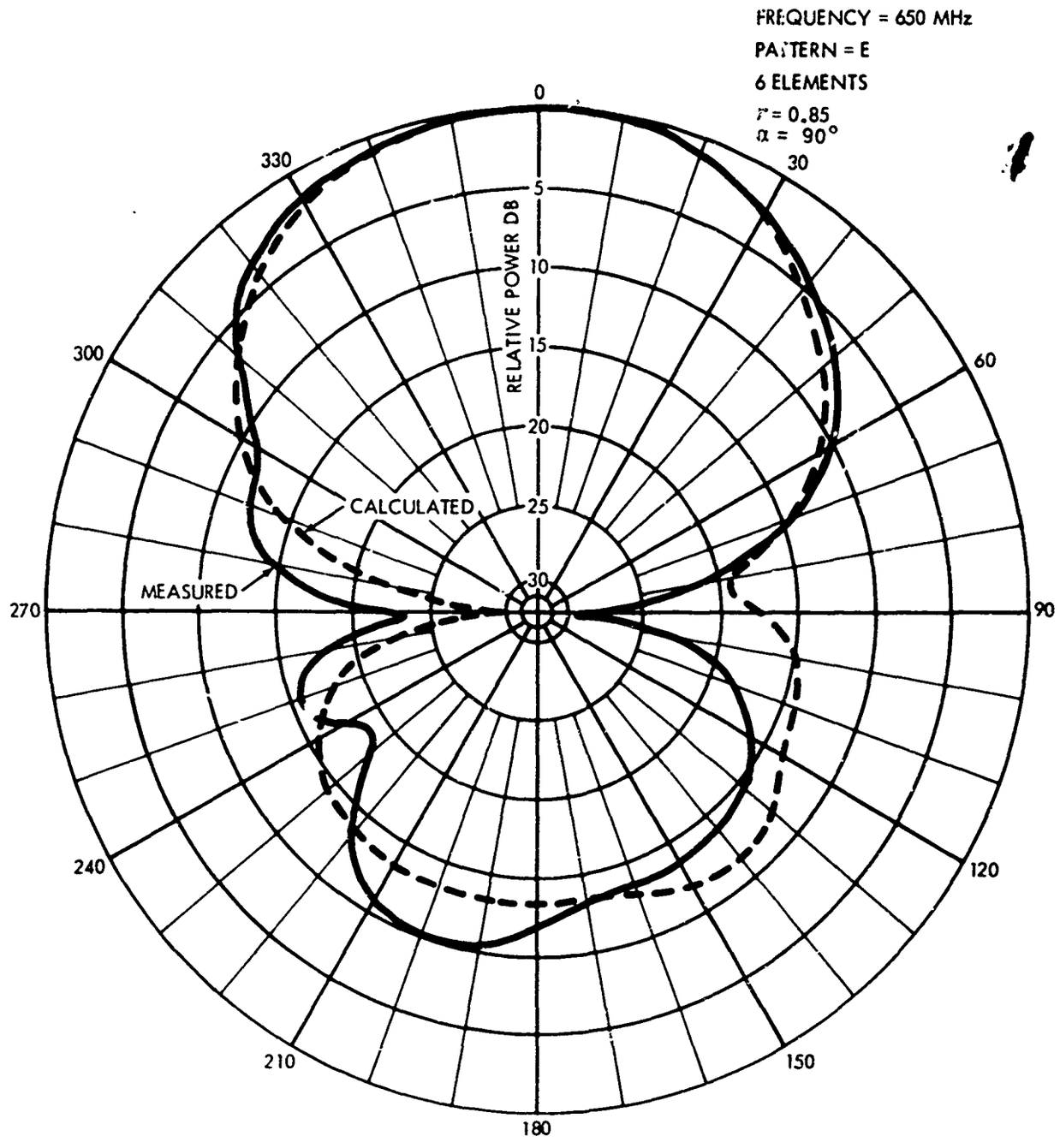

Figure III-11. Log Periodic E-Plane Pattern - 650 MHz

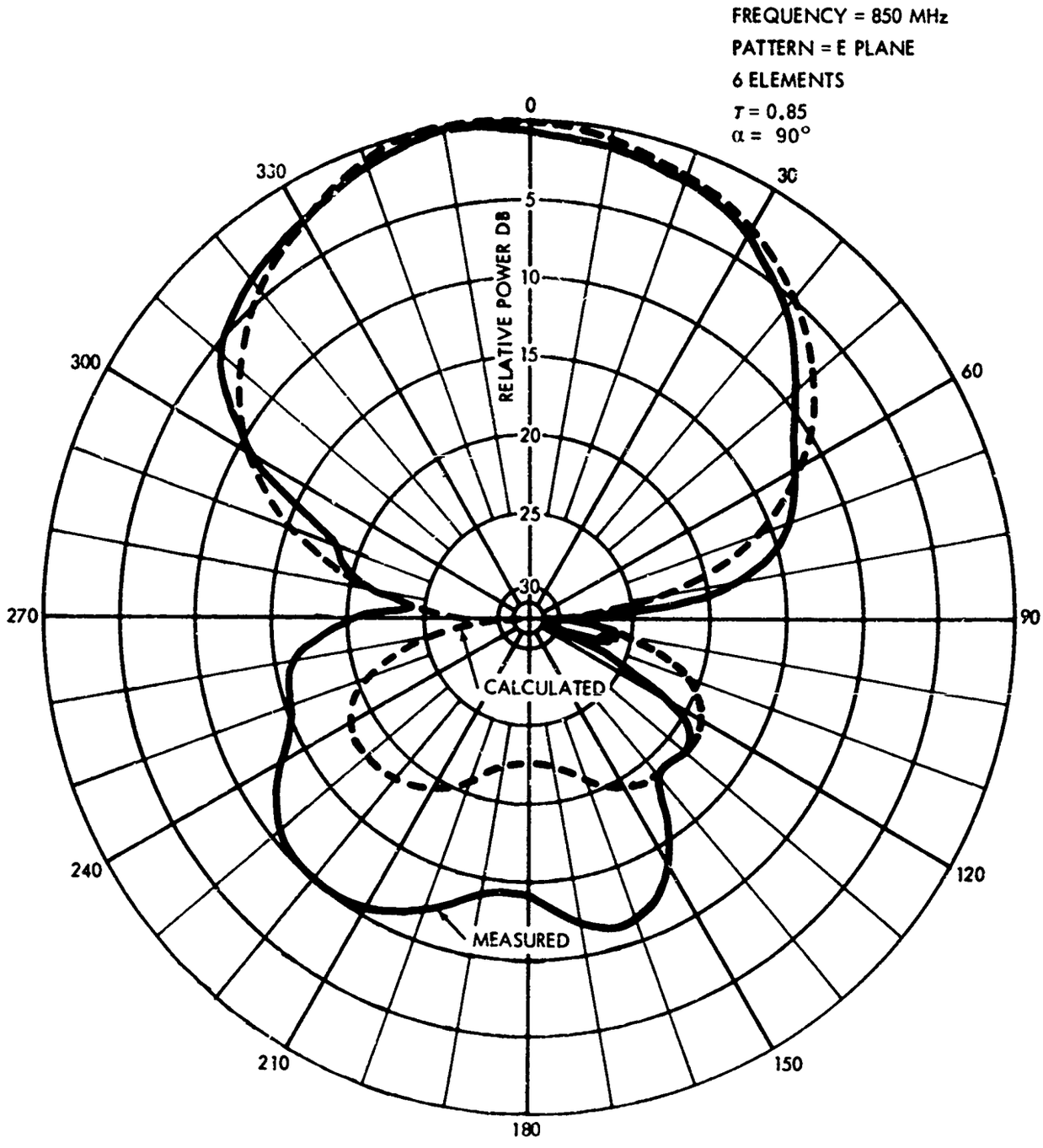

Figure III-12. Log Periodic E-Plane Pattern - 850 MHz

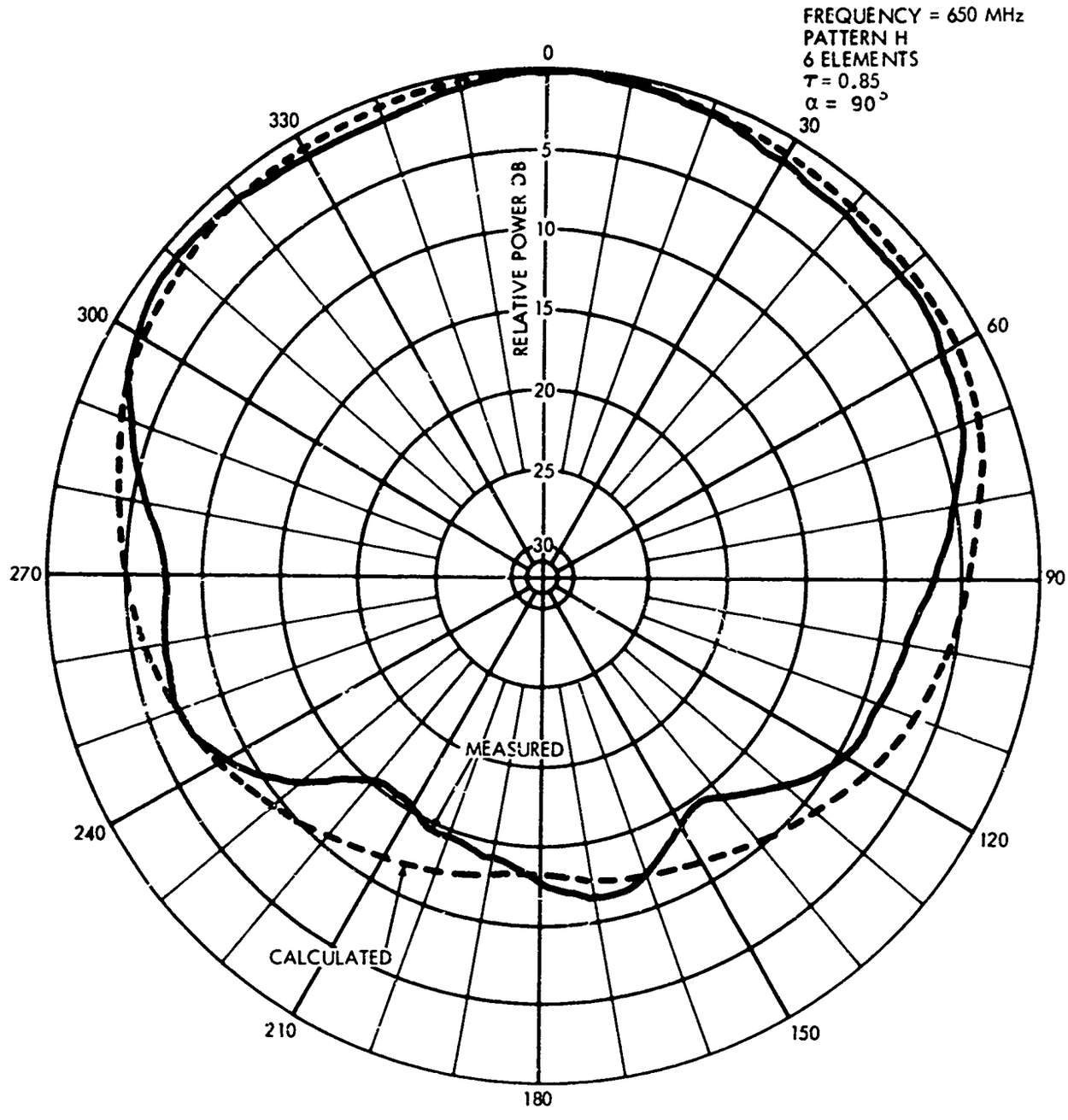

Figure III-13. Log Periodic H-Plane Pattern - 650 MHz

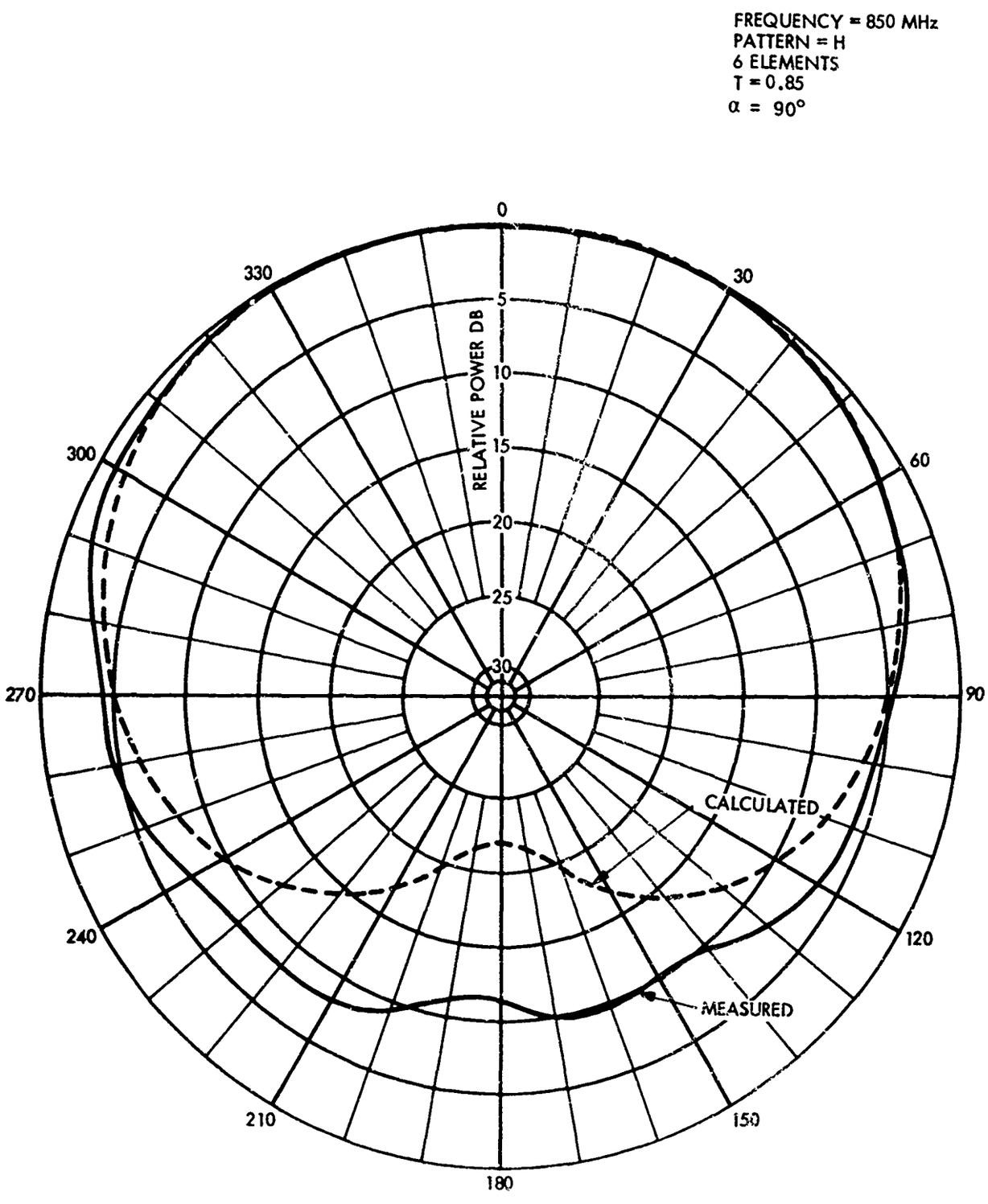

Figure III-14. Log Periodic H-Plane Pattern - 850 MHz

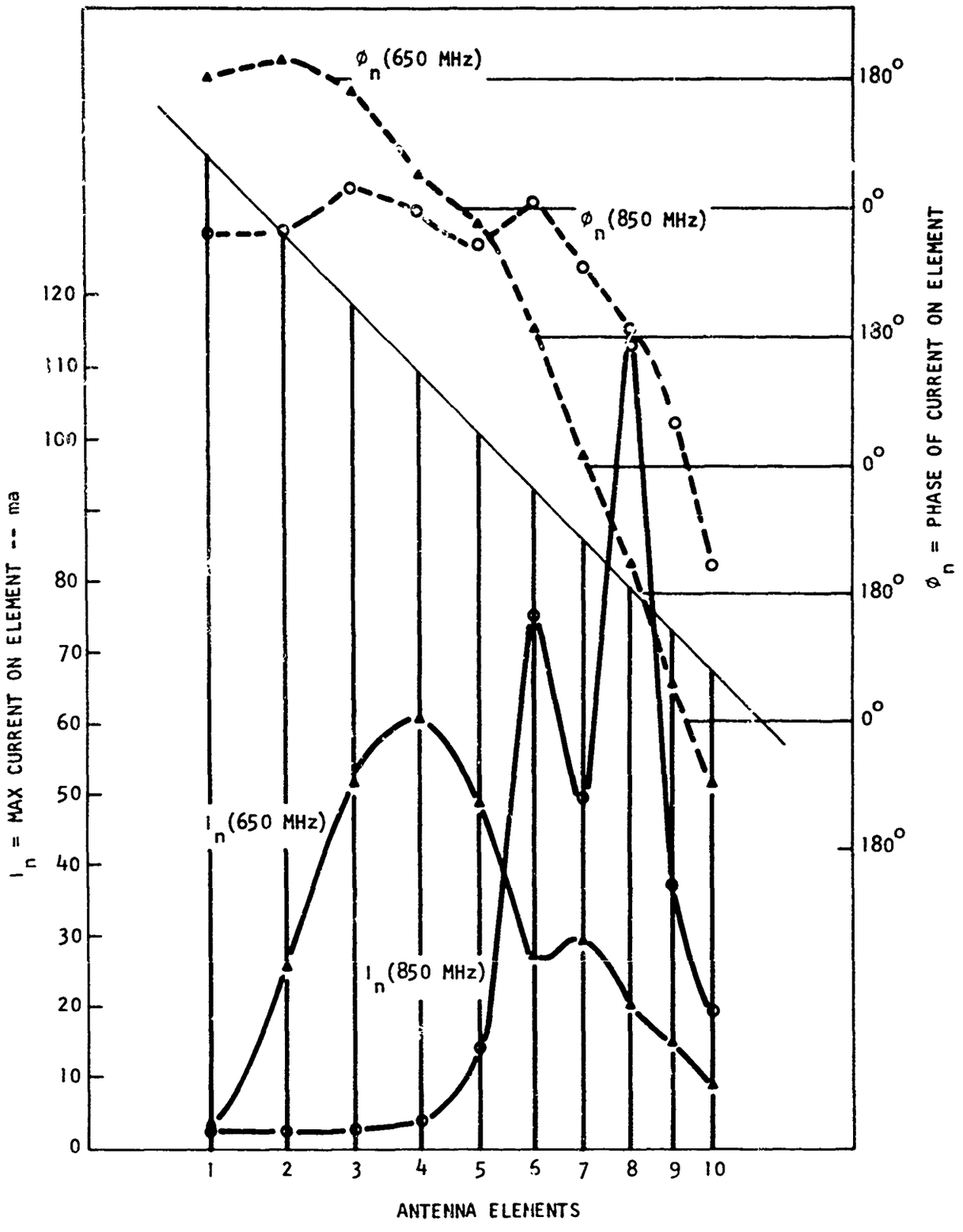

Figure III-15. Current Amplitude and Phase Distribution 10-element Log Periodic. $\tau = 0.922$, $\alpha = 90°$.

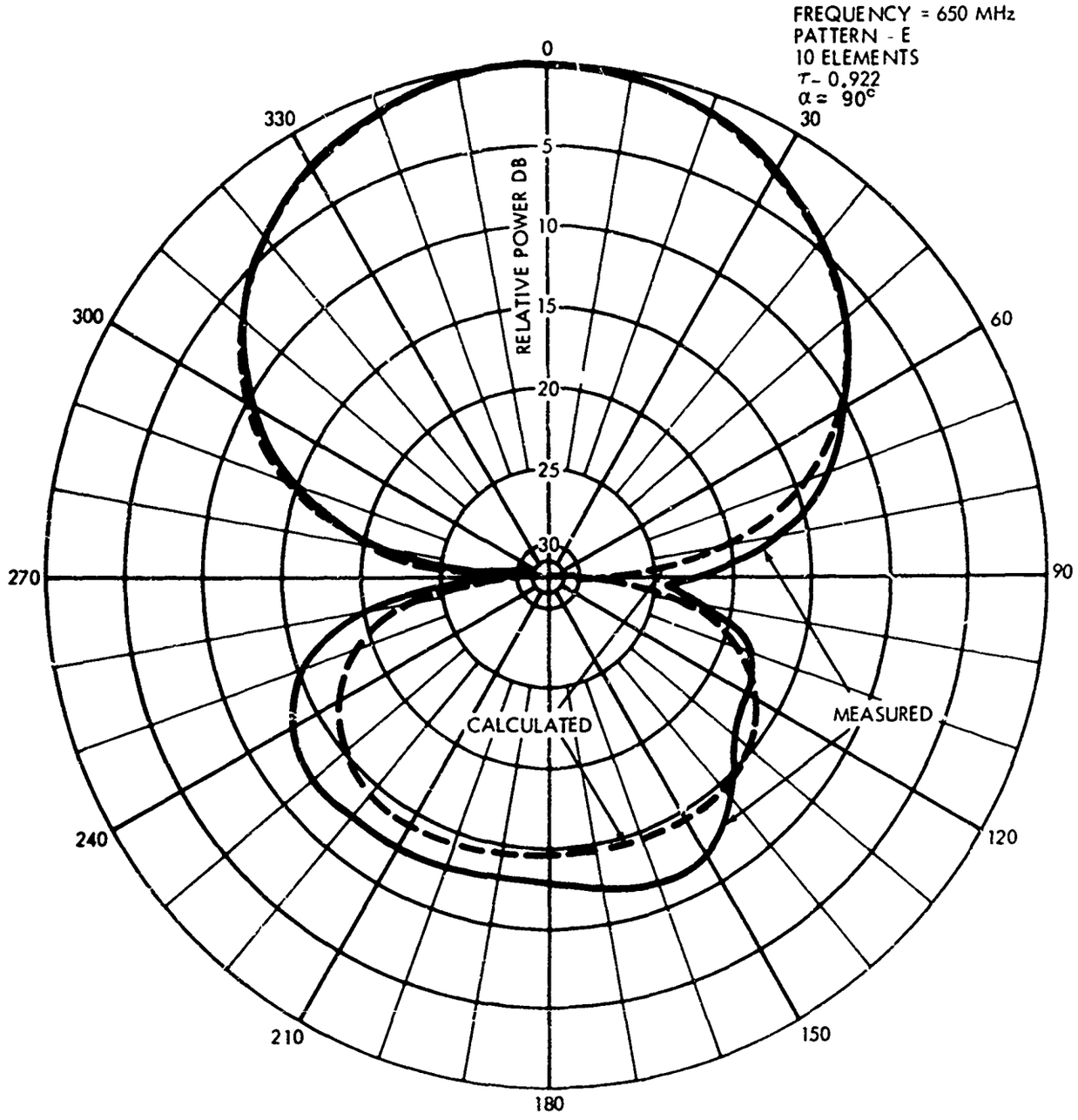

Figure III-16. Log Periodic E-Plane Pattern - 650 MHz

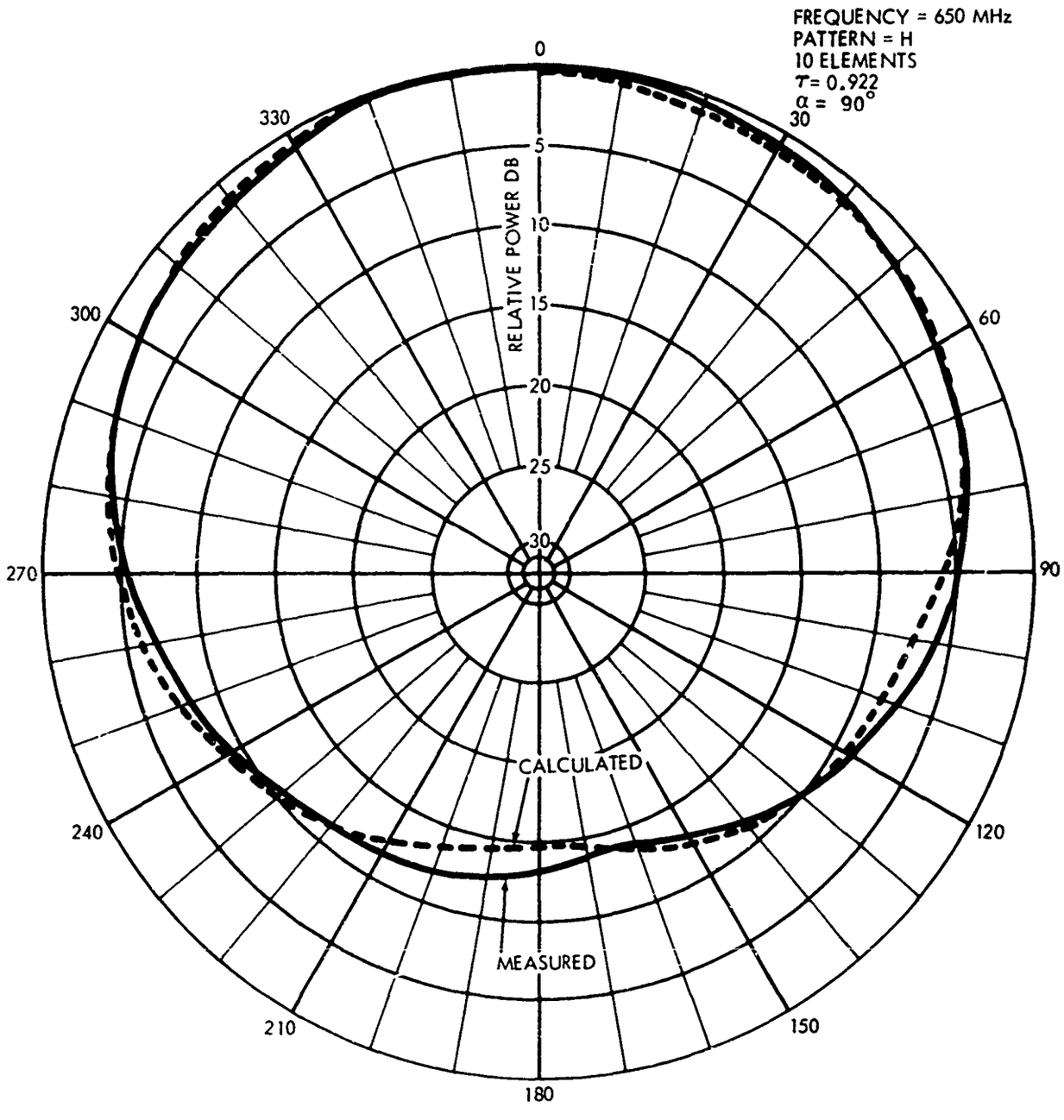

Figure III-17. Log Periodic H-Plane Pattern - 650 MHz

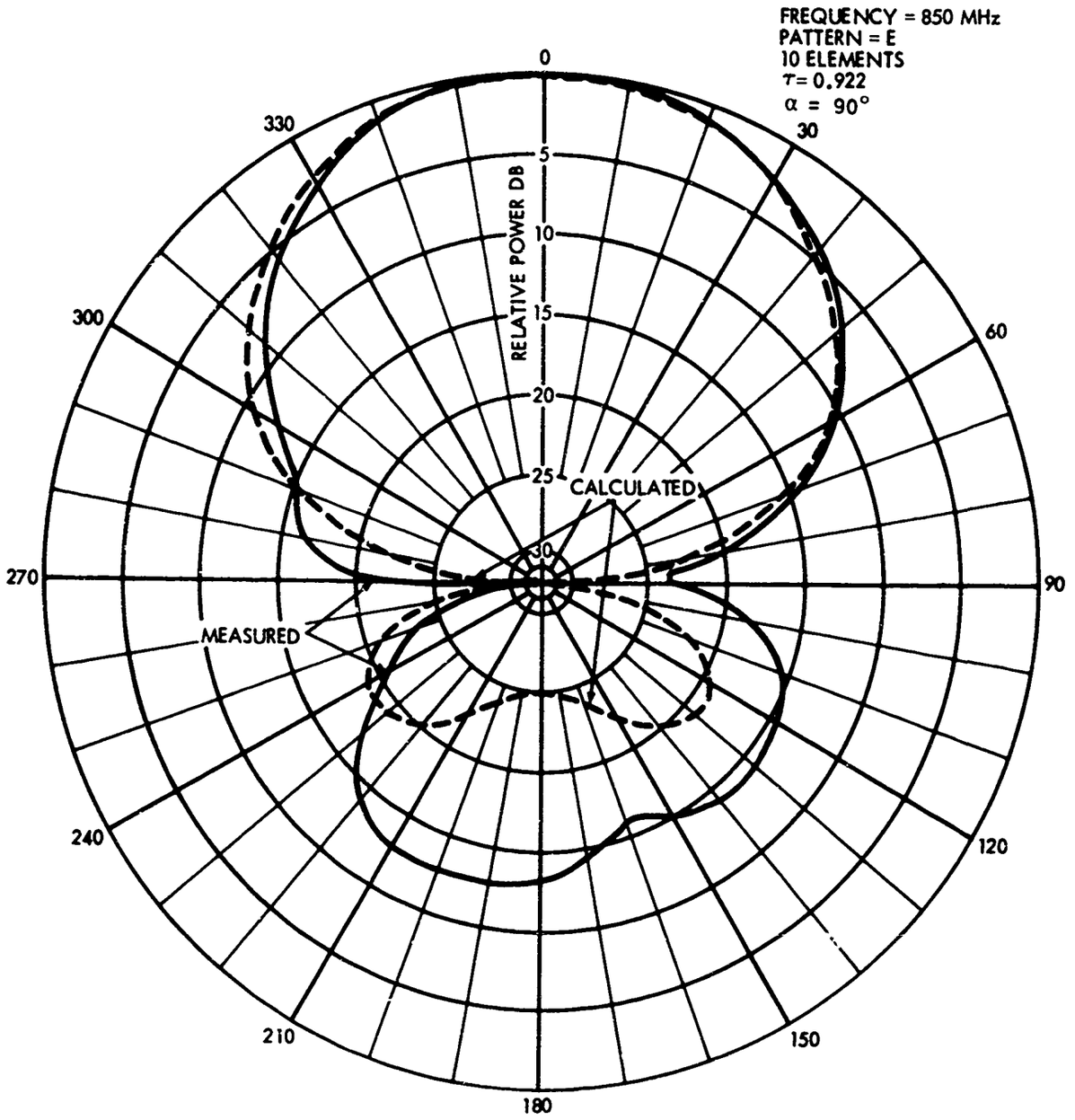

Figure III-18. Log Periodic E-Plane Pattern - 850 MHz

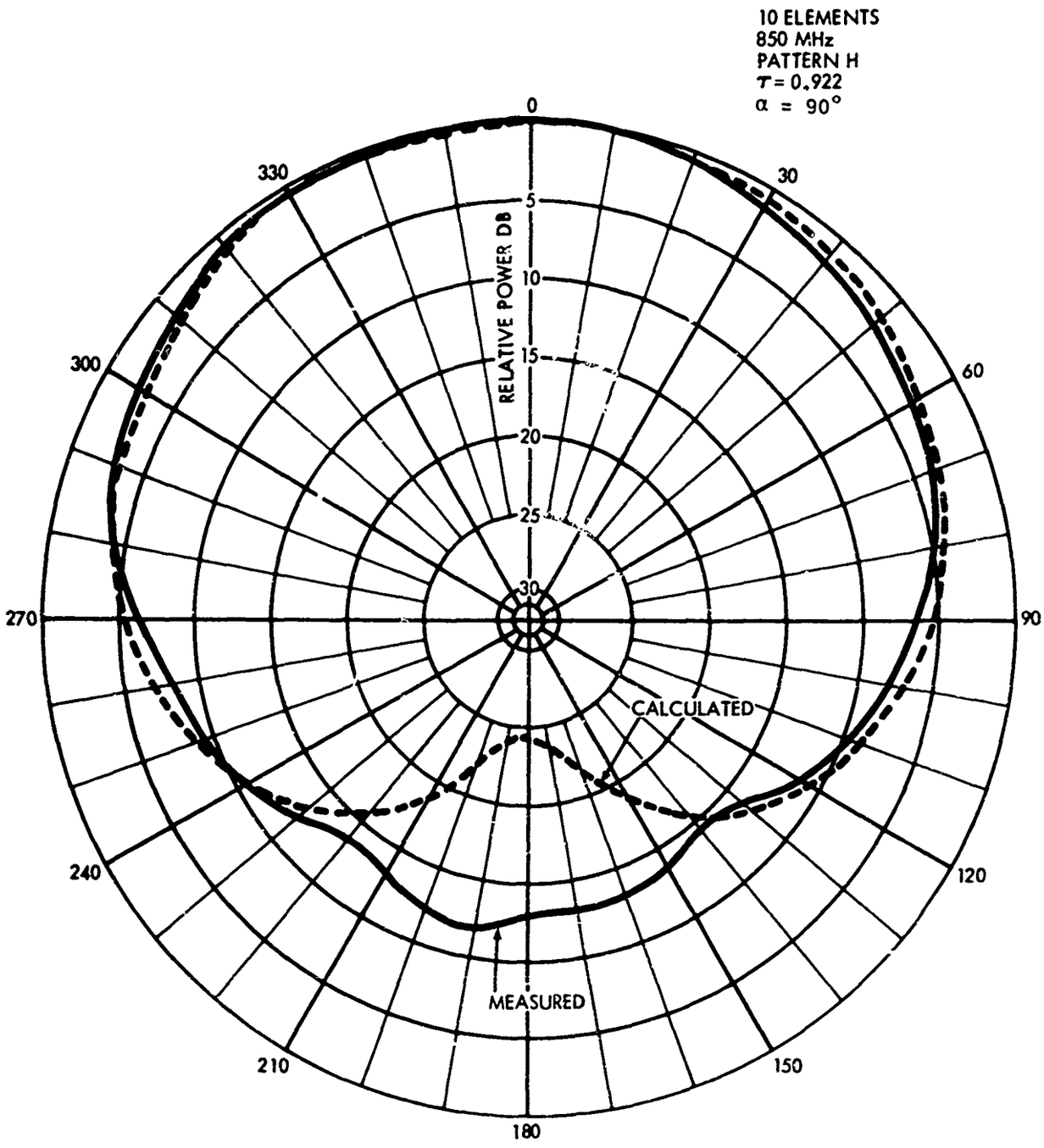

Figure III-19. Log Periodic H-Plane Pattern - 850 MHz

D. --Continued.

The patterns shown in Figures III-6-9, 11-14, and 16-19 are probably the most conclusive proof available to show that the theory and computer program are valid when applied to a log-periodic antenna. The discrepancies between calculated and measured data that show up in the back lobes of the patterns are due to environmental conditions at the test site and to the lack of perfection in model building techniques. One argument that indicates that the physical model is at fault instead of the mathematical model, is the fact that the measured data is not symmetrical where the differences in the two sets of data occur. For future work, higher quality models will be used and tested in a controlled environment.

Figures III-20 and III-21 show the current distribution and far-field patterns of a log periodic dipole array when the α angle is 45 degrees. Antennas with angles this high are sometimes used in broadside or billboard arrays. Since the computer outputs are symmetrical about the 0-90 degree line, only half of the E- and H-plane patterns are included in Figure III-21 and many of the succeeding patterns.

Figures III-22 through III-24 show the current distribution and far field patterns of a 10-element array designed for maximum gain using the techniques developed by R. L. Carrel. The maximum gain was found to be 10.7 dbi while Carrel's method predicted a gain to 11 dbi.

Figures III-25a through c show that the computer program that has been developed will predict the existence of the so-called 3/2 moding. Three-halves moding occurs when only part of the available energy is radiated in the active region around the half wave element with the remainder being radiated in the region of the three-halves wave element. The effect shown probably would have been more pronounced if the operating frequency had been a little higher.

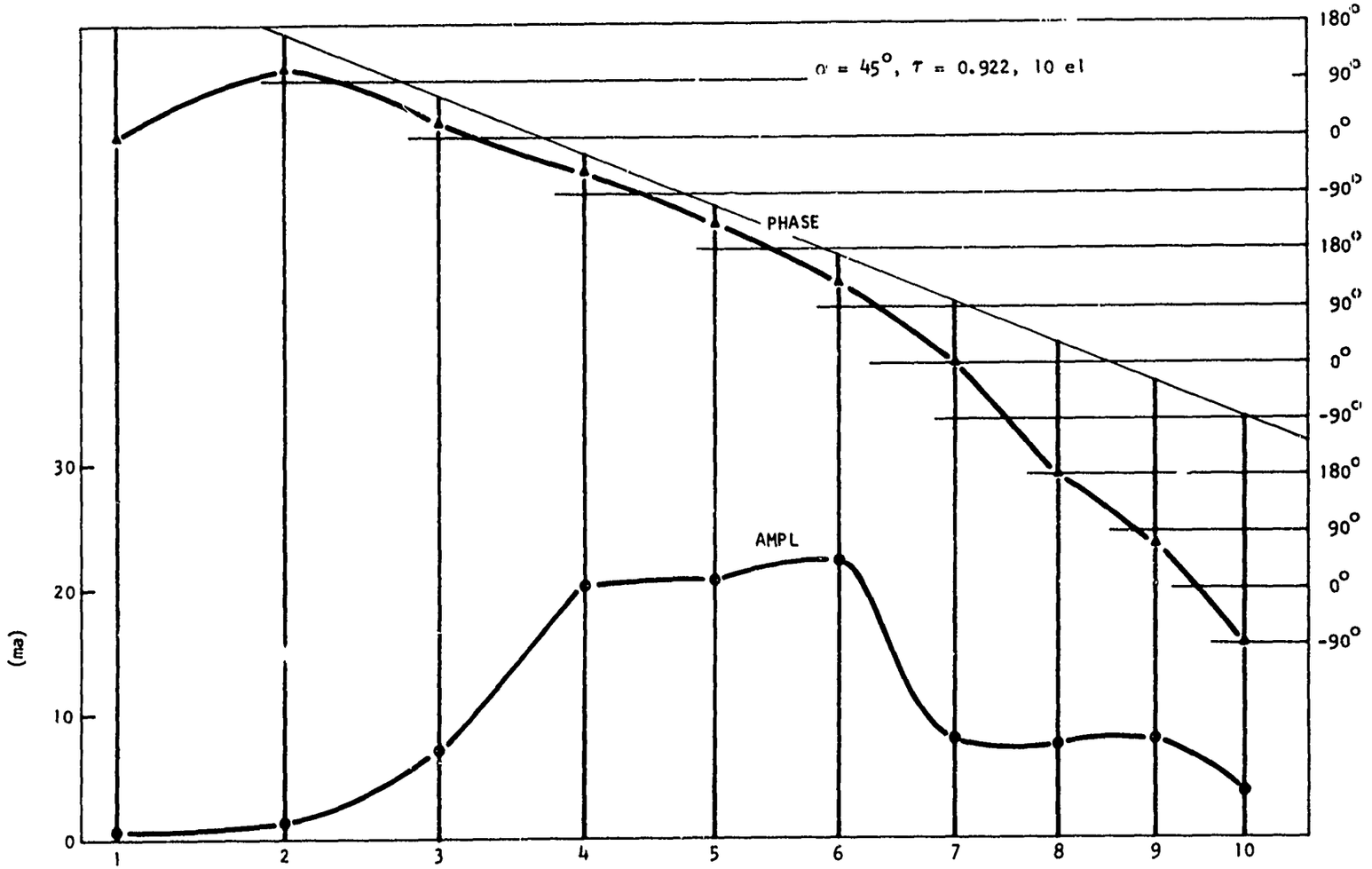

Figure III-20. Log-Periodic Current and Phase Distribution

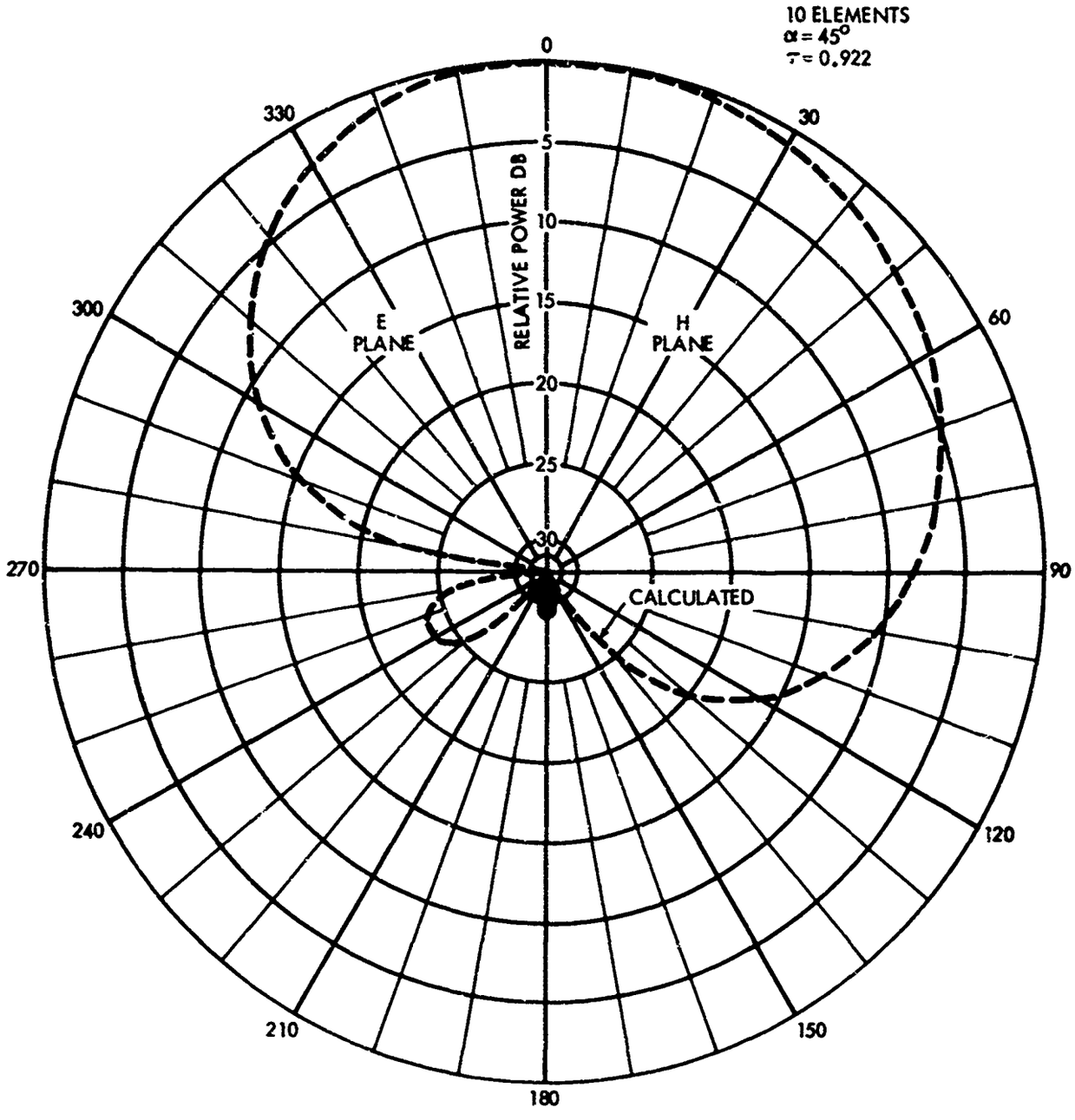

Figure III-21. Log-Periodic Azimuth and Elevation Pattern

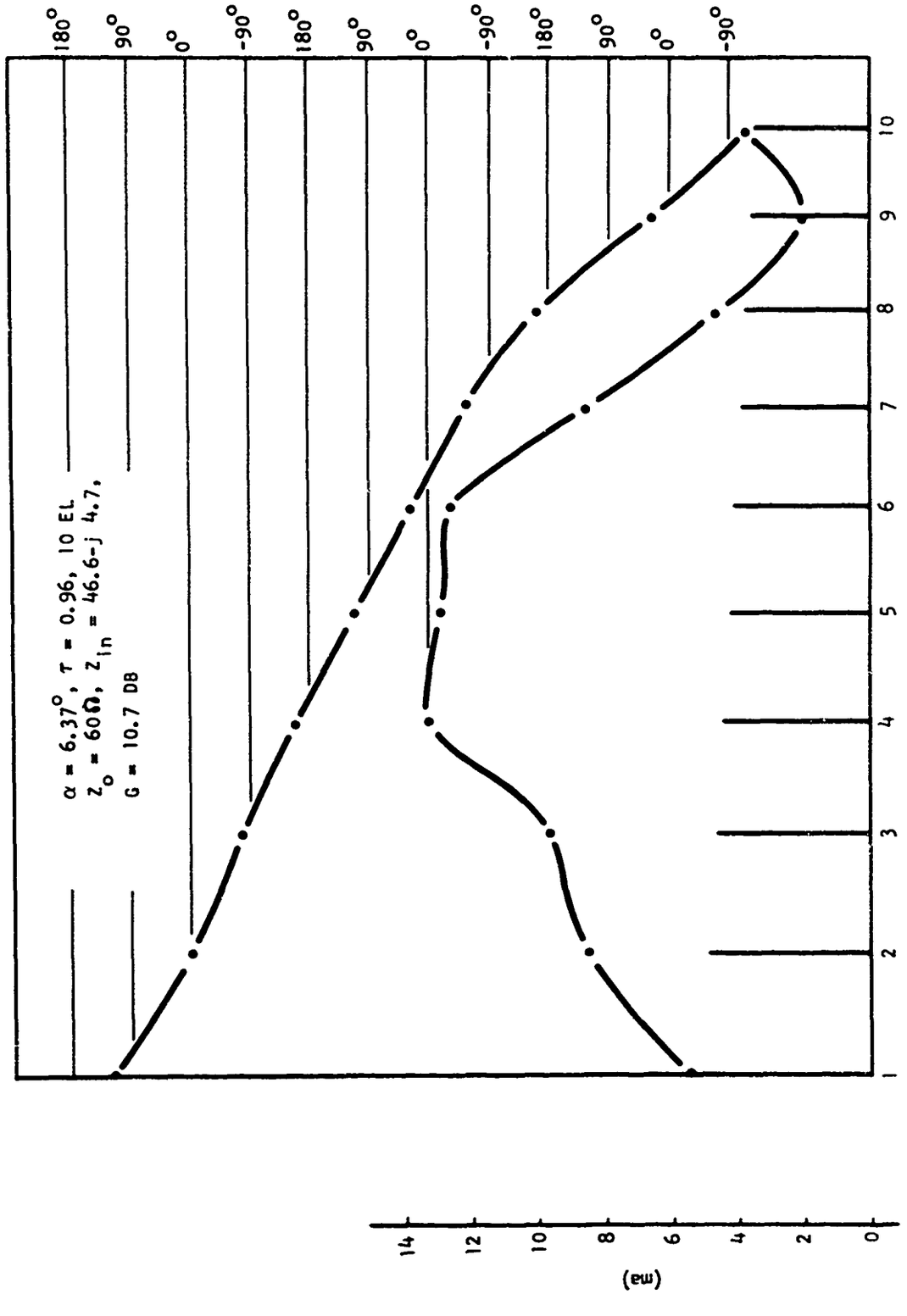

Figure III-22. Current Amplitude and Phase Distribution High Gain Log Periodic

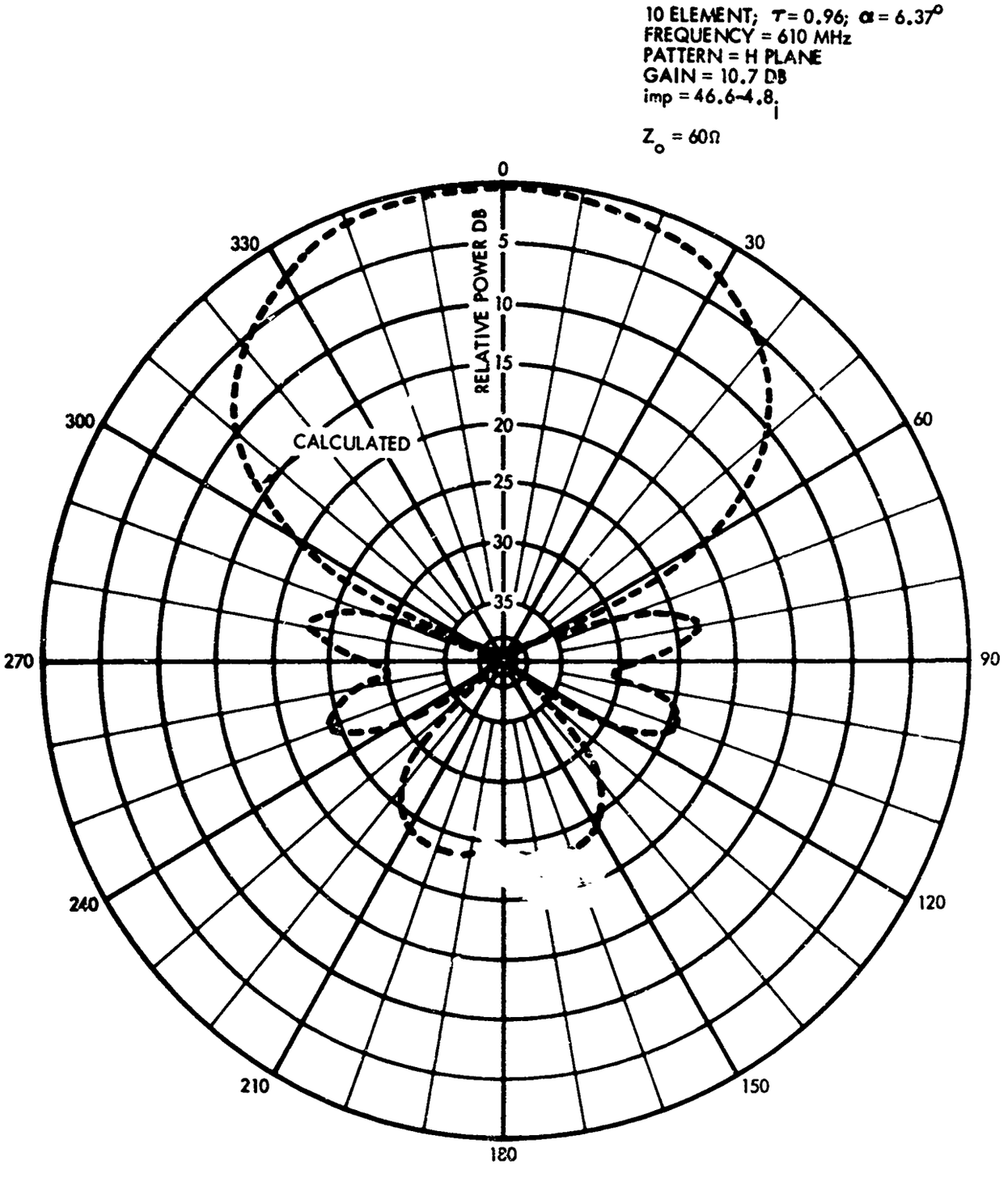

Figure III-23. Log Periodic H-Plane Pattern

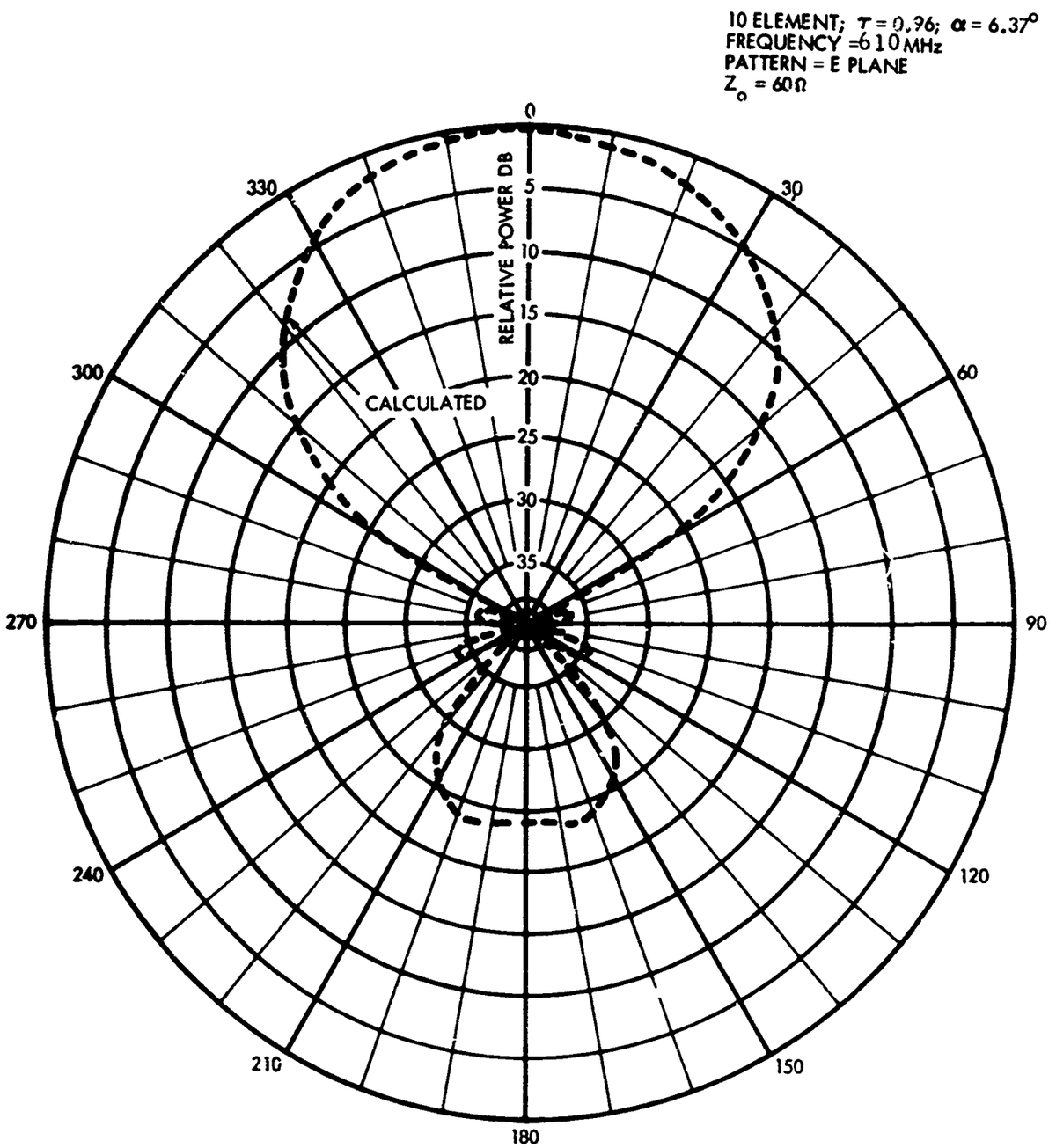

Figure III-24. Log Periodic E-Plane Pattern

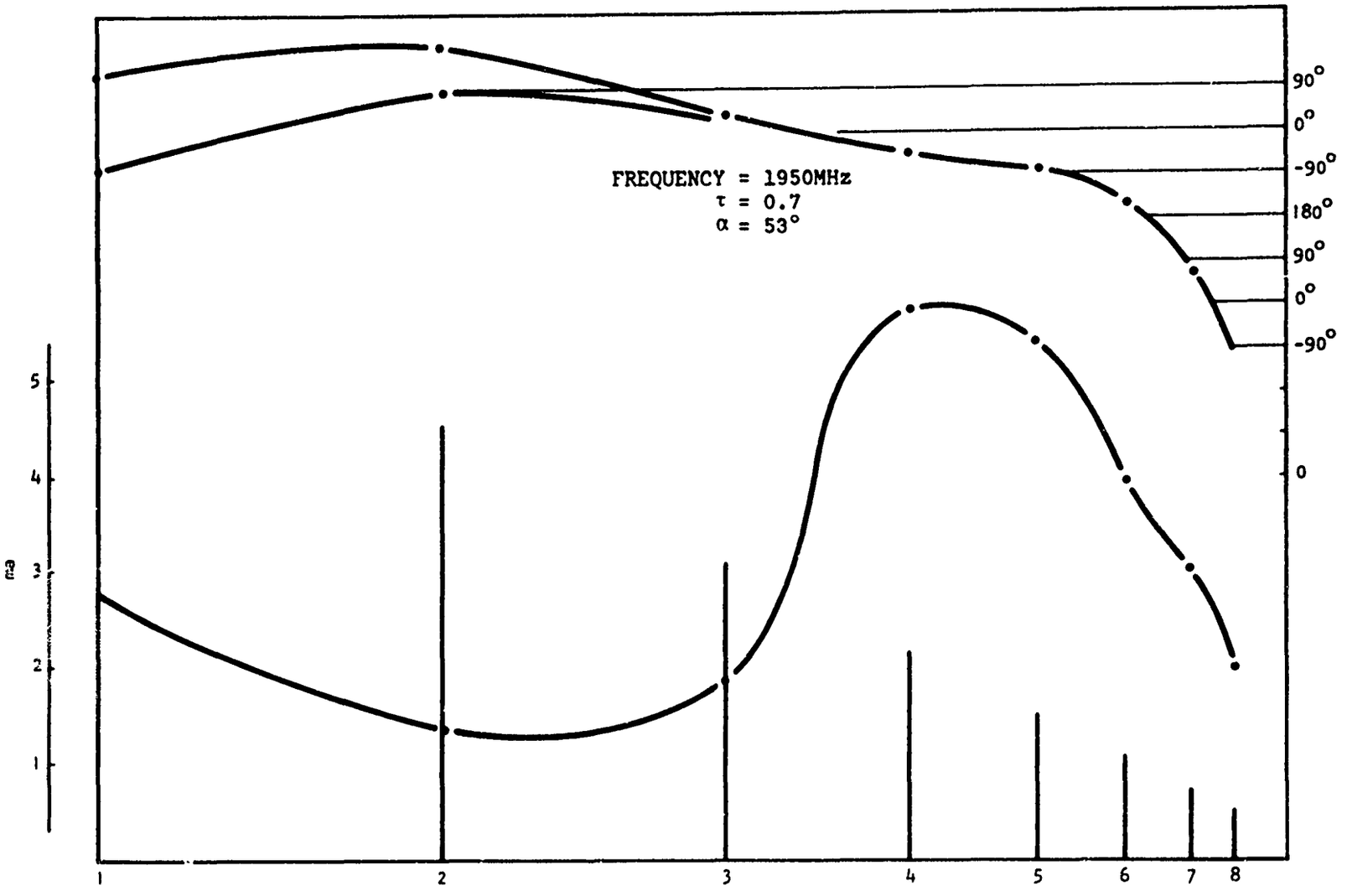

Figure III-25 a Current Amplitude and Phase Distribution Log Periodic with $3\lambda/2$ Moding

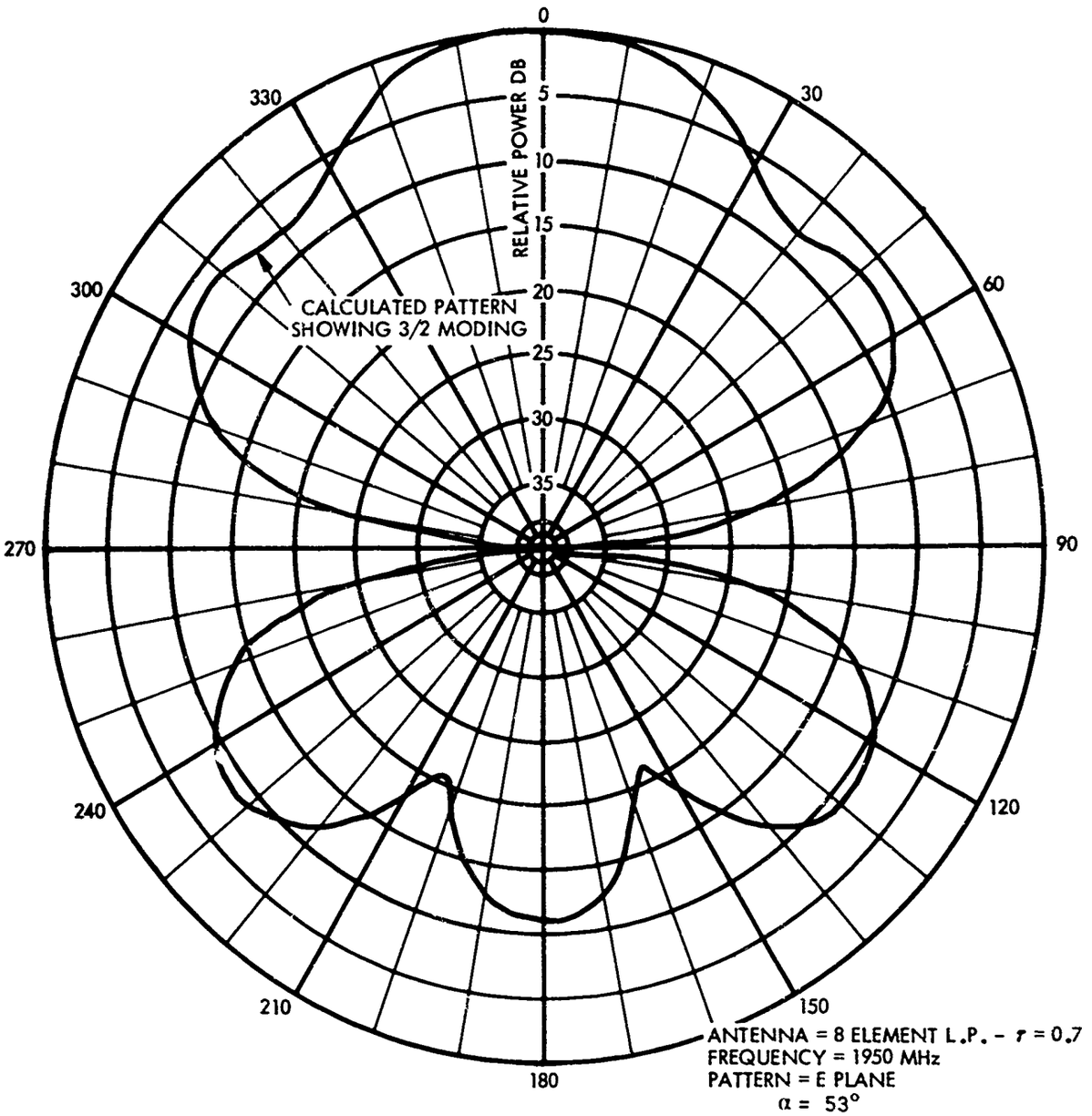

Figure III-25b. Log Periodic E-Plane Pattern

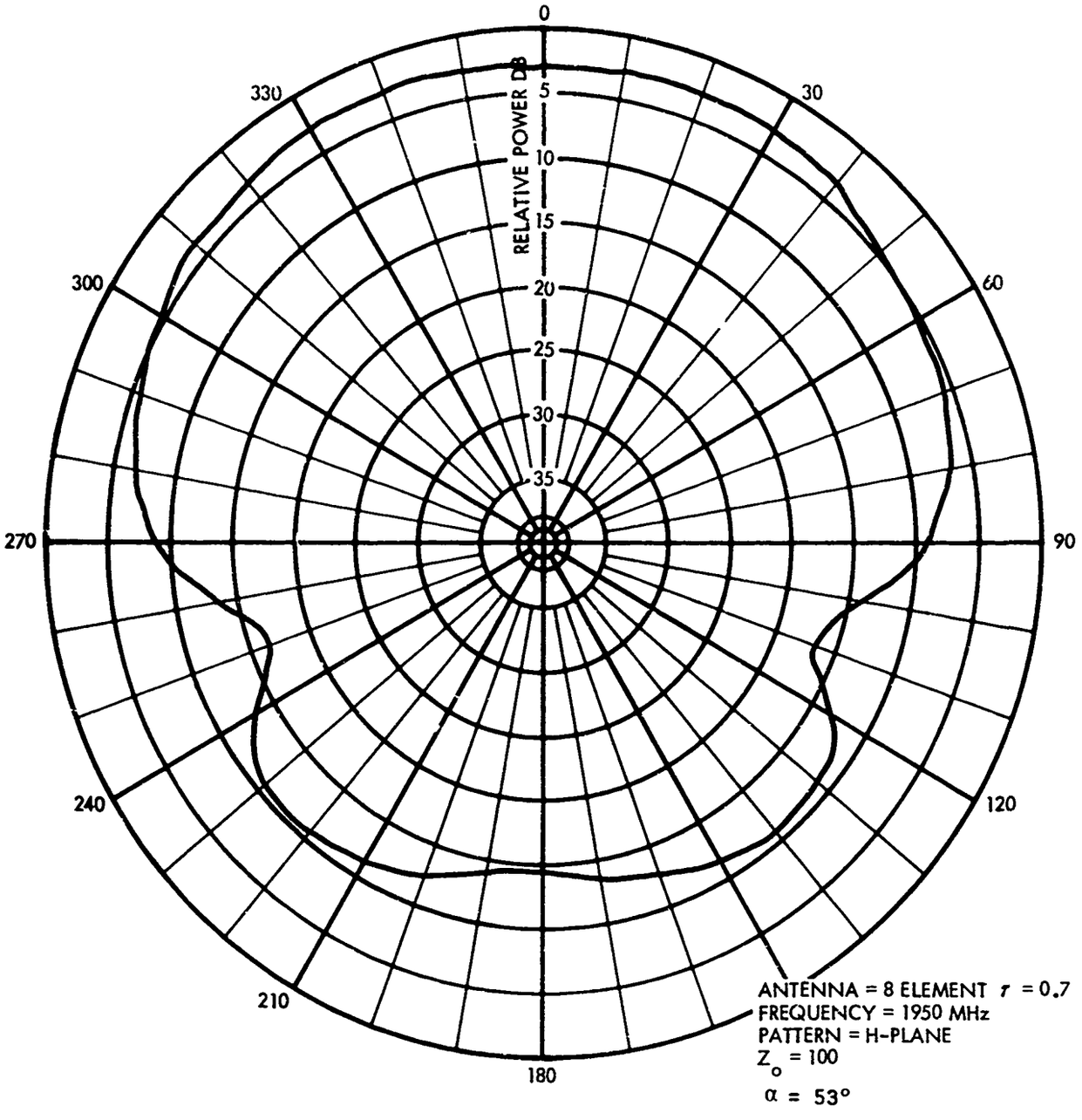

Figure III-25c. Log Periodic H-Plane Pattern

E. LOG-PERIODIC ARRAYS

As a final step in the computer solution of log-periodic antennas an array of LP's was analyzed. The arrays were of two types -- the DuHamel array where all log periodic antennas making up the array are identical and the Mei array where all elements of equal length lie in a straight line, thereby making it necessary for each LP in the array to be of a different design (See Figure III-26). The DuHamel array has a circular phase front whereas the Mei array has a flat phase front. Of the computer runs made, the DuHamel array was the most often used while the Mei array was used only occasionally as a check against the DuHamel designs.

Two basic LP designs were used as elements in forming the LP arrays. These were a high gain LP (10 dipoles, $\alpha = 6.37^{\circ}$, $\tau = 0.96$) and a medium gain LP (9 dipoles, $\alpha = 44.34^{\circ}$, $\tau = 0.78$). Both medium and high gain antennas were designed to operate in the upper UHF region (length of longest dipole =0.25 meters) so models could be constructed and tested easily if a comparison between computer and empirical data was desired. This choice in design frequencies is not a restriction for antennas operating in free space, however, since the computer program in this mode works only with relative and not absolute values, i.e., a half wavelength antenna looks electrically the same at all frequencies. The only case where actual frequencies must be analyzed in the computer program is that in which the antenna is to be placed over real earth which is frequency sensitive in the absolute sense. For the sake of convenience, all patterns for the medium and high gain antenna arrays in the remainder of the report were run at frequencies of 1100 MHz and 665 MHz, respectively. See Figures III-27 and III-28 for single LP patterns at these frequencies.

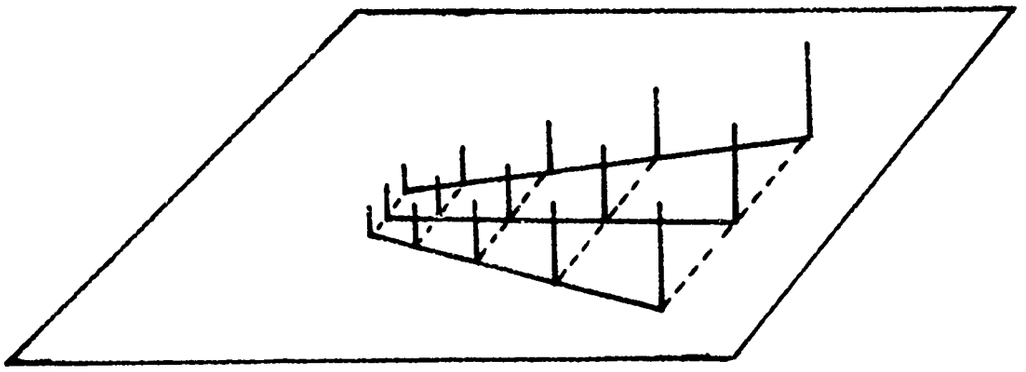

Mei Array

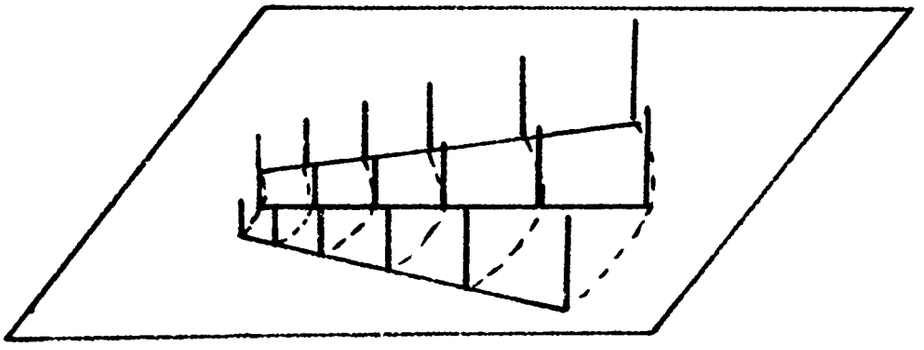

DuHamel Array

Figure III-26 Mei and DuHamel Arrays

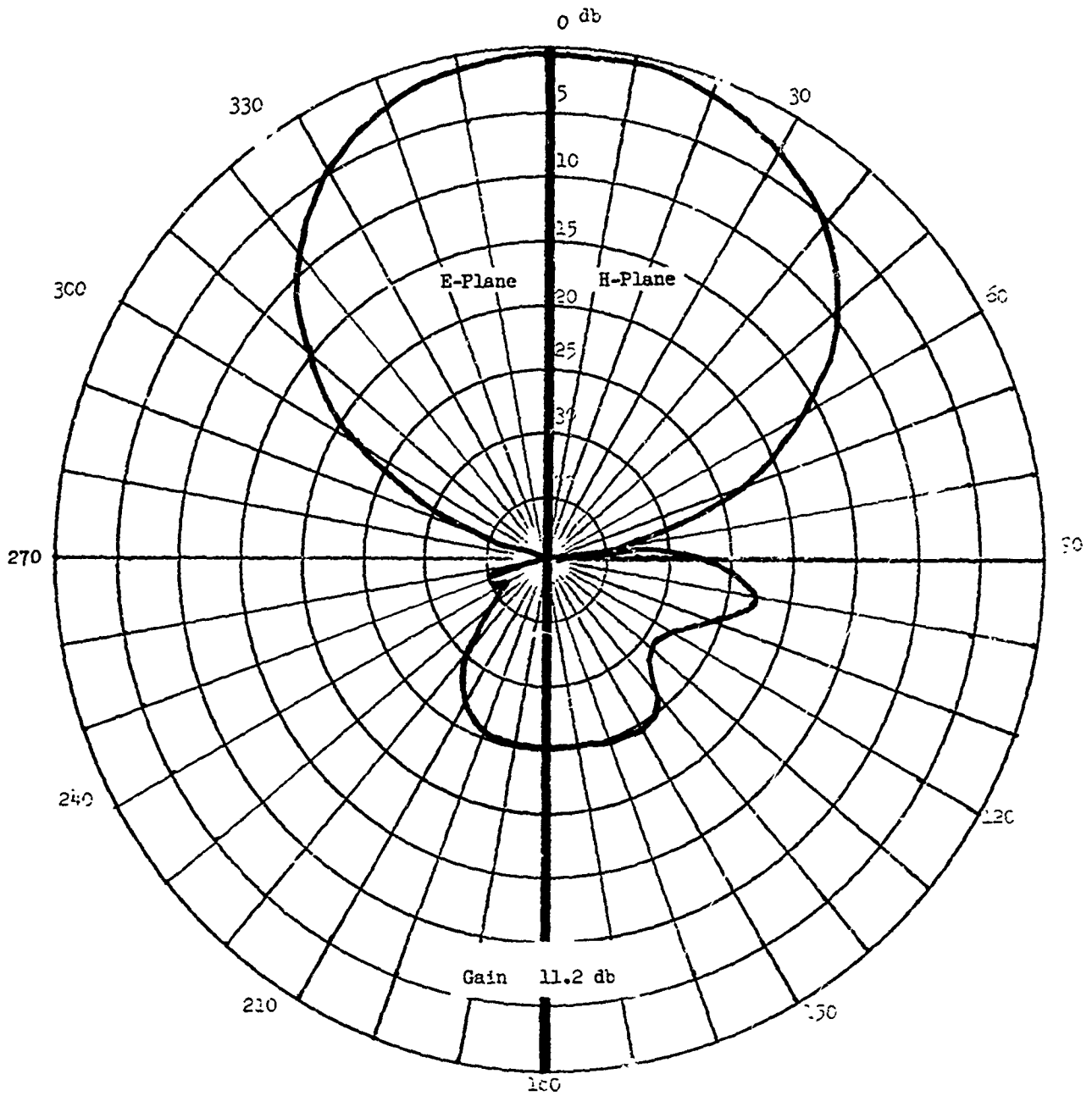

Figure III-27. Single High Gain LP.

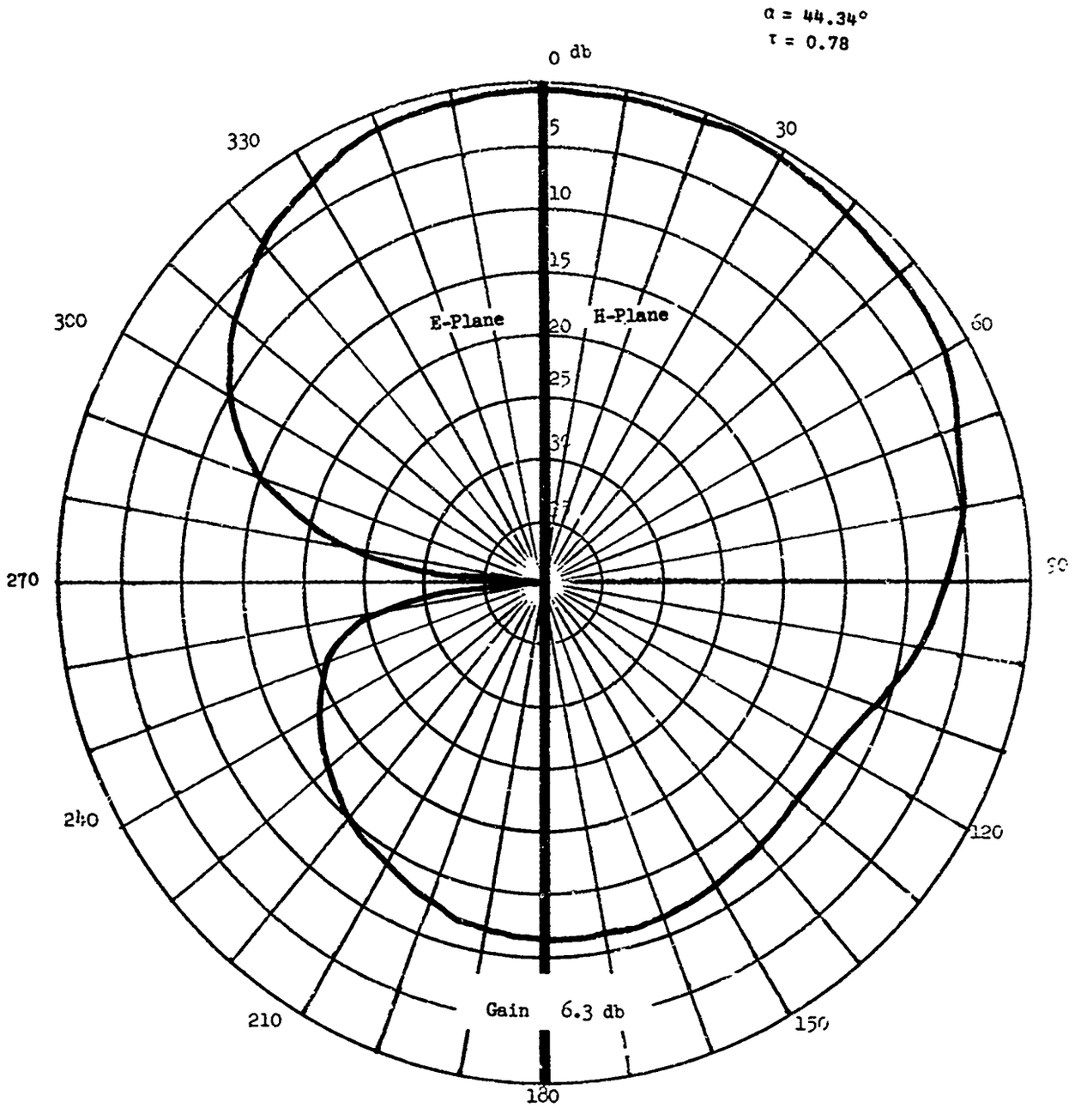

Figure III-28 Single Medium Gain LP

E. --Continued

In switching from single LP antennas to LP arrays the interests in electrical characteristics changes also. Previously, current distributions were of prime concern, but now the gain and pattern coverage that can be achieved with different antenna designs is of interest. The major factors affecting the gain and pattern coverage of an array are the individual LP designs, of which we have chosen two as being representative, the manner in which the LP's are arrayed and the number of LP's in the array. The particular array, DuHamel or Mei, once chosen, leaves only the spacing between LP's and the number of LP's in the array as the variables to be optimized.

The process used to find an optimum set of array variables was one of choosing the spacing to be used between LP's and then to make computer runs with varying numbers of LP's in the array. Figure III-29 shows a graph of maximum gain versus the number of LP's in the array for various DuHamel spacings. The term LP spacing as used here means the distance in wavelengths between the half wave dipoles of neighboring LP's in the array. The data for this graph was obtained from computer runs for high gain LP's in an array. It is interesting to note that the array gain does not necessarily increase with an increase in the number of LP's in the array, but often decreases. If one visualizes the geometry of an LP array he sees that each additional element placed in the array must be positioned at an ever increasing angle from the direction of radiation for the array. The radiation from these off-axis LP's contributes significantly to the side lobe level thereby decreasing the amount of gain that could be realized with the additional element. This increase in sidelobe

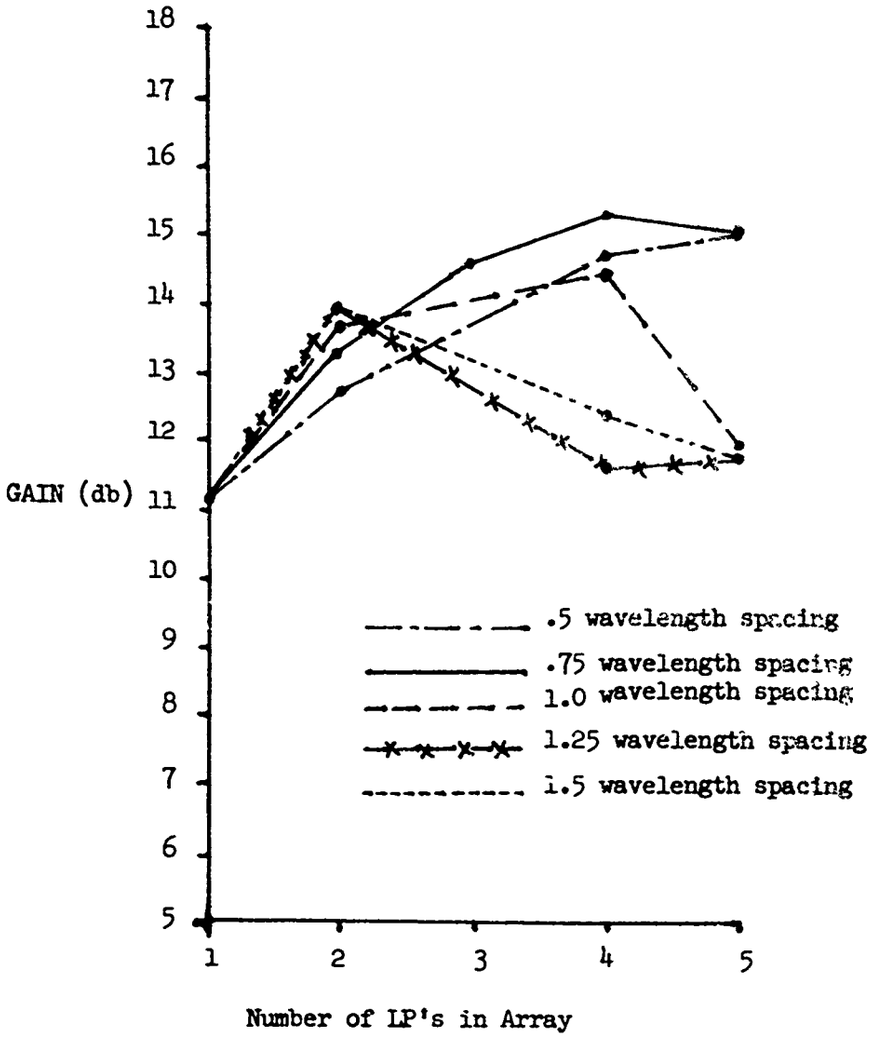

Figure III-29 High Gain LP's in a DuHamel Array

E. --Continued

level coupled with that due to arraying when some of the LP elements in the array are separated by more than a wavelength can cause an overall decrease in array gain, especially when the LP to LP spacing in the array becomes large.

Figure III-30 is a graph, similar to that of Figure III-29, for medium gain LP's in an array. This graph shows trends identical to those of the previous graph with the only difference being an overall lower gain for the medium gain LP arrays.

The two graphs just mentioned do not tell the complete story of arraying trends; however, a closer look at some radiation patterns indicates that a particular array may have more gain than another, but its radiation coverage could be completely unacceptable. For example, Figure III-29 shows that a DuHamel array with four LP's spaced 1.5 wavelengths apart has a higher maximum gain than a similar array with elements spaced 1.25 wavelengths apart, but a glance at the radiation patterns shows that the peak of the beam (actually two peaks -- one on either side of boresight) occurs about 6 degrees off boresight for the higher gain array (Figures III-31a, b). See Part IV - Appendix for a complete set of E-and H-plane radiation patterns and gains of all designs run on the computer. Even though the 1.5 wavelength spaced array has higher maximum gain, the 1.25 wavelength spaced array has a higher boresight gain.

In all previous examples the arrays analyzed have been of the DuHamel or circular phase front type. The Mei array, however, offers an alternate design approach which seems to be somewhat superior to the DuHamel

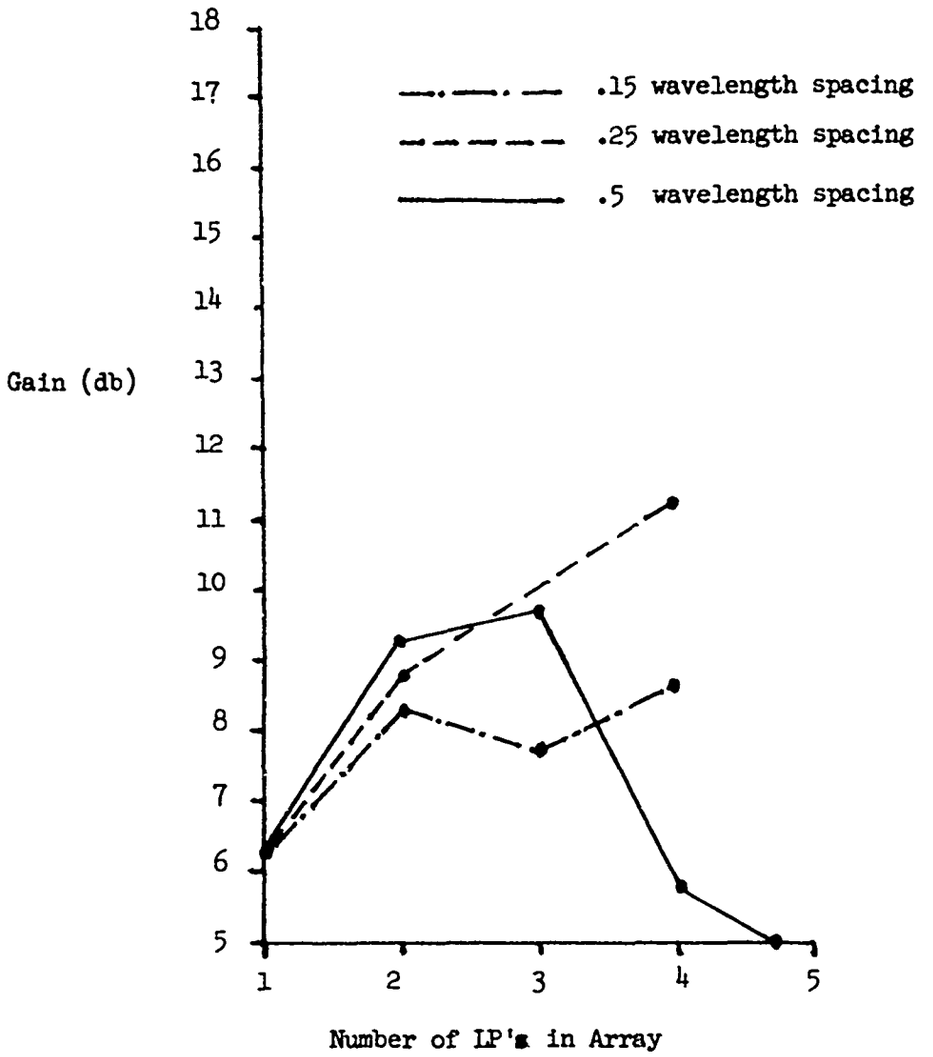

Figure III-30 Medium Gain LP's in a DuHamel Array

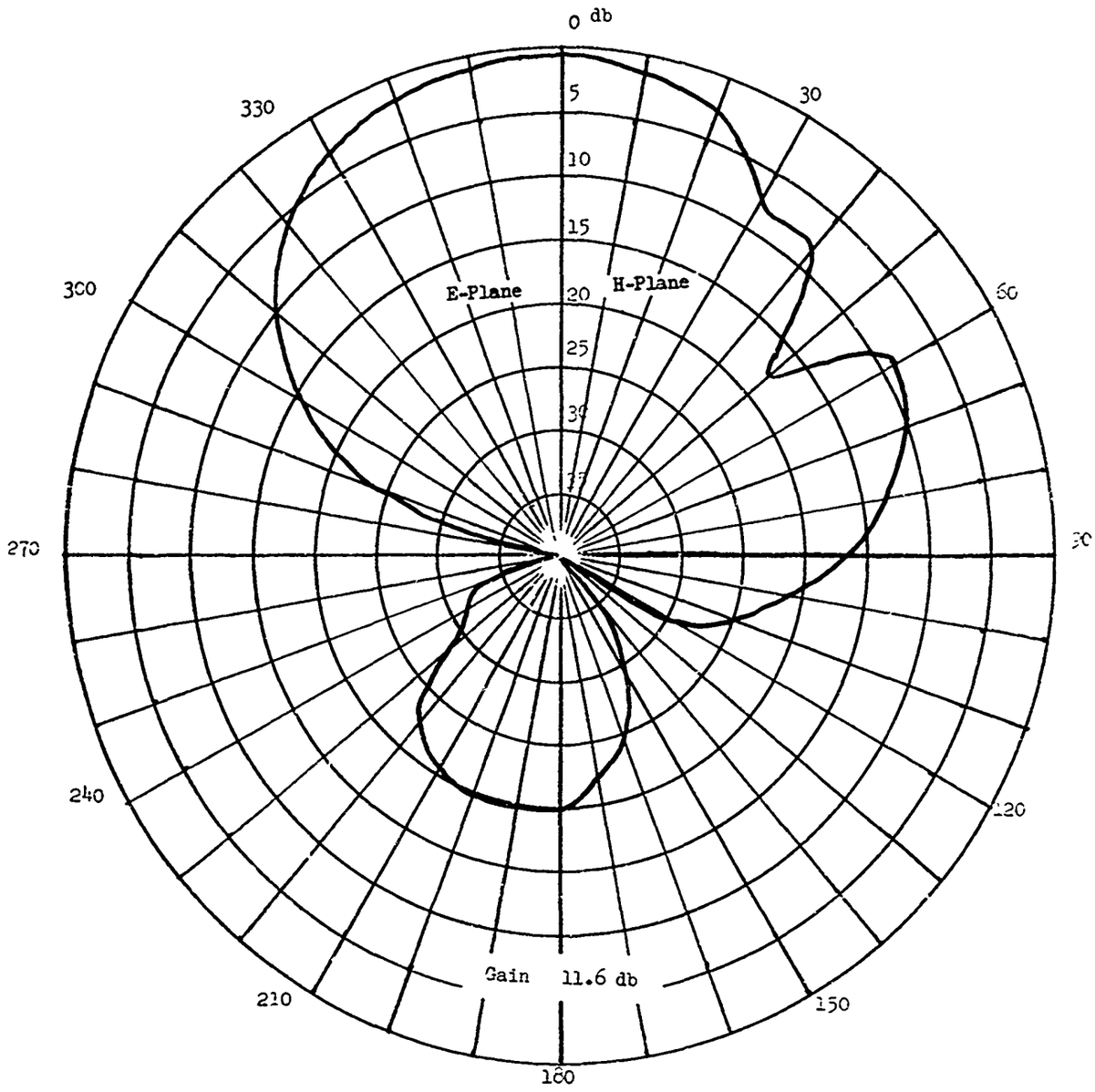

Figure III-31a Four Element DuHamel Array with 1.25 Wavelength Spacing

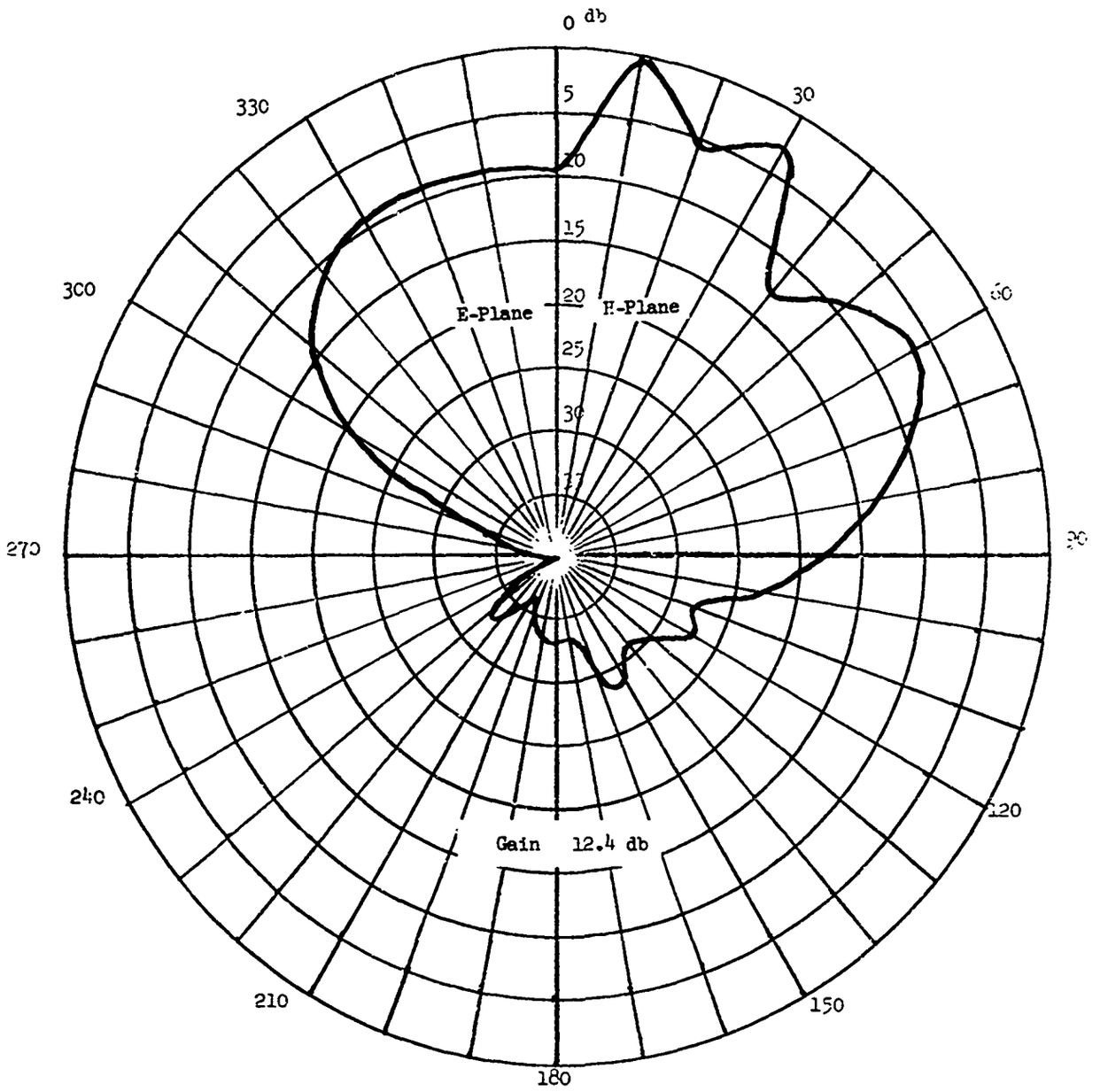

Figure III-31b Four Element DuHamel Array with 1.5 Wavelength Spacing

E. --Continued

array. Figure III-32 is a bar graph showing a comparison of the two arrays for different designs and as can be seen the Mei array is significantly higher in gain for all designs. The designs used for this comparison were not preselected, but were chosen simply because they happened to be the only designs for which both array types were run on the computer. The comparison is by no means exhaustive in the number of different designs used, but the results are so decidedly one way that the Mei array could safely be called the superior array type at least in terms of array gain. One also notes that the gain of the Mei array does not decrease in going from four to five element arrays unlike that of the DuHamel designs. There is nothing to indicate that this trend won't reverse with the addition of the sixth element, but at least up to five elements the gain of the Mei array increases with additional elements. See Figure III-33 for the radiation pattern of a 5 element Mei array-the highest gain array run.

Before concluding this section on the comparison of array types we note that the one comparison involving medium gain LP's shows the Mei array with higher gain than the DuHamel array, but with the radiation in the opposite direction. Even though the Mei array gain is higher, the fact that it radiates in the backward direction seems to indicate an unstable design. Unfortunately there are no other computer runs on medium gain LP Mei arrays available to indicate whether or not this instability is a property of the array type.

In our final step in the analysis of LP arrays we have placed the arrays over real earth. Due to an oversight on the part of the author, the computer runs were made at UHF instead of HF and, because of a shortage

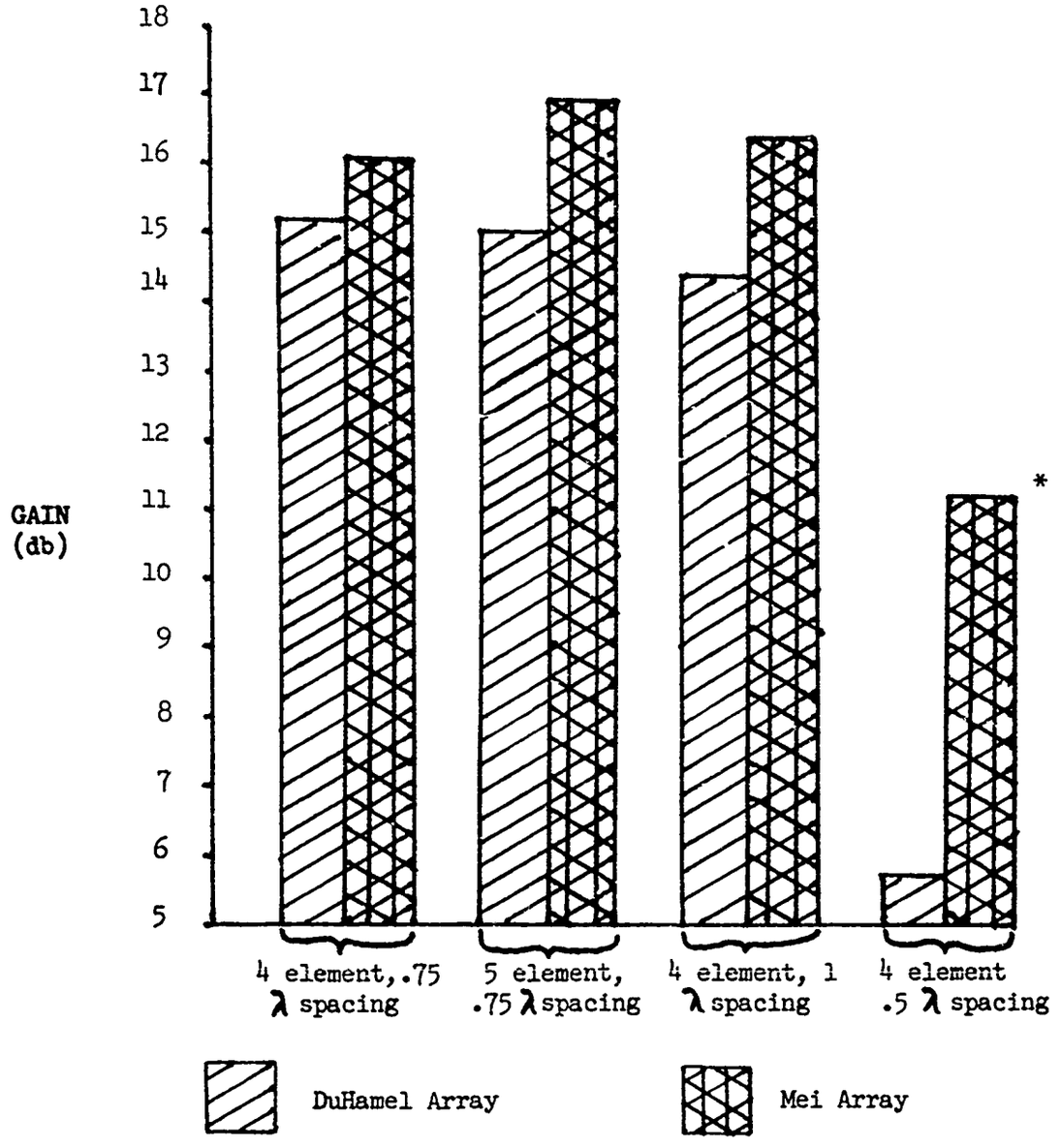

Figure III-32 Comparison of DuHamel and Mei Arrays

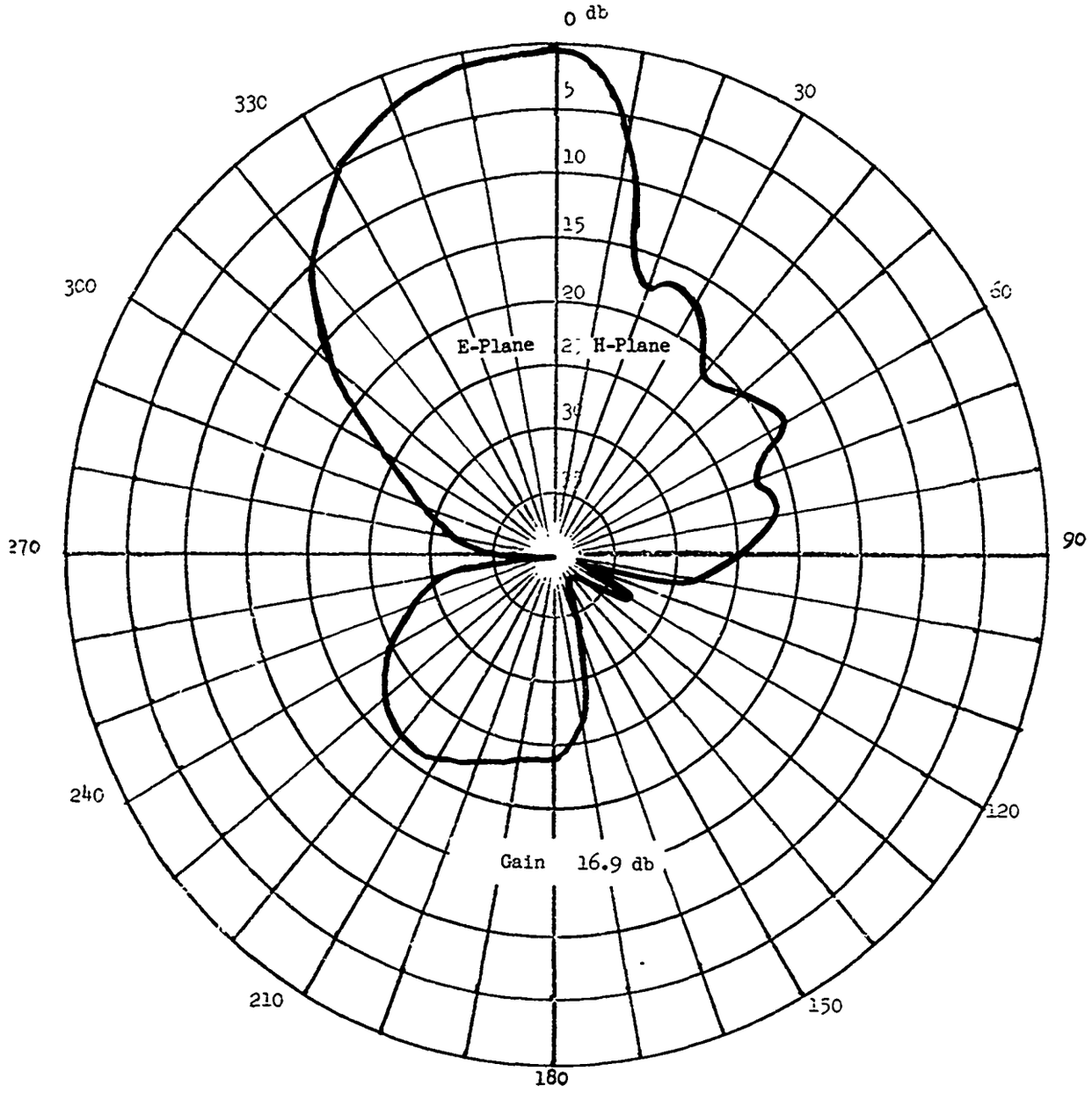

Figure III-33 Five High Gain Element Mei Array

of time, reruns on these arrays at the proper frequencies were not obtained. The two cases of arrays over real earth that were run are of some interest, however, and are shown in Figures III-34a and b. The ground chosen for the runs had a conductivity, σ, of 5×10^{-14} emu and a relative dielectric constant, ε, of 15 - a rather mediocre earth. The gain of these arrays is slightly less than there counterparts in free space (See Part IV) and if one were to speculate he could draw the conclusion that this decrease in gain would be less at HF frequencies. Speculating further we can say that most probably the take-off angle at the lower frequencies would be somewhat higher than that for the UHF case at hand, although there is no way of specifying exactly what it would be. The parameters affecting the radiation characteristics of an HF array are so numerous that drawing exact conclusions from the available UHF runs would not only be meaningless, but would be impossible. It is only possible to speculate about the direction of change that might occur in going from UHF to HF.

Until now this section has simply provided the results of the various computer runs on LP arrays with only some of the more interesting results being pointed out. It is time to draw some conclusions and apply these conclusions to a specific array design. At the beginning of this study a set of design goals to be achieved was specified. With the limited data at hand we can see which goals can be fulfilled, which goals seem likely to be fulfilled and which goals will take considerably more study to determine whether or not they are possible to meet.

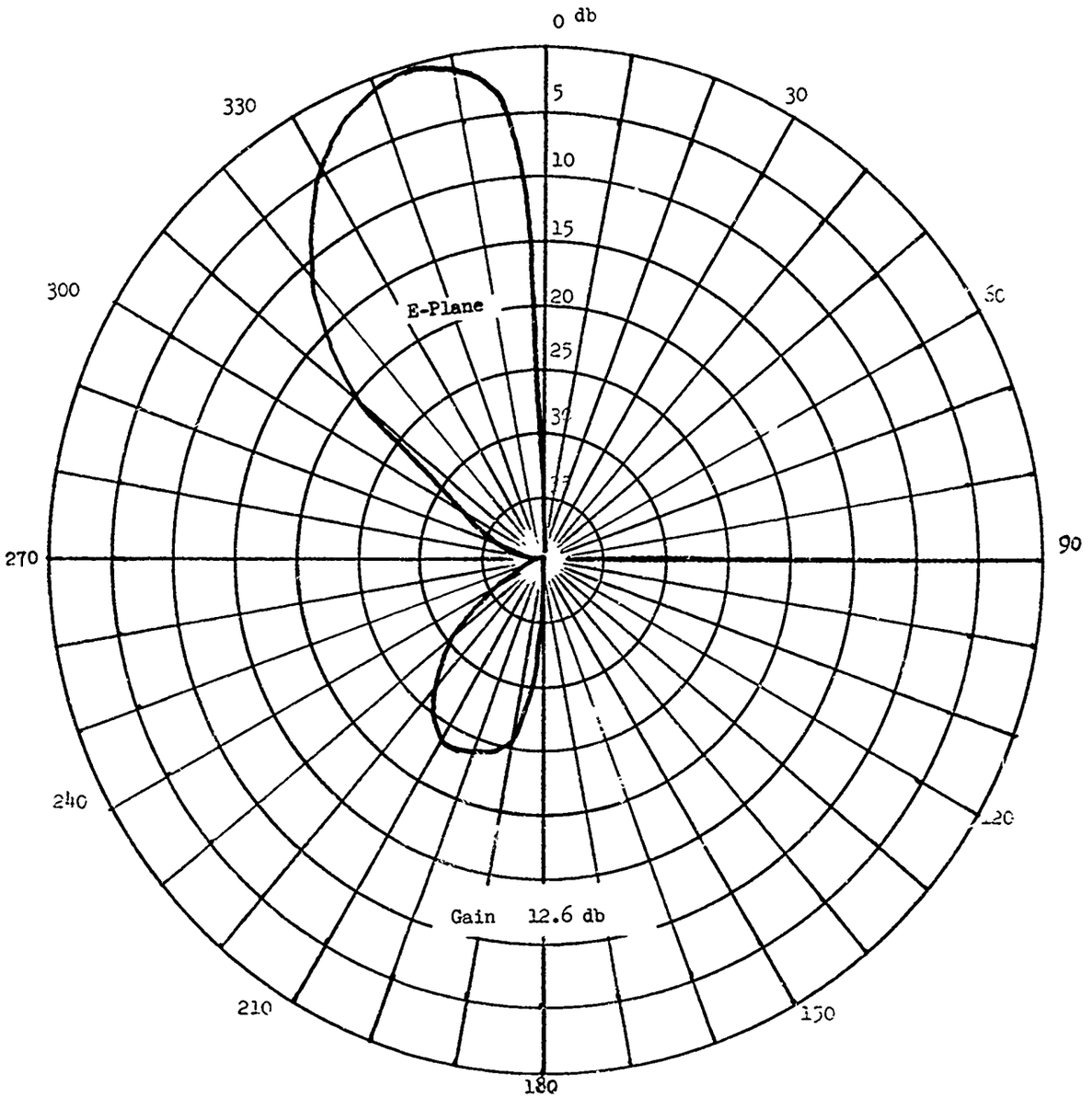

Figure III-34a Four Element DuHamel Array with .75 Wavelength Spacing Over Real Earth

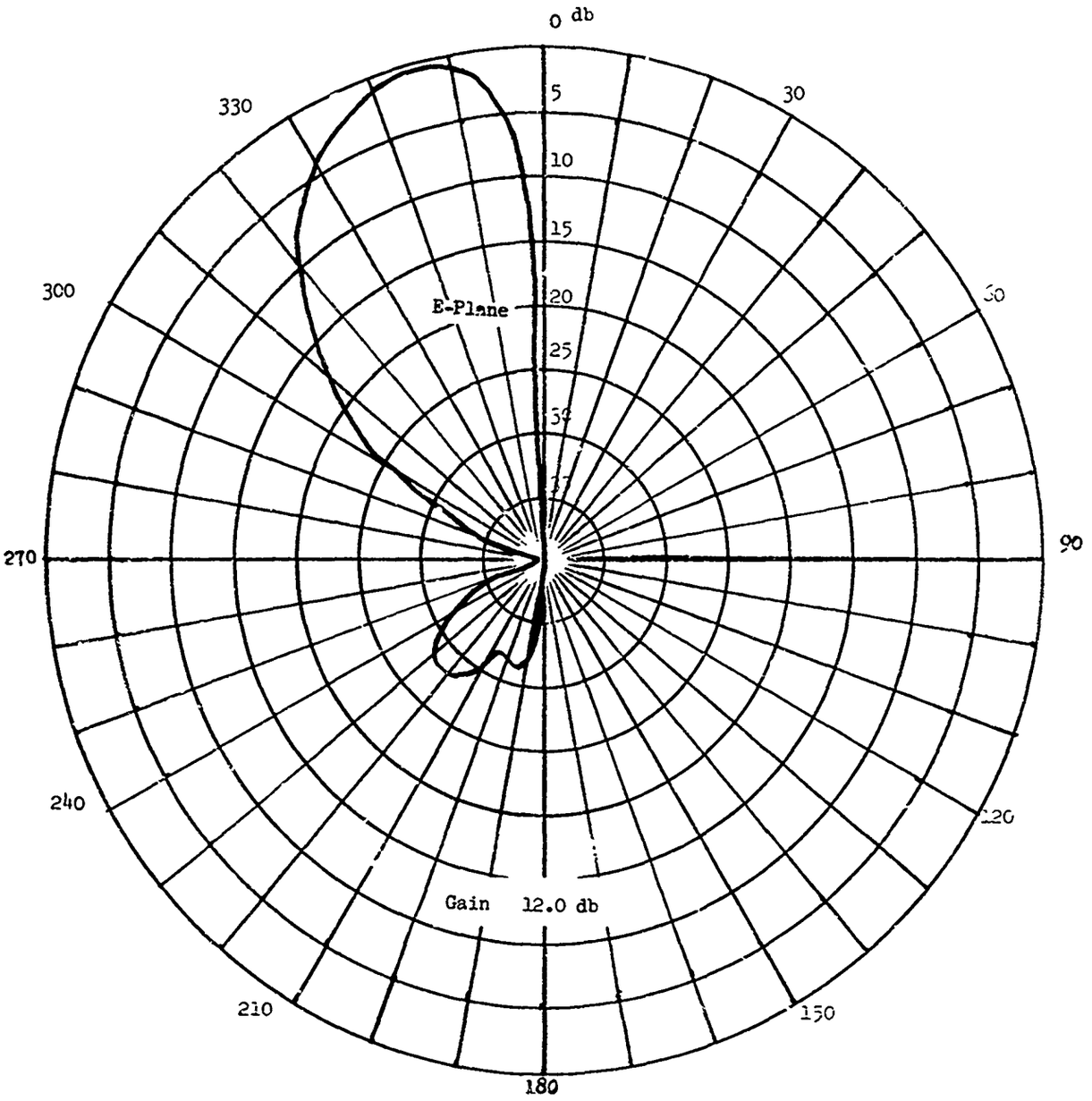

Figure III-34b Four Element DuHamel Array with 1. Wavelength Spacing Over Real Earth

E. --Continued

One of the foremost design goals is the gain which has been specified as a minimum of 17 dbi at the beam peak. A 5 element Mei array with 3/4 wavelength spacing has a free space gain of 16.9 dbi, nearly enough to meet the requirements. However, the Mei array seems to increase in gain with additional elements so that a minimum gain of 17 dbi should be easily achieved with a 6 or 7 element array even over real earth.

The second design goal, equally important as gain, is the coverage that can be obtained. The azimuth coverage was specified as a 16 degree beamwidth at and near the peak of the beam in elevation. Since the azimuth coverage should change only slightly between a free space situation and over real earth, the free space patterns available should give a good indication as to the coverage that can be achieved by an HF antenna. Another look at the same 5 element Mei array shows a beamwidth of 15 degrees with the first sidelobe 17 db below the beam peak. The beamwidth is only a degree under the design goal, hardly enough to bother with since the beamwidth will probably change more than a degree with a change in frequency. The sidelobe level of -17 db is 2 db better than the -15 db specified in the design goal requirements.

The elevation coverage is to have a beamwidth from 2 to 16 degrees. We can see from the UHF pattern that this goal cannot be achieved with a simple HF antenna above ground, there must ba a ground screen in front of the array to lower the beam peak. No more can be said about the elevation pattern or screen effects since the HF information is not available

E. --Continued

By using the data that is available on the five element Mei array, we can now proceed with the design of an optimum 3-30 MHz HF array. As mentioned previously, the number of elements would be increased from five to six with an inter-element spacing of 0.75 wavelengths.

With a τ of 0.96 each LP element of the array would consist of 62 dipoles for a total of 372 dipoles for the array. The longest dipole would be 164 feet tall while the shortest would be 13.59 feet tall. Four dipoles have been added to the high frequency end of each LP element to insure that maximum gain is achieved at 30 MHz.

The spacing between the longest dipoles of adjacent LP elements would be 0.75 λ or 246 feet for a total array width of 1230 feet at the low frequency end. Similarly, the spacing between the shortest dipoles of adjacent LP elements would be 20.4 feet giving an array width of 102 feet at the high frequency end.

Since we are designing a Mei array, the spacing between dipoles of an LP element is dependent on element placement in the array (See Figure III-26). Although the dipole spacings differ from element to element, only the inter dipole spacings of an imaginary LP in the center of the array need

E. --Continued

to be specified since all dipoles of the same length on the various LP elements will fall on a line perpendicular to this imaginary centerline. Of course, if there were an odd number of LP elements in the array, then there would be an actual center LP element. The best choice for the imaginary center LP element would be the high gain LP discussed previously with an α angle of 6.37°. Using this information and some simple geometry, the spacing between the longest and the next longest element in the imaginary LP can be found from the expression

$$S = \frac{(1-\tau)\ell_{max}}{2\tan(\alpha/2)} \tag{153}$$

where S is the desired spacing and ℓ_{max} is the length of the longest element. For the particular array at hand this spacing is 59 feet. Making use of geometrical progression formulas one can determine the total length, L, of the array from

$$L = \frac{\ell_{max}-\ell_{min}}{2\tan(\alpha/2)} \tag{154}$$

where ℓ_{min} is the length of the smallest element. The total length of our array is 1352.1 feet.

E. --Continued

Until now only the dimensions of the longest dipole and the spacing between the two longest dipoles in the imaginary center LP have been presented. Obtaining the dimensions of the remainder of the elements and spacings is simply a matter of successive multiplication by τ.

The only remaining parameter that must be specified for a complete array design, is the line length between adjacent dipoles in an LP element. Although the physical spacing between dipoles of an LP element depends on the placement of the element in the array, the line length connecting any two dipoles in an LP element must be the same for similar dipoles in each LP element in the array to maintain a flat phase front. The line lengths can be obtained by letting the electrical spacing equal the physical spacing for the outer most elements in the array since the outer elements will have the largest separation between dipoles. Again using some simple geometry we find that the line length from the largest to next largest dipole in the outer LP elements is 63.9 feet. To obtain the other line lengths from dipole to dipole in the LP's all that is required is successive multiplication of the largest line length by τ.

The design of the HF Mei array is now complete and may be summarized as follows:

Frequency	3 - 30 MHz
No. of LP Elements	6
No. of Dipoles/Element	62
No. of Dipoles/Array	372

E. --Continued

τ	0.96
Spacing Between Elements	246 ft. Low Frequency End
	20.4 ft. High Frequency End
Array Width	1230 ft. Low Frequency End
	102 ft. High Frequency End
Array Length	1352.1 ft.
Largest Dipole-to-Dipole Spacing on Centerline	59 ft.
Largest Line Length	63.9 ft.

The characteristic impedance of the transmission line was 60 ohms for the computer runs used in designing this array. However, no attempt has been made to optimize this impedance, therefore no transmission line impedance will be specified in this design. Similarly, there is not enough information available to specify the type and size ground plane necessary to make this array meet the elevation coverage specified.

There are other design goals such as VSWR that were specified at the beginning of the study, but the program has changed scope to such an extent that these goals are no longer in the realm of the study. Such design goals are secondary, however, compared to the primary objective of proper gain and coverage.

E. --Continued

Although not every aspect of the original study has been considered because of the redirection in emphasis from antenna physical modeling to mathematical modeling, it is felt that an optimum HF array design has been achieved to the extent intended in the study. During the course of the study an extremely valuable tool in the form of a computer LP array analysis program has been developed and furnished to the customer for optimizing arrays with different design goals.

The mathematical model developed under this study was the best at the time of its writing, but use of the program and an analysis of the results show that there are changes that would improve and expand this model. It is felt that these changes would greatly benefit the user of such a model and that a future study be undertaken to incorporate any desireable changes in the model and computer program.

IV APPENDIX

A. SINGLE LOG PERIODIC ANTENNAS

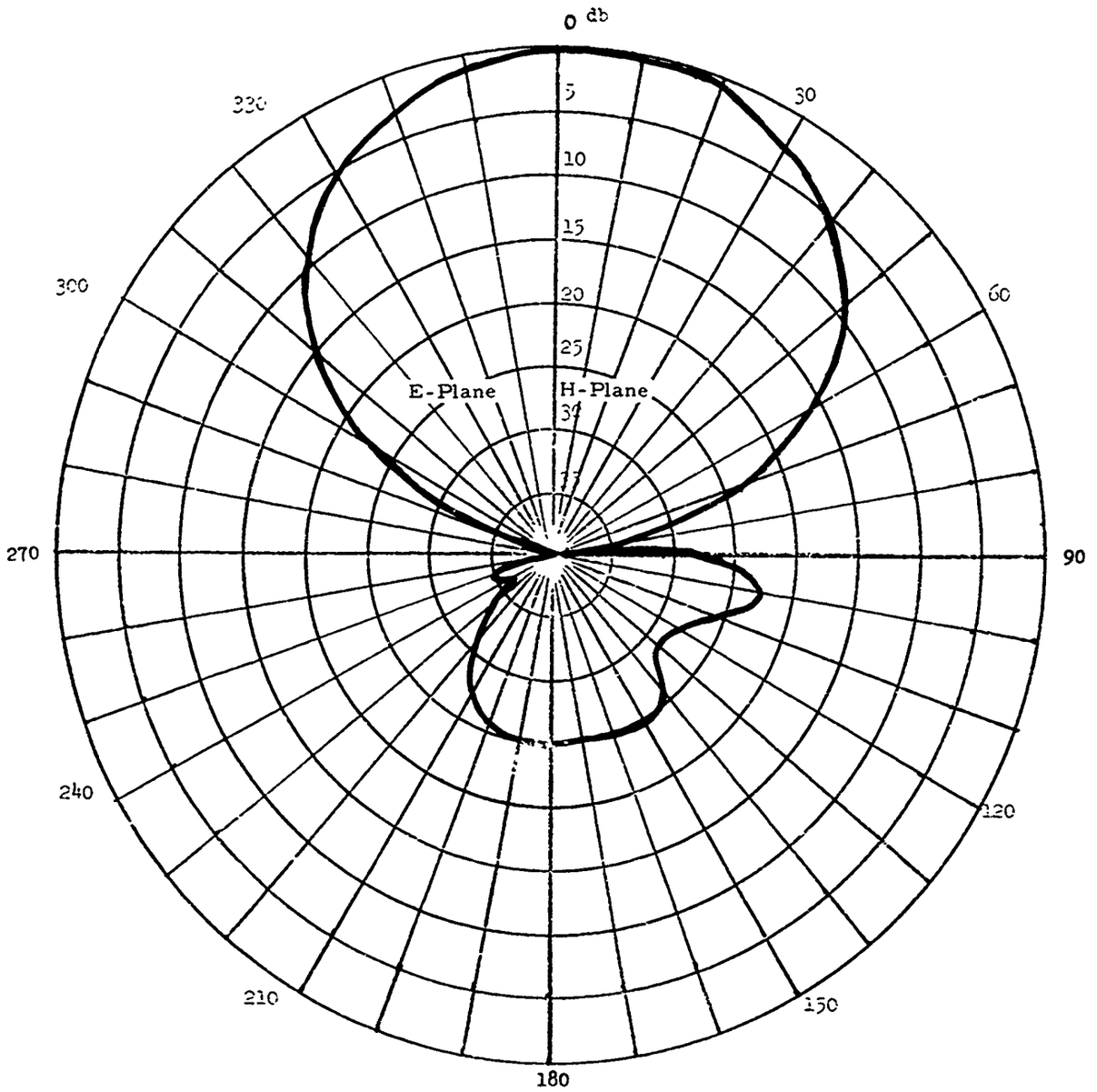

Figure IV A-1 High Gain LP - Gain 11.2 db

A. (Continued)

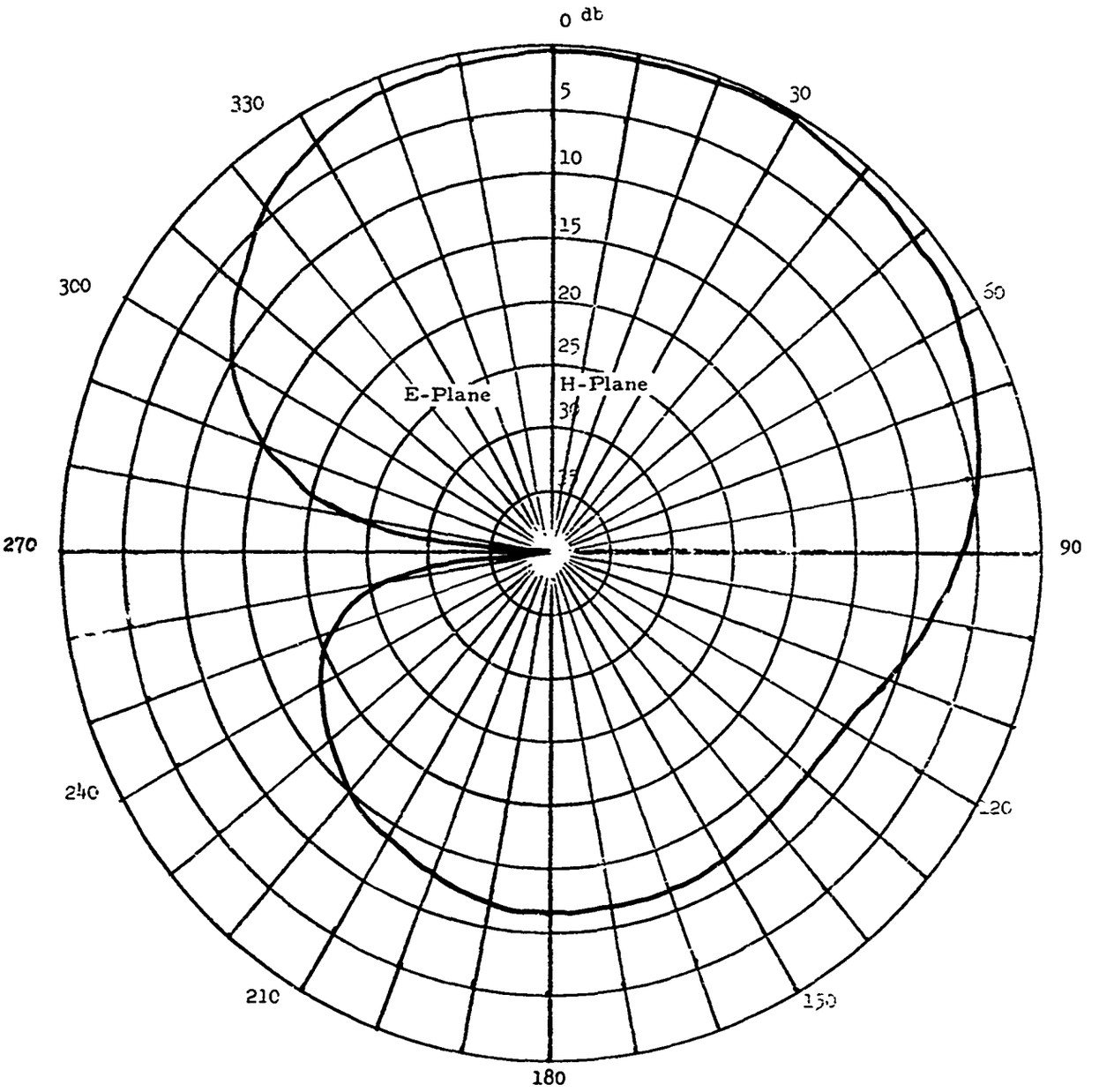

Figure IV A-2 Medium gain Lp - Gain 6.3 db

B. HIGH GAIN ELEMENT DUHAMEL ARRAYS

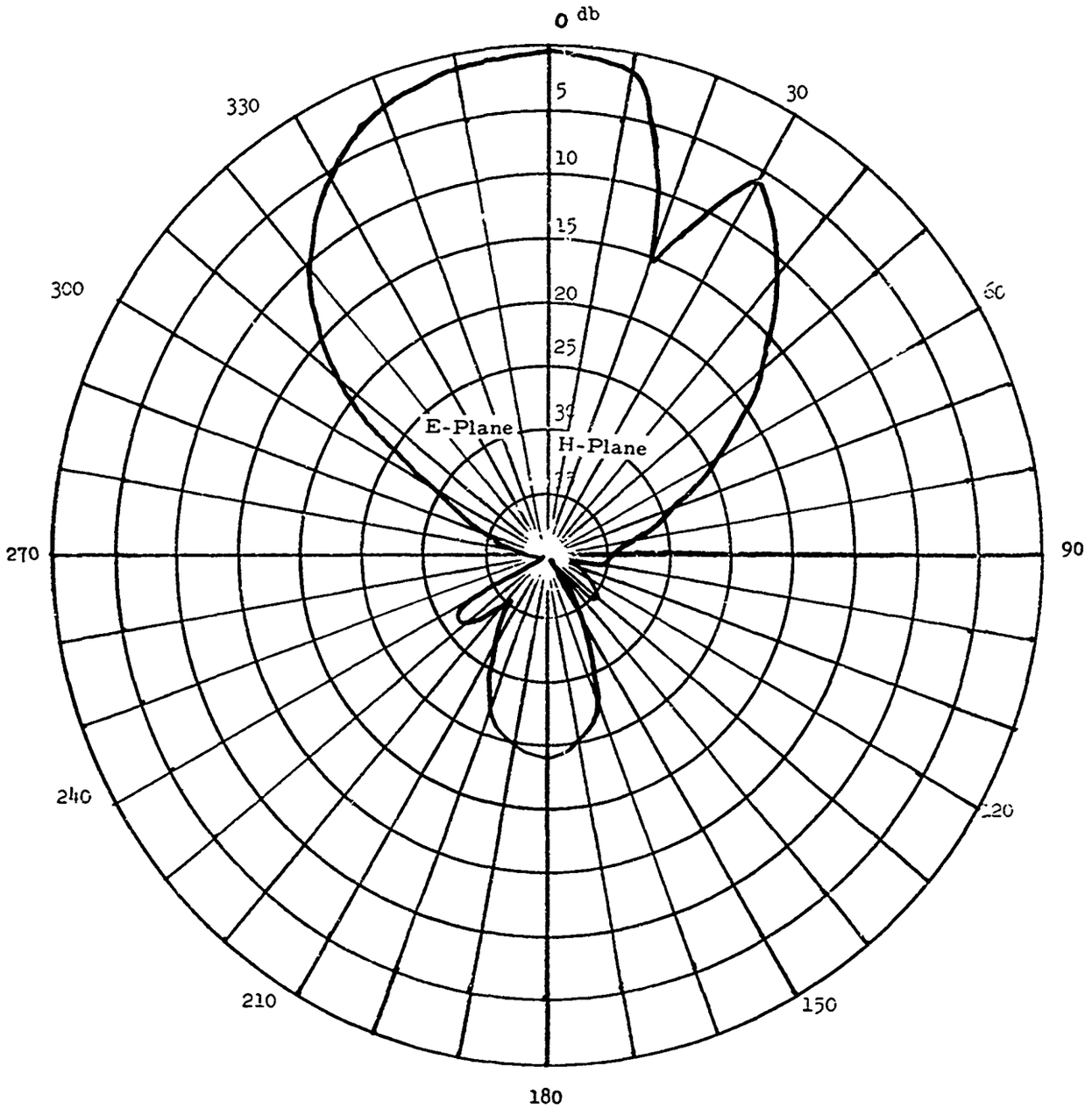

Figure IV B-1 2 Element array - .5 wavelength spacing - Gain 12.8 db

B. (Continued)

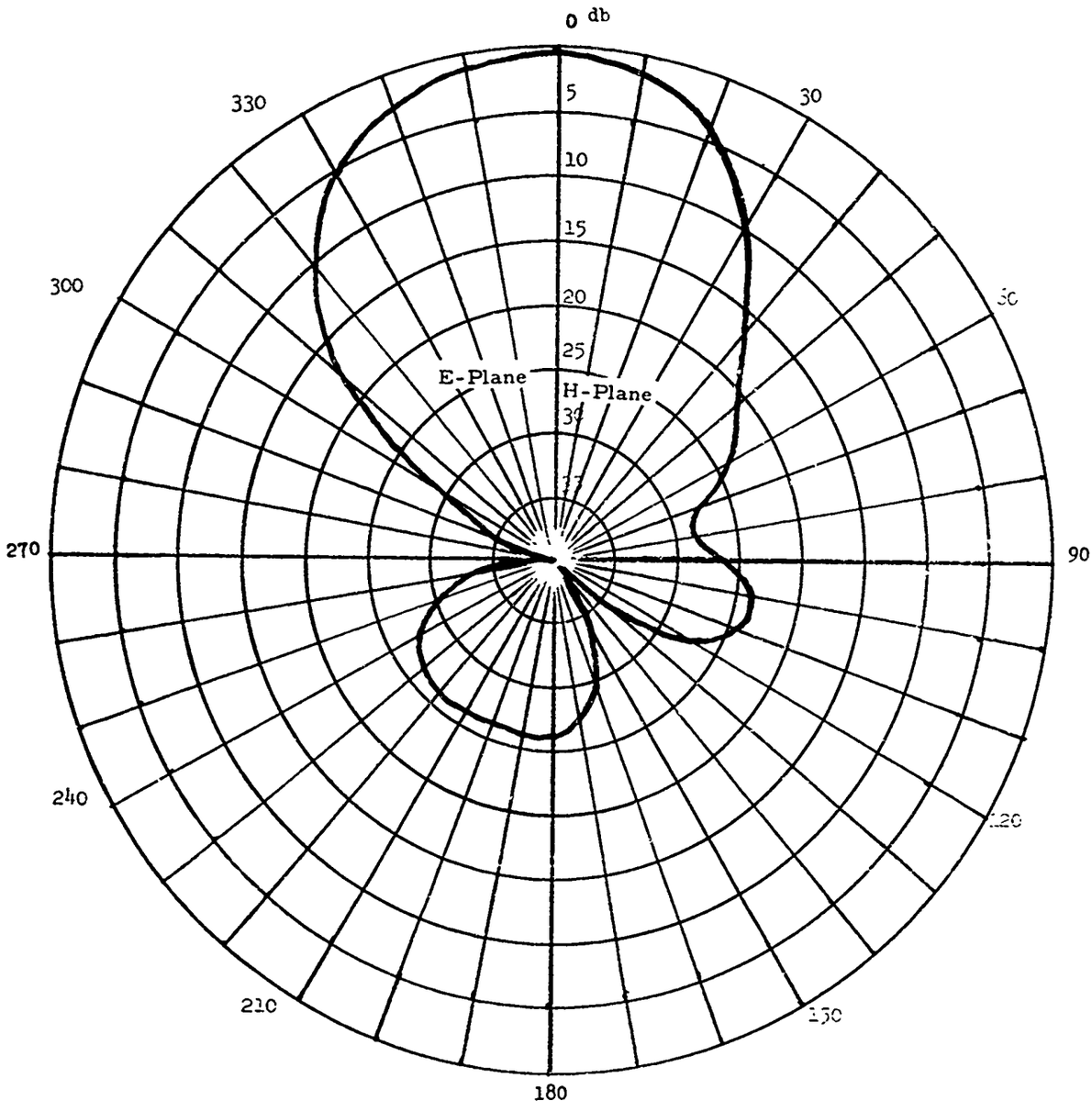

Figure IV B-2 2 Element Array - .75 Wavelength Spacing - Gain 13.4 db

B. (Continued)

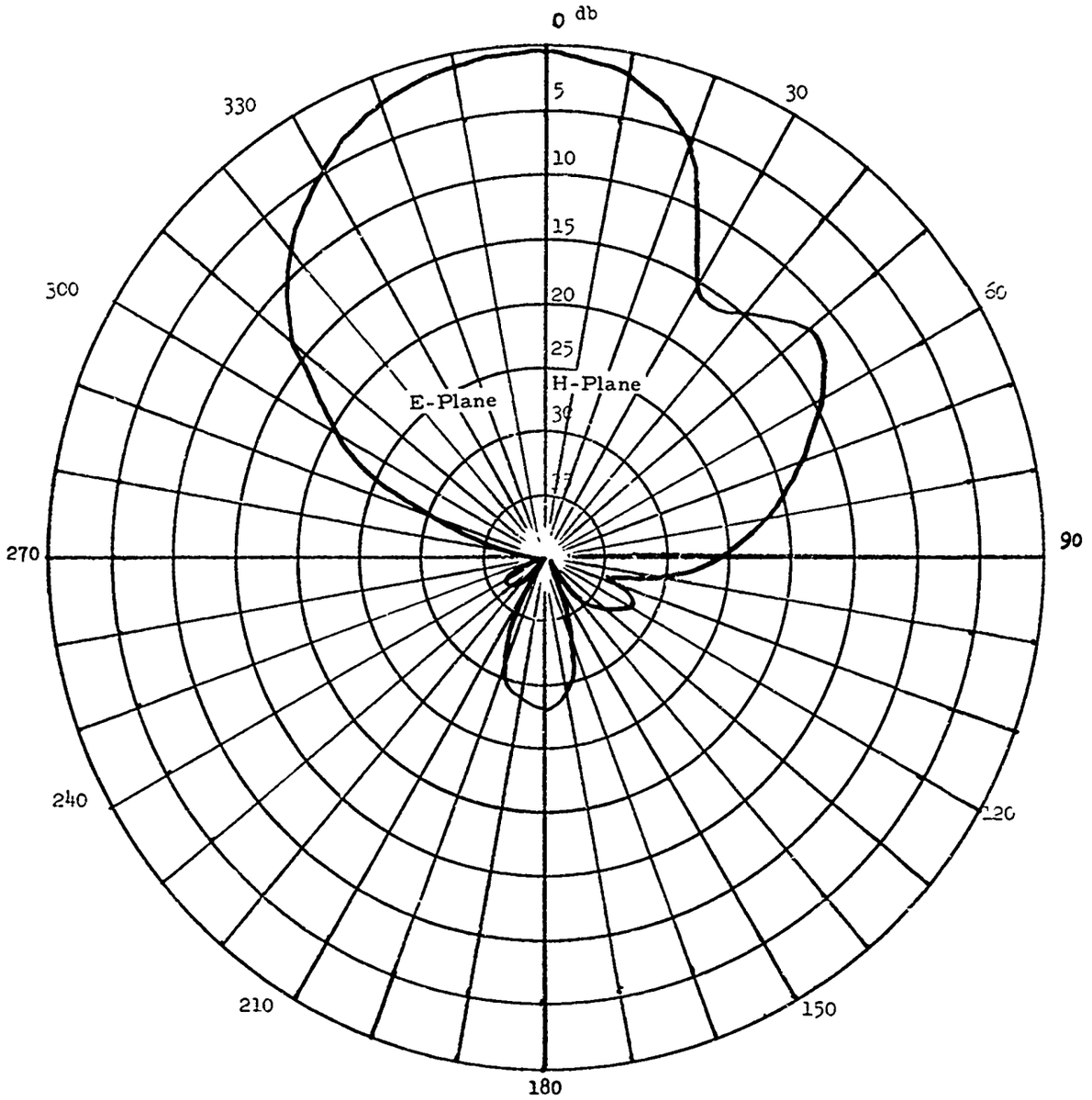

Figure IV B-3 2 Element Array - 1.0 Wavelength Spacing - Gain 13.7 db

B. (Continued)

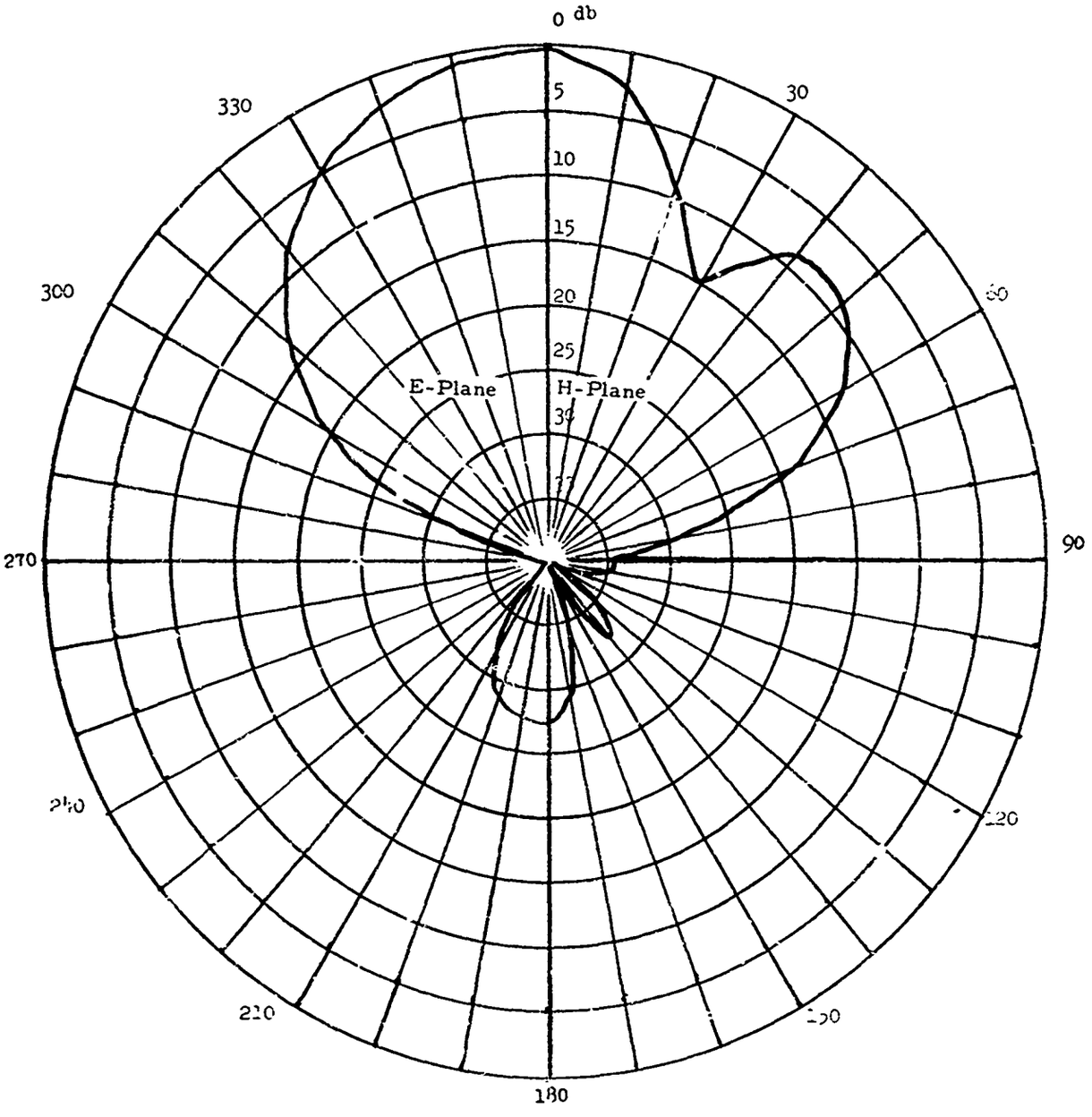

Figure IV B-4 2 Element Array - 1.25 Wavelength Spacing - Gain 14.0 db

B. (Continued)

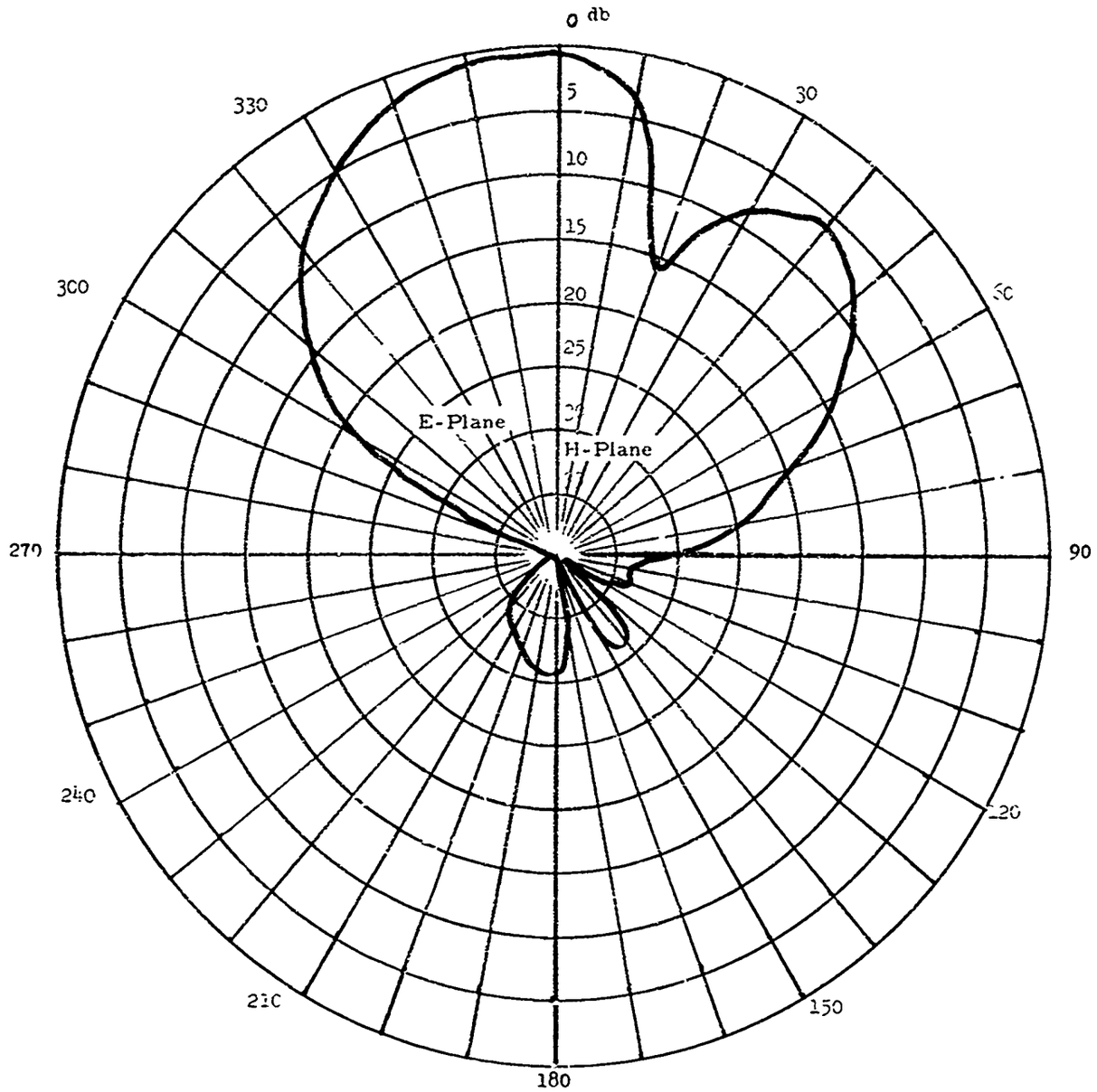

Figure IV b-5 2 Element Array - 1.5 Wavelength Spacing - Gain 14.0 db

B. (Continued)

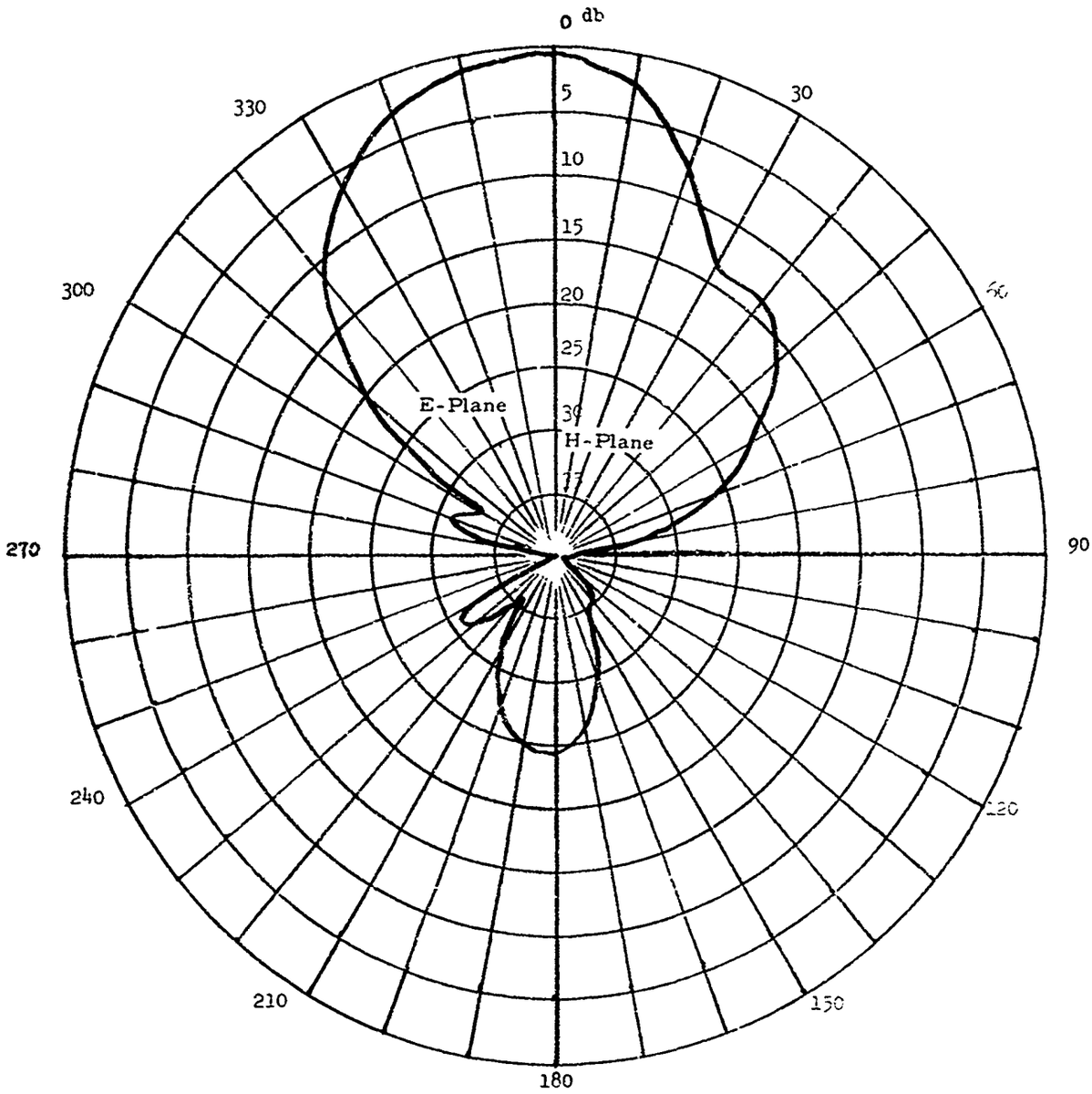

Figure IV B-6 4 Element Array - .5 Wavelength Spacing - Gain 14.7 db

B. (Continued)

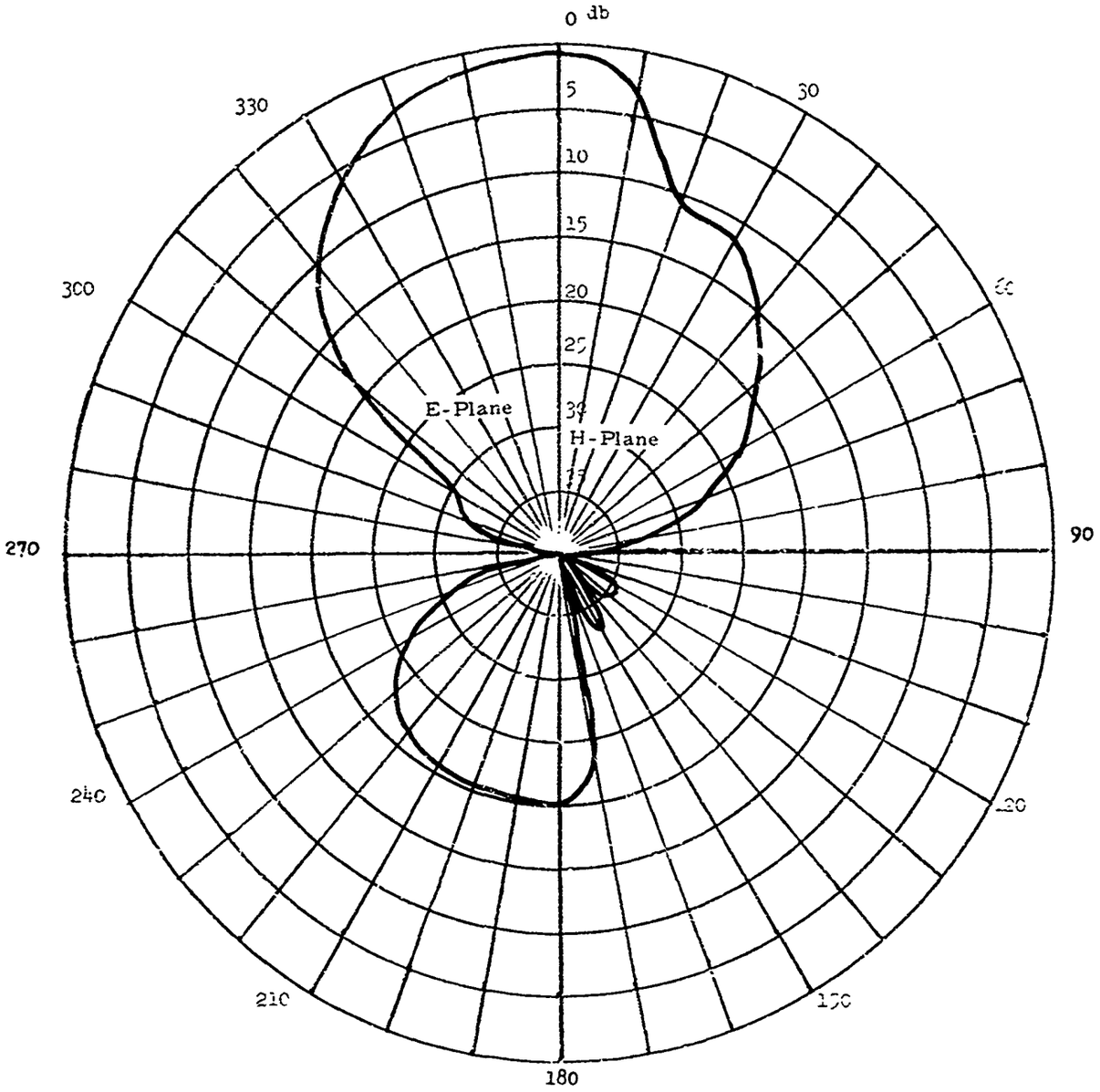

Figure IV B-7 4 Element Array - .75 Wavelength Spacing - Gain 15.2 db

B. (Continued)

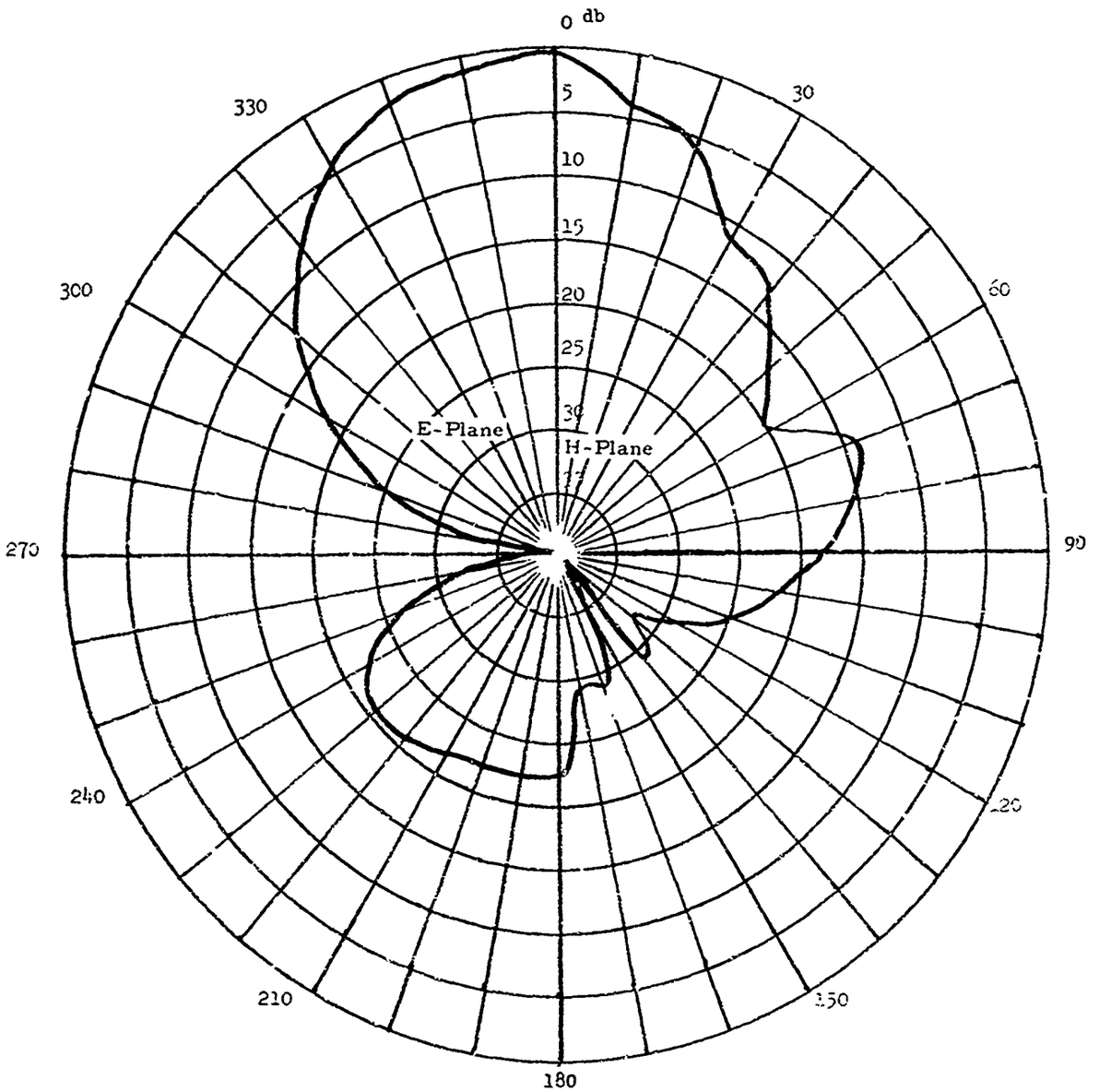

Figure IV B-8 4 Element Array - 1.0 Wavelength Spacing - Gain 14.5 db

B. (Continued)

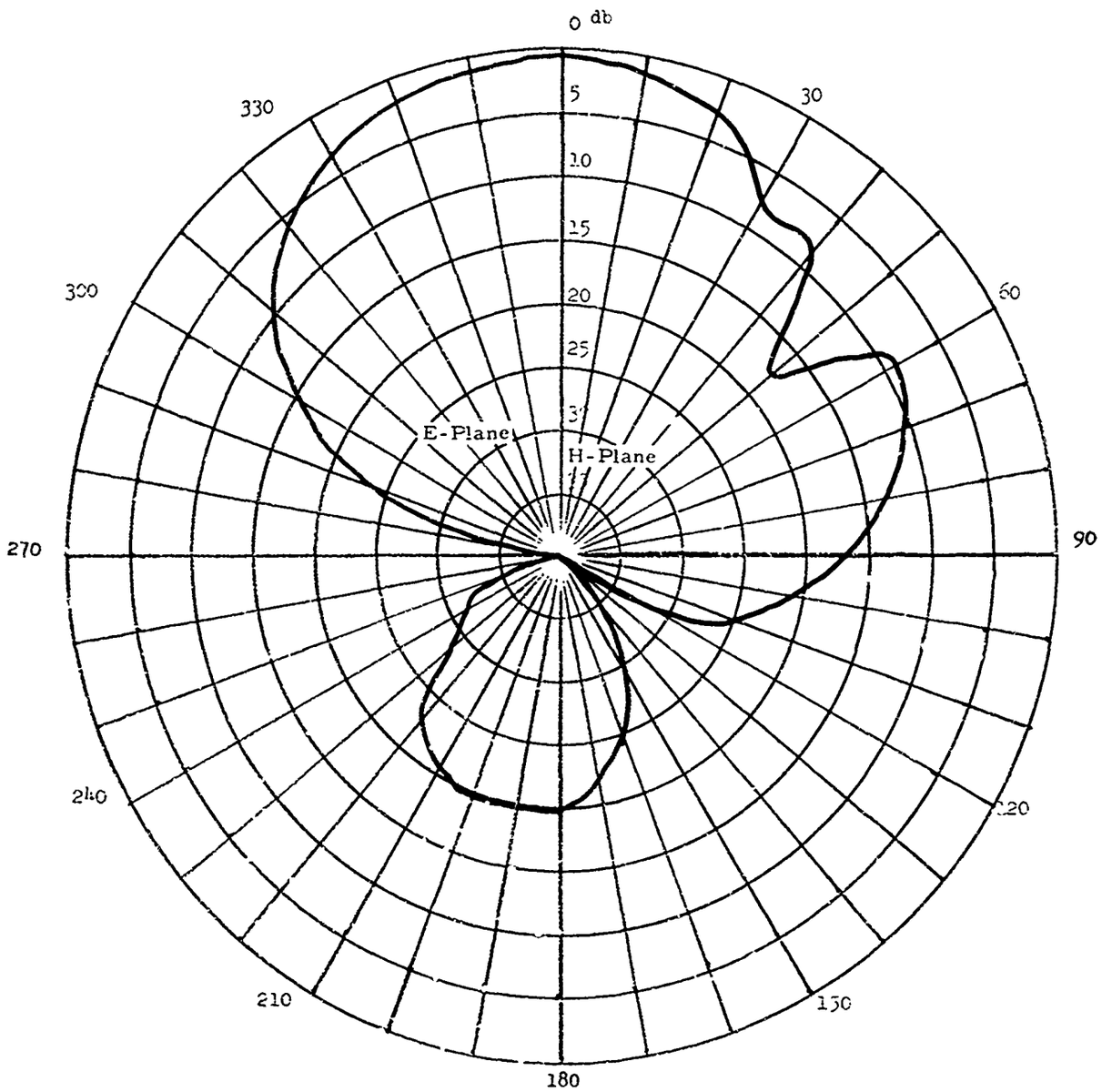

Figure IV B-9 4 Element Array - 1.25 Wavelength Spacing - Gain 11.7 db

B. (Continued)

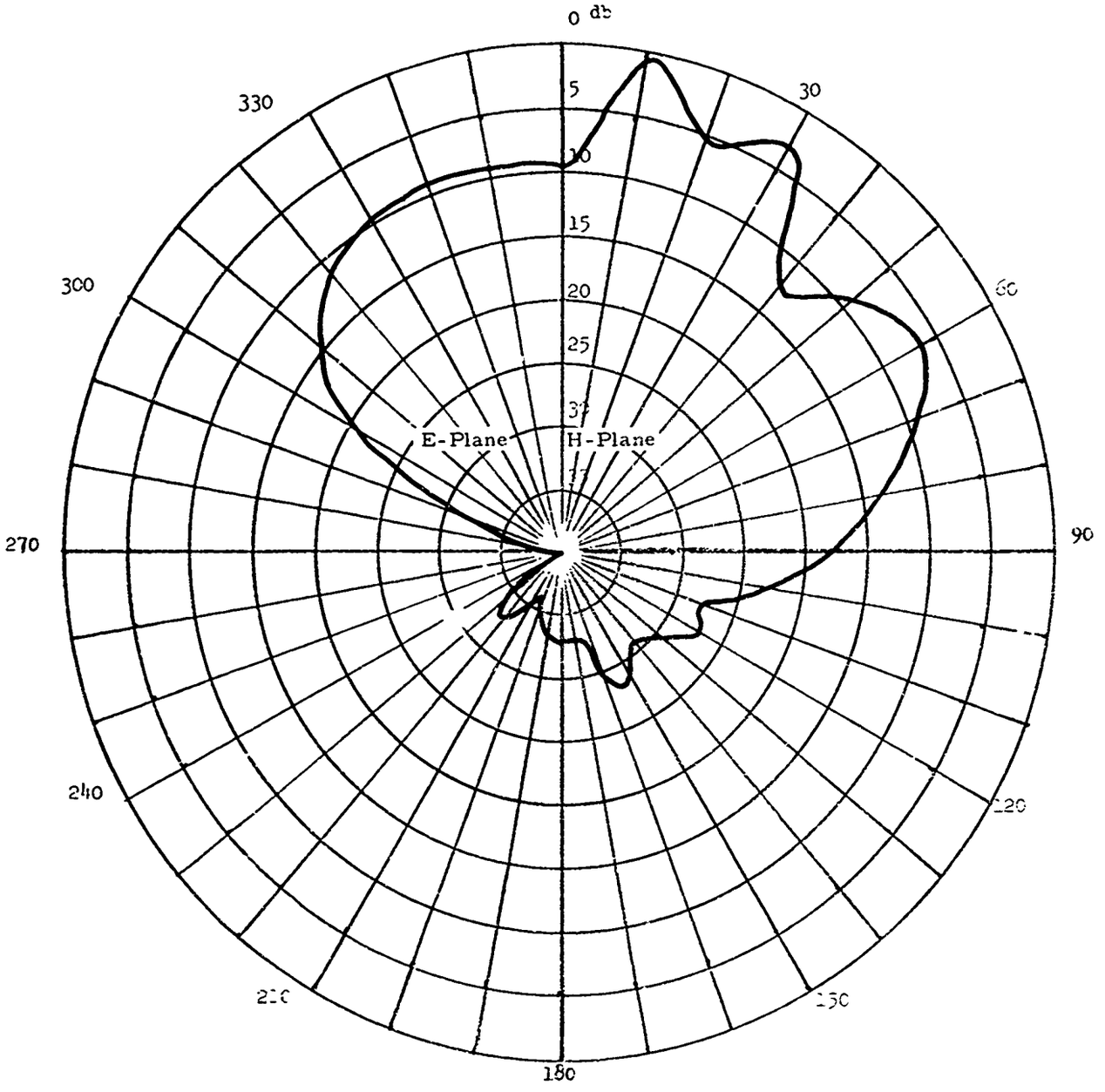

Figure IV B-10 4 Element Array - 1.5 Wavelength Spacing - Gain 12.4 db

B. (Continued)

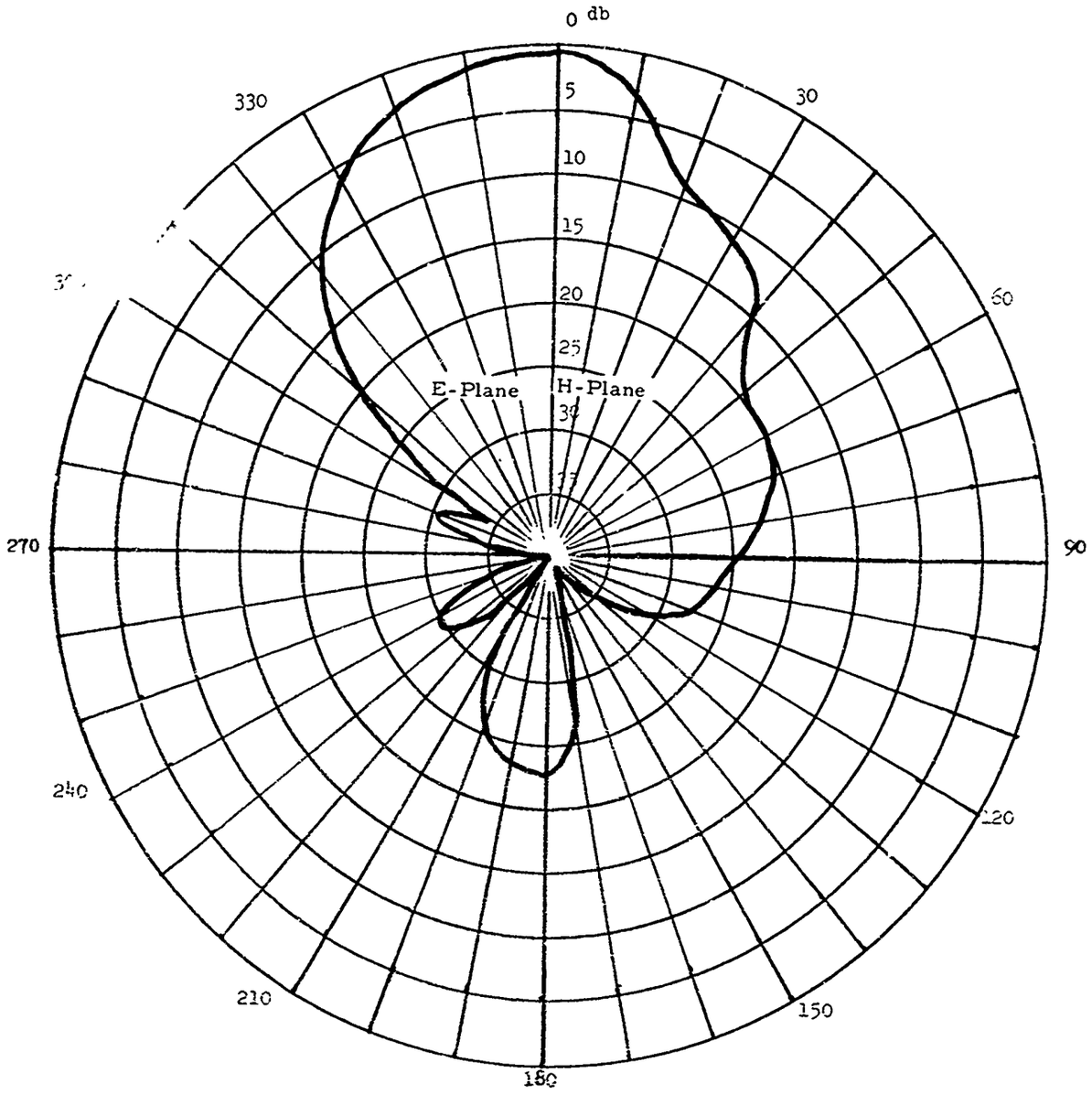

Figure IV B-11 5 Element Array - .5 Wavelength Spacing - Gain 15.1 db

B. (Continued)

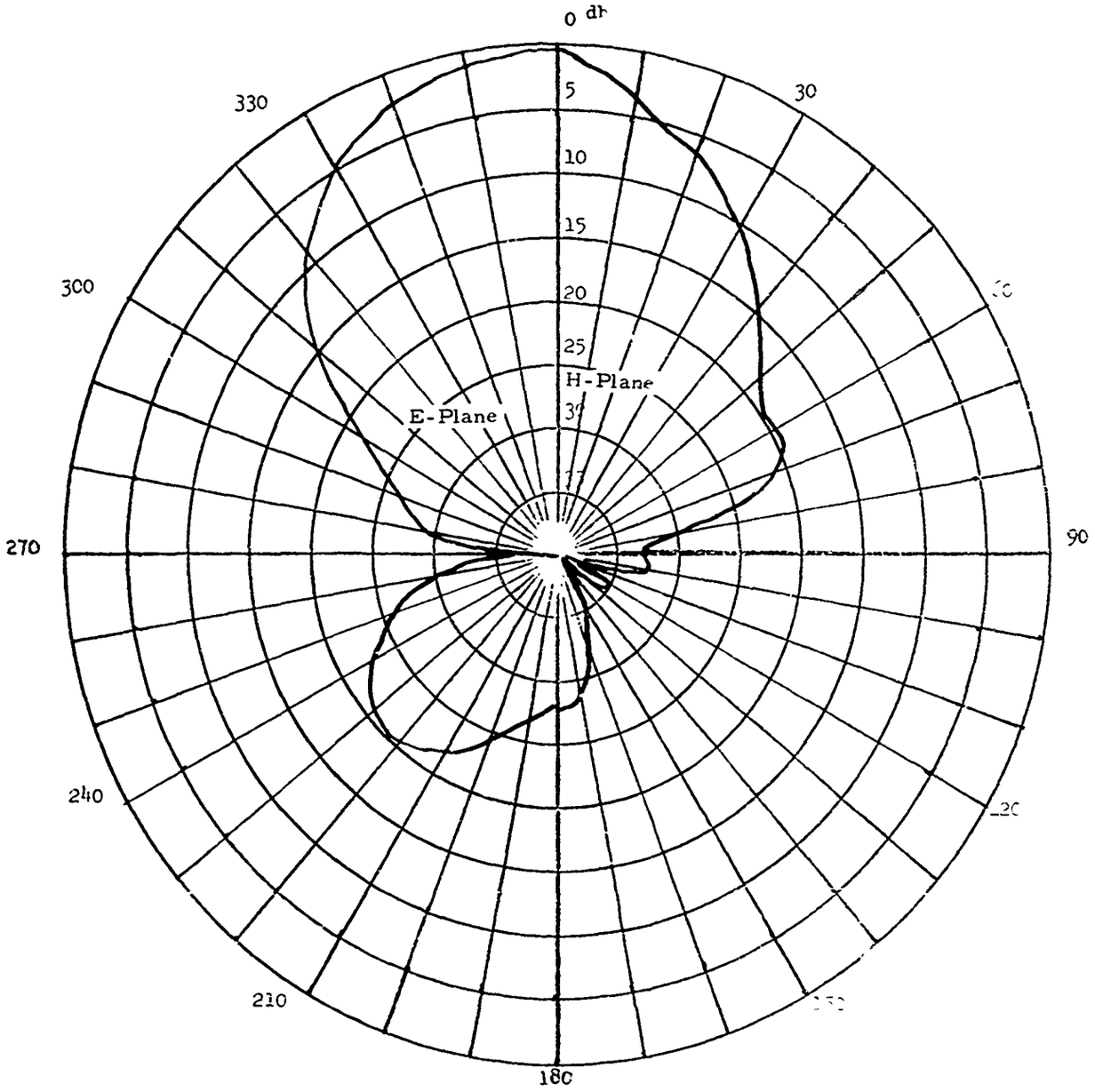

Figure IV B-12 5 Element Array - .75 Wavelength Spacing - Gain 15. db

B. (Continued)

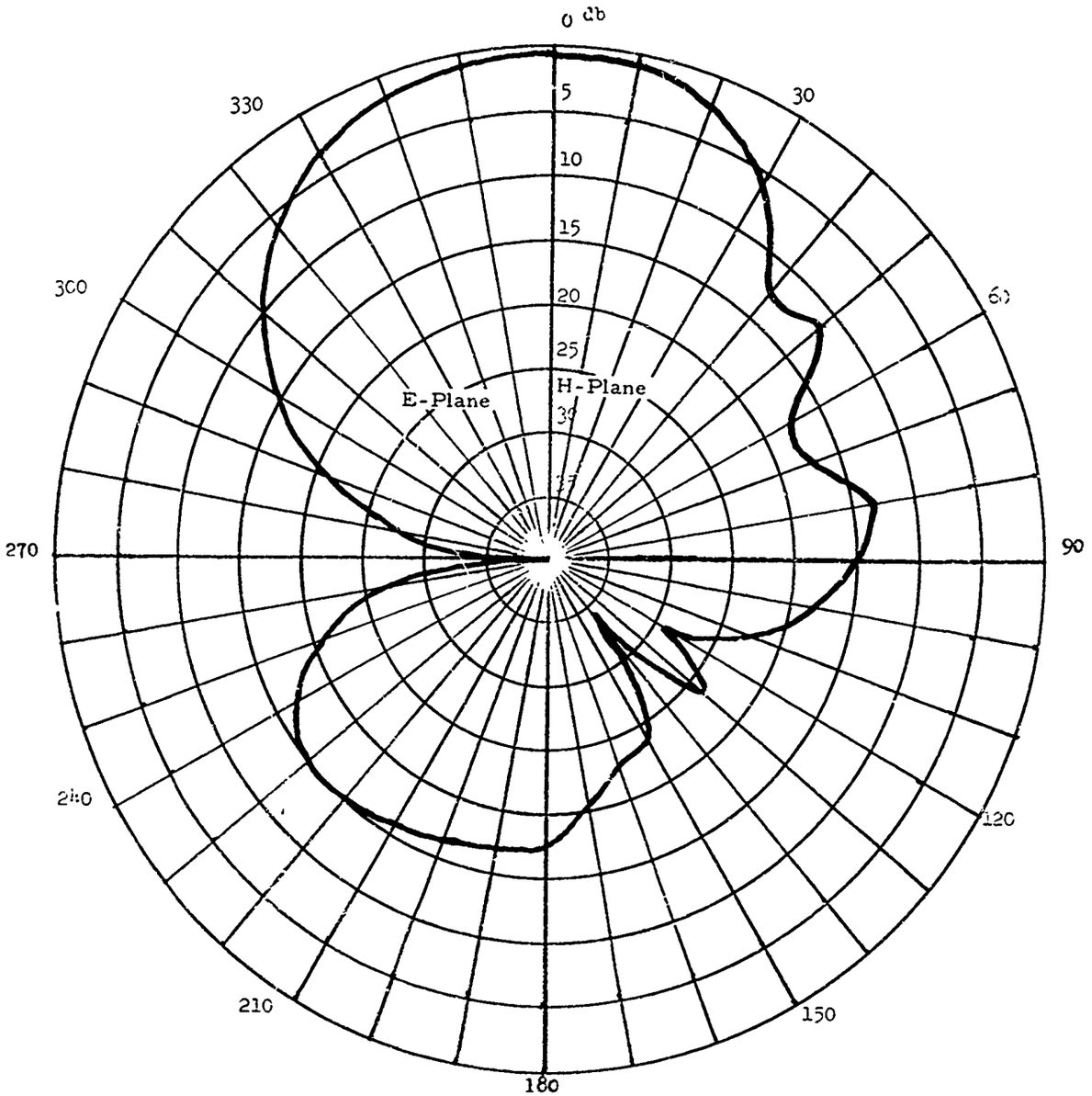

Figure IV B-13 5 Element Array - 1.0 Wavelength Spacing - Gain 11.9 db

B. (Continued)

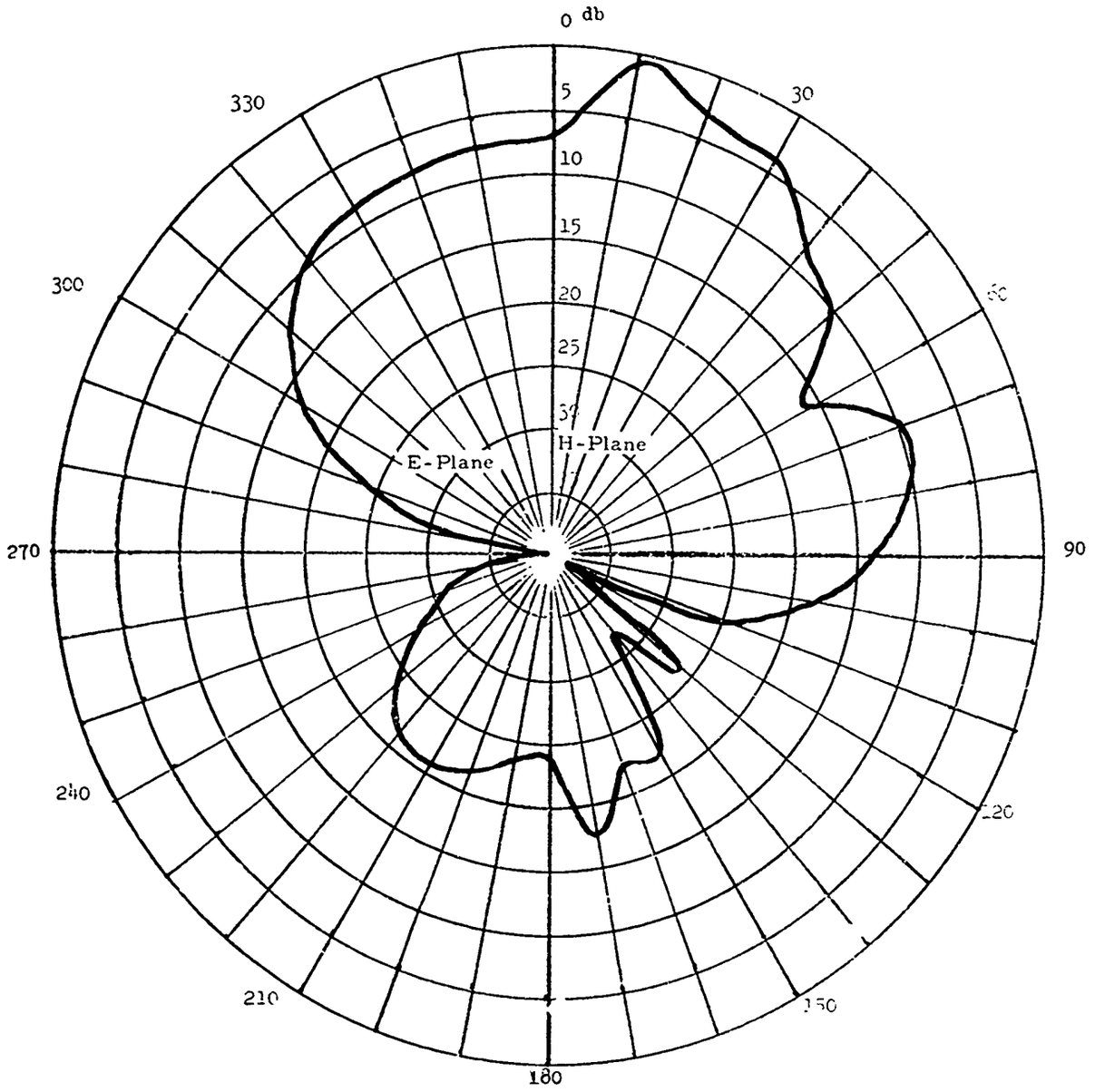

Figure IV B-14 5 Element Array - 1.25 Wavelength Spacing - Gain 11.8 db

B. (Continued)

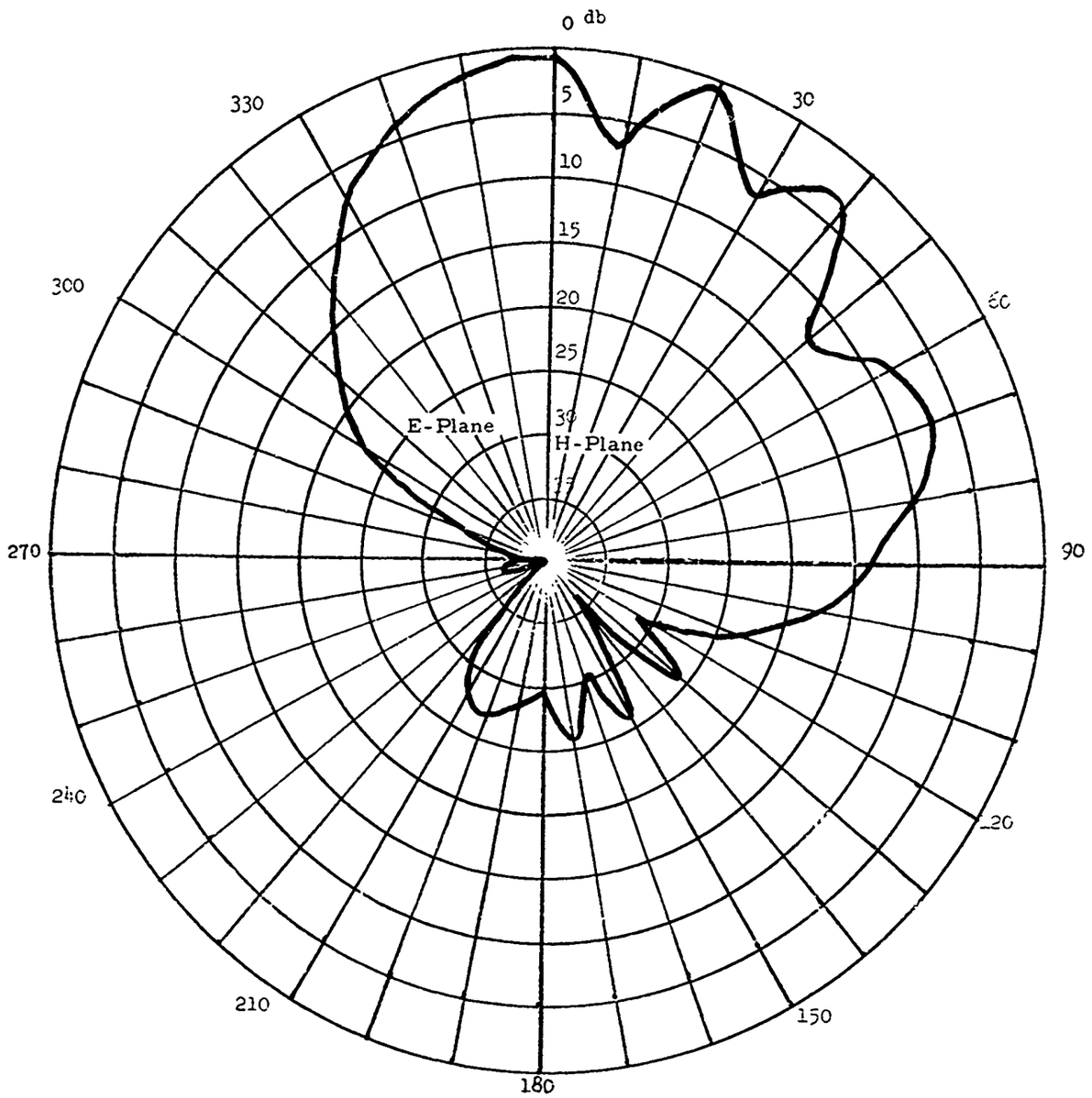

Figure IV B-15 5 Element Array - 1.5 Wavelength Spacing - Gain 11.8 db

C. MEDIUM GAIN ELEMENT DUHAMEL ARRAYS

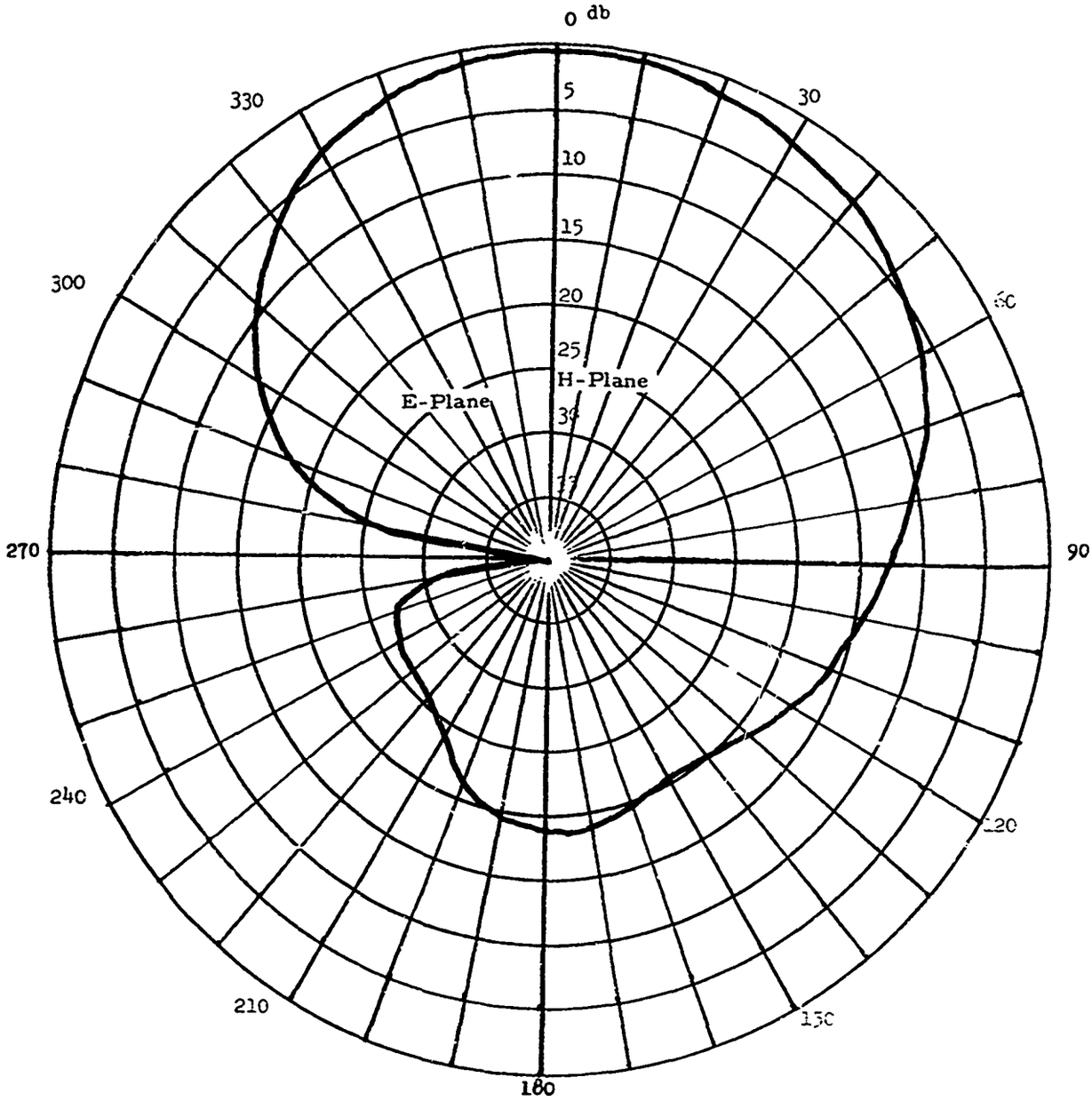

Figure IV C-1 2 Element Array - 0.15 Wavelength Spacing - Gain 8.4 db

C. (Continued)

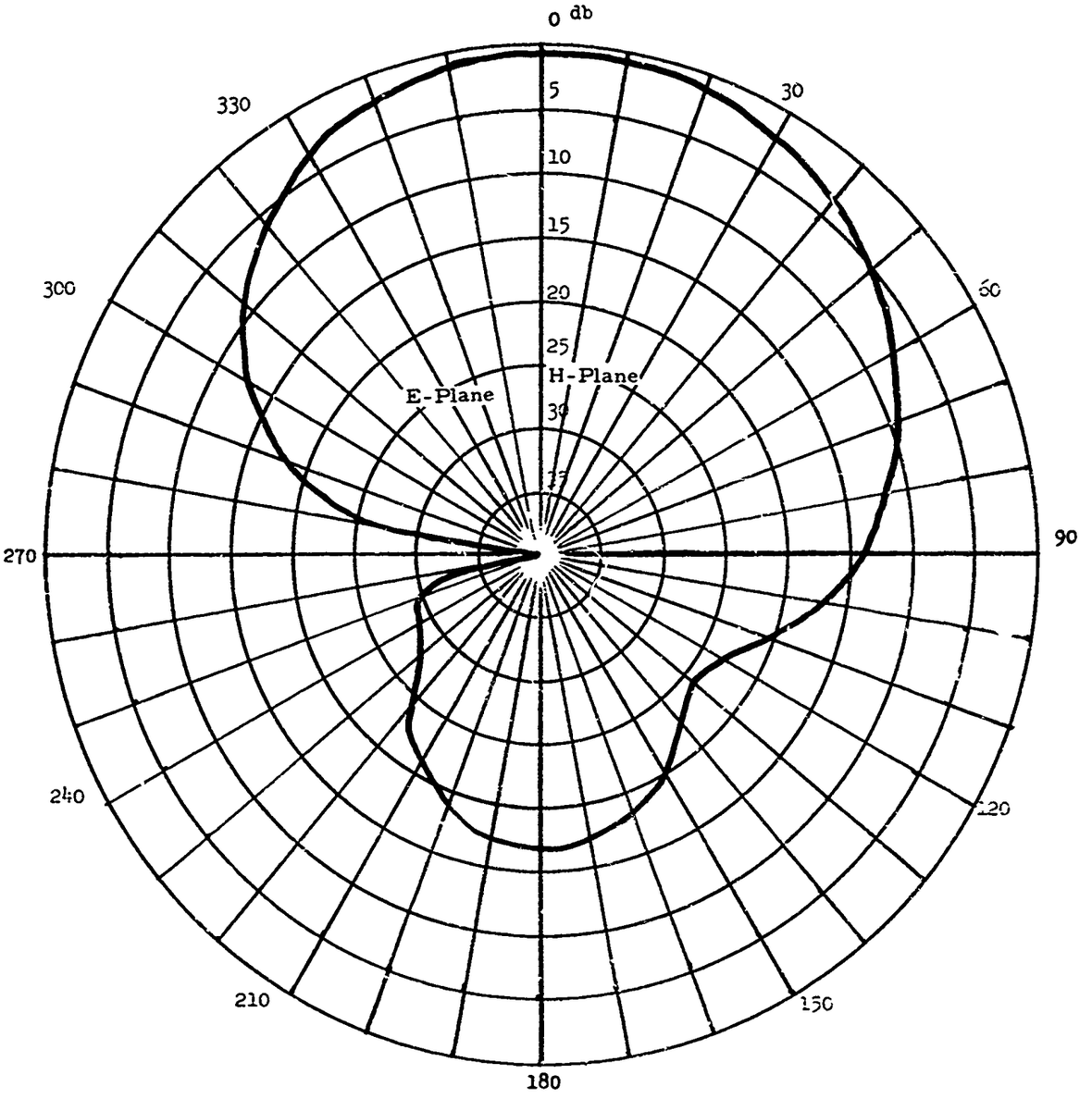

Figure IV C-2 2 Element Array - 0.25 Wavelength Spacing - Gain 8.8 db

C. (Continued)

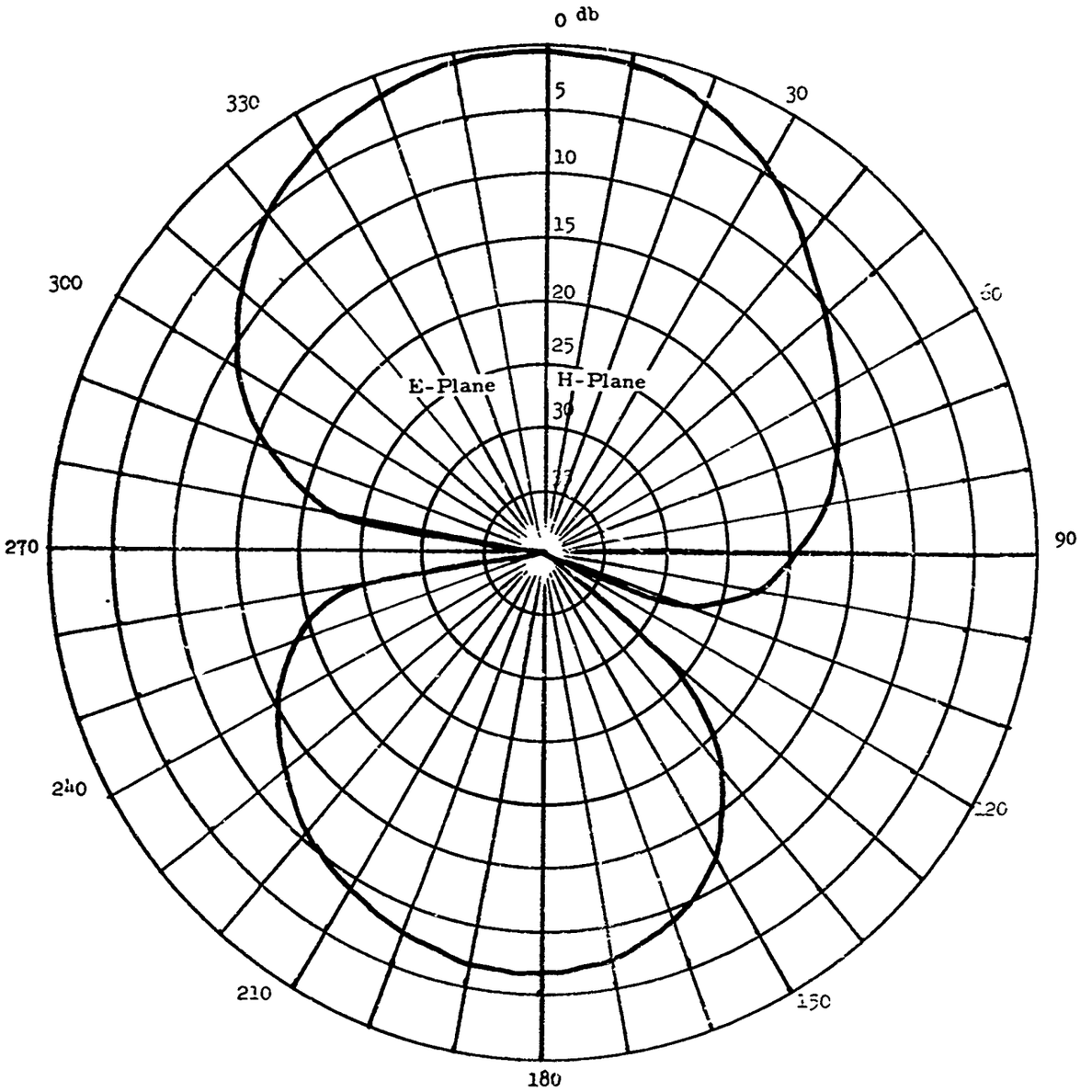

Figure IV C-3 2 Element Array - 0.5 Wavelength Spacing - Gain 9.4 db

C. (Continued)

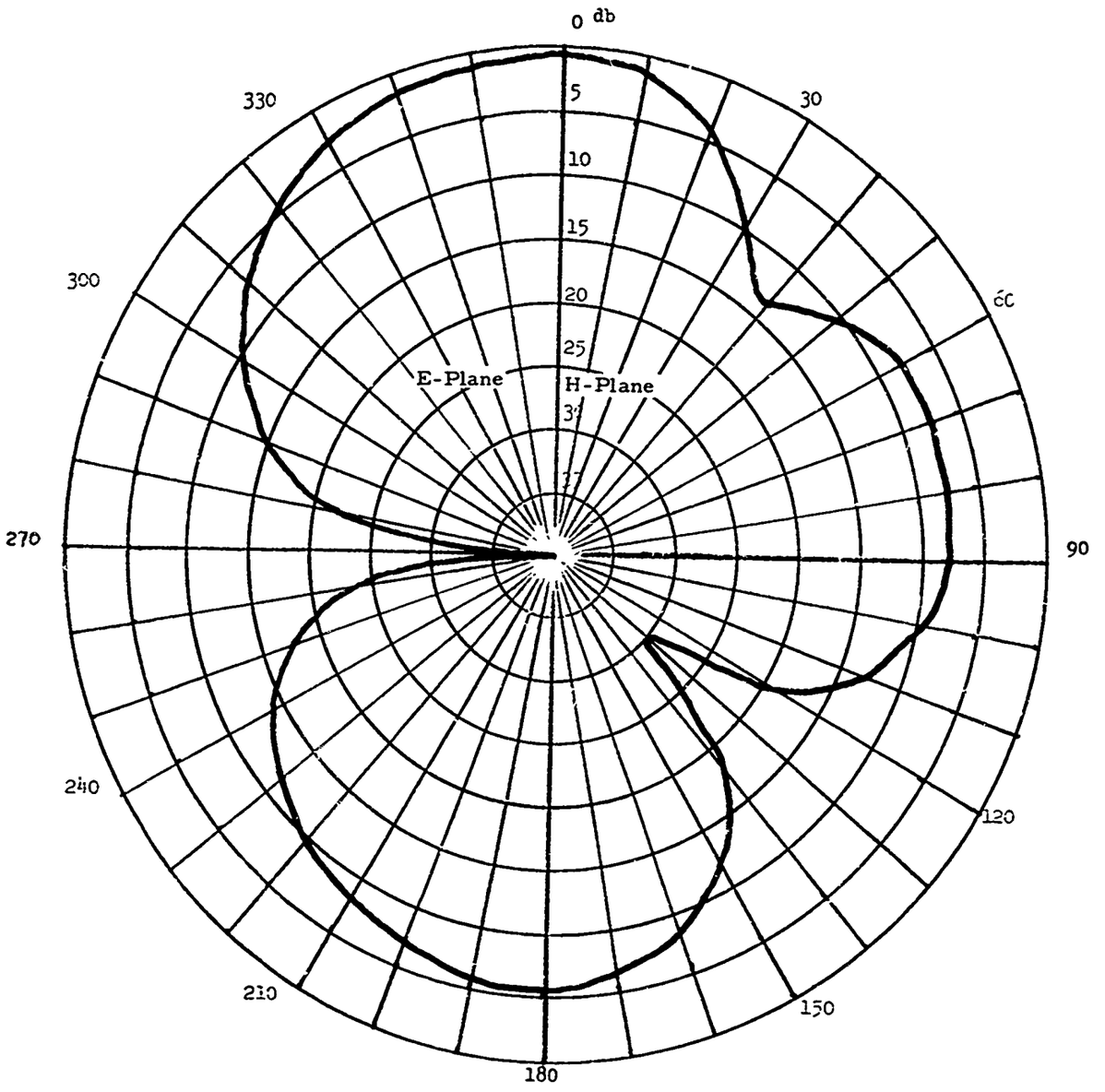

Figure IV C-4 2 Element Array - 0.75 Wavelength Spacing - Gain 9.5 db

C. (Continued)

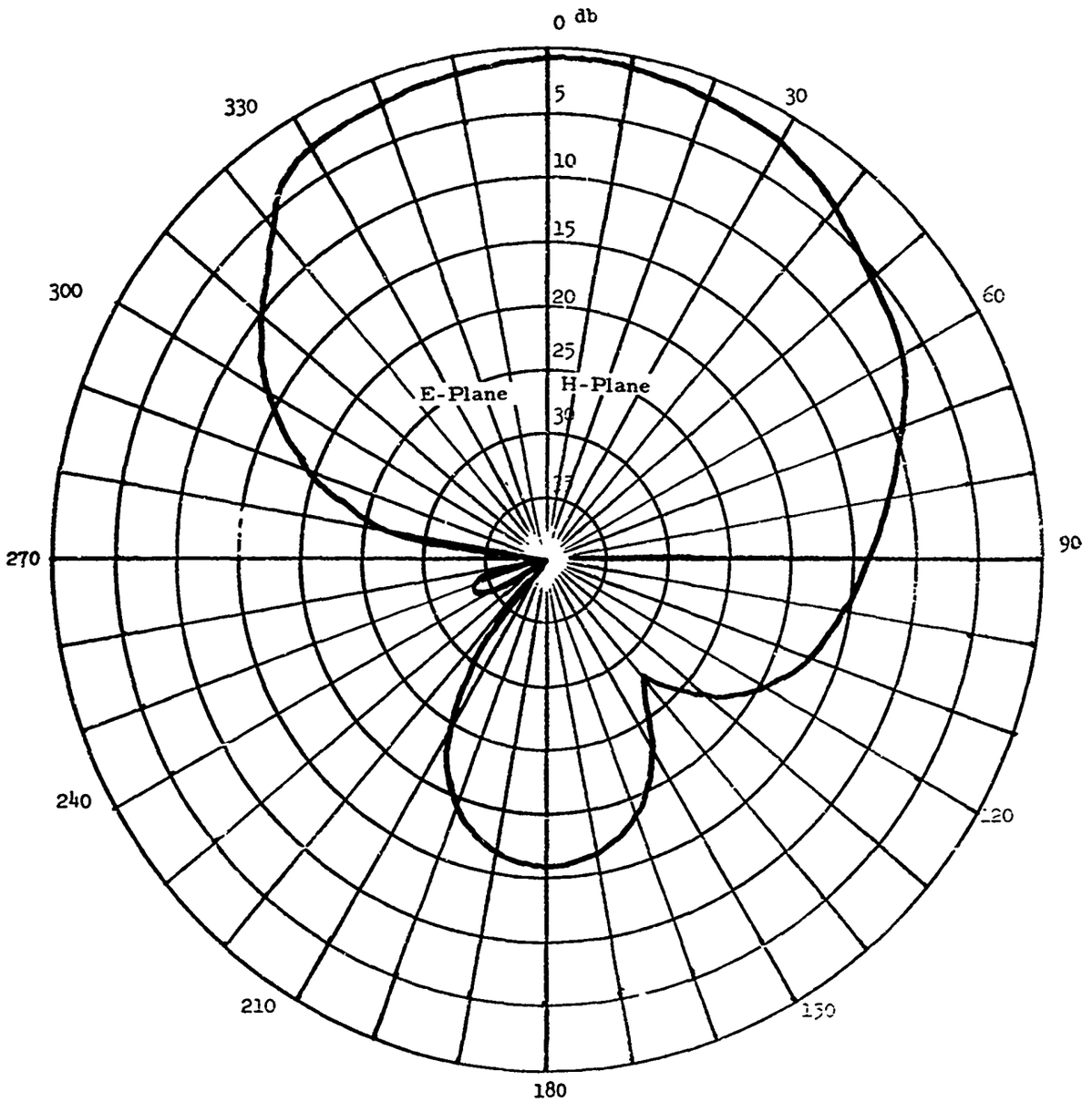

Figure IV C-5 3 Element Array - 0.15 Wavelength Spacing - Gain 7.8 db

C. (Continued)

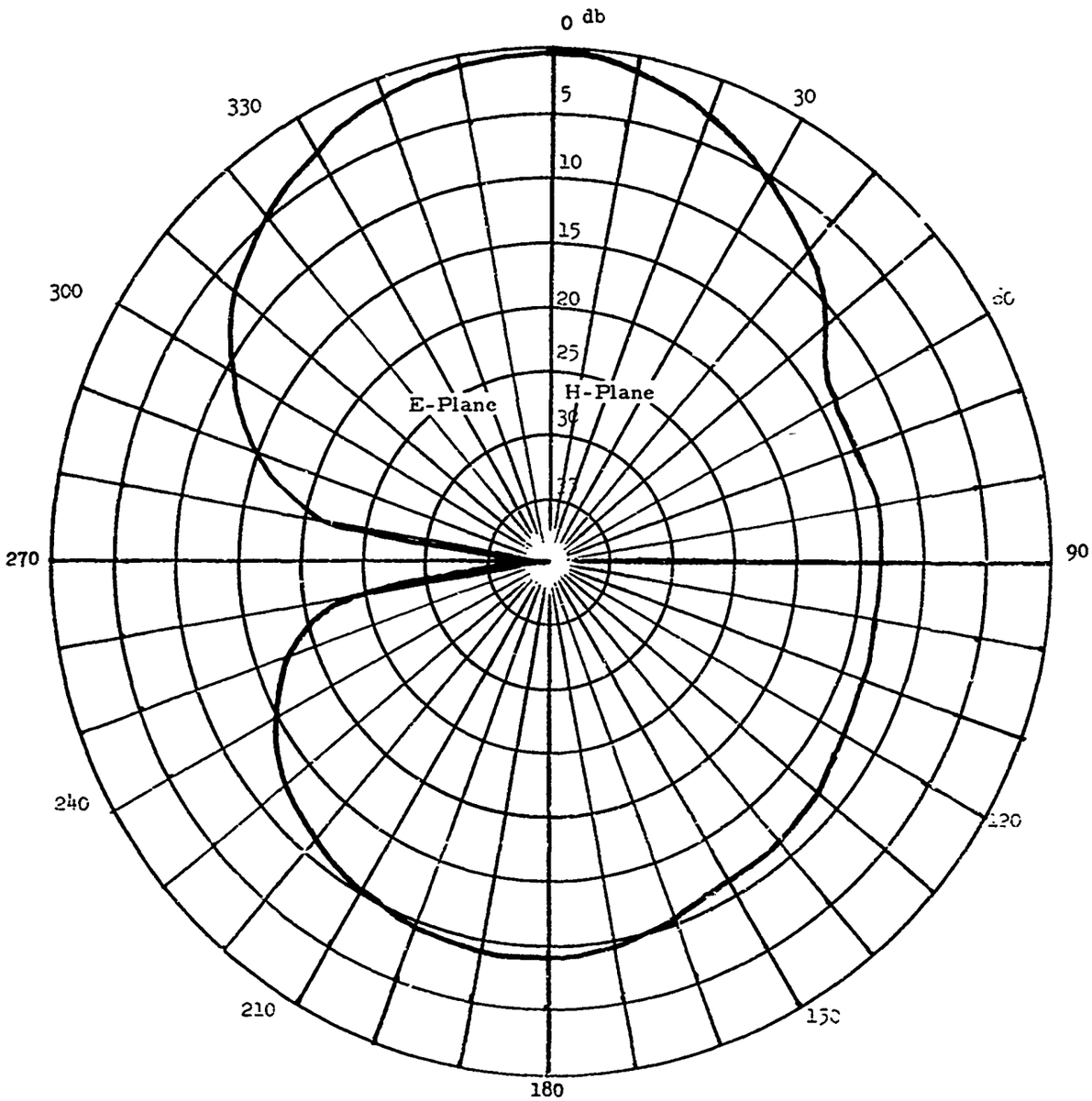

Figure IV C-6 3 Element Array - 0.5 Wavelength Spacing - Gain 9.8 db

C. (Continued)

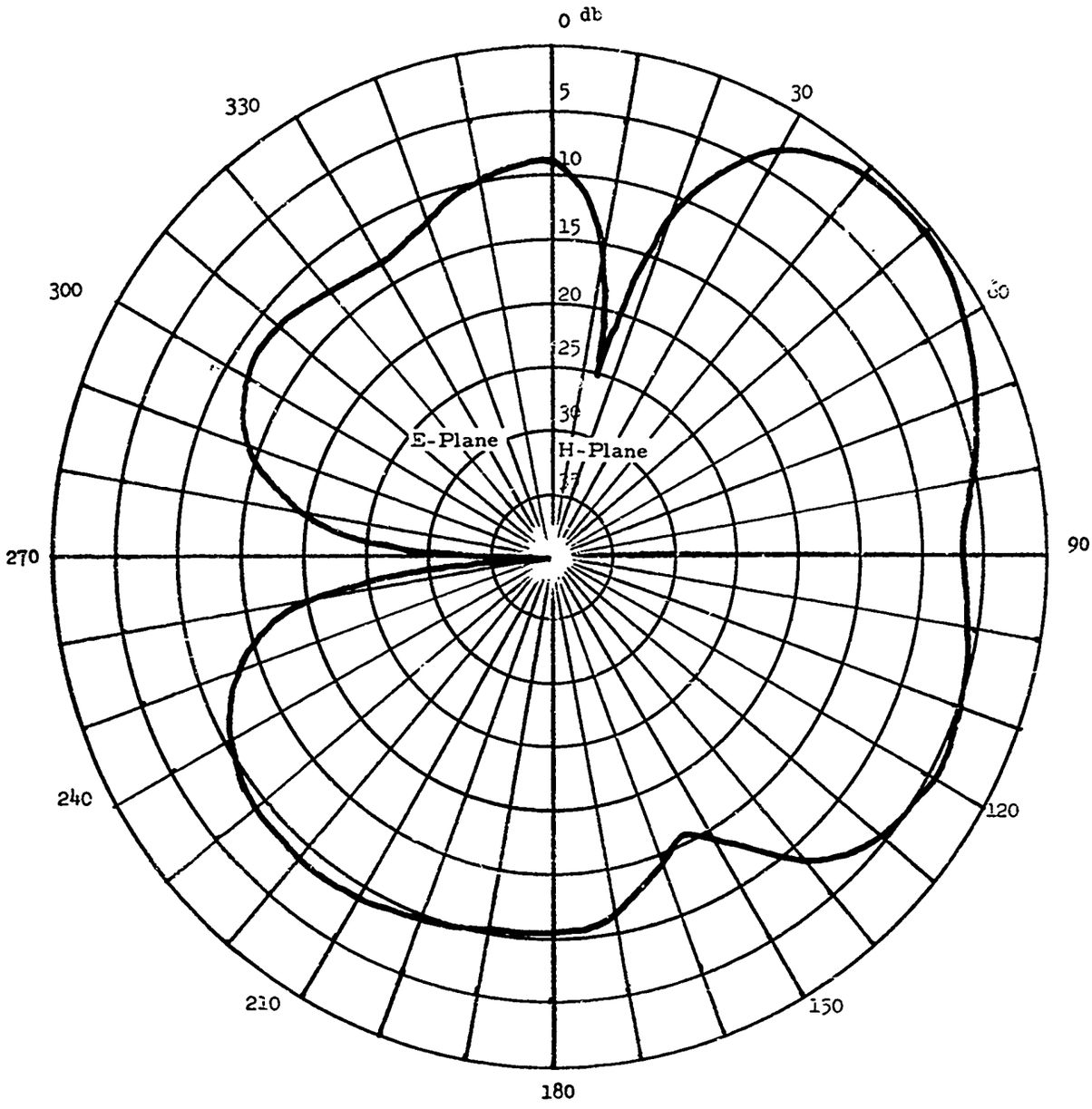

Figure IV C-7 3 Element Array - .75 Wavelength Spacing - Gain 7.5 db

C. (Continued)

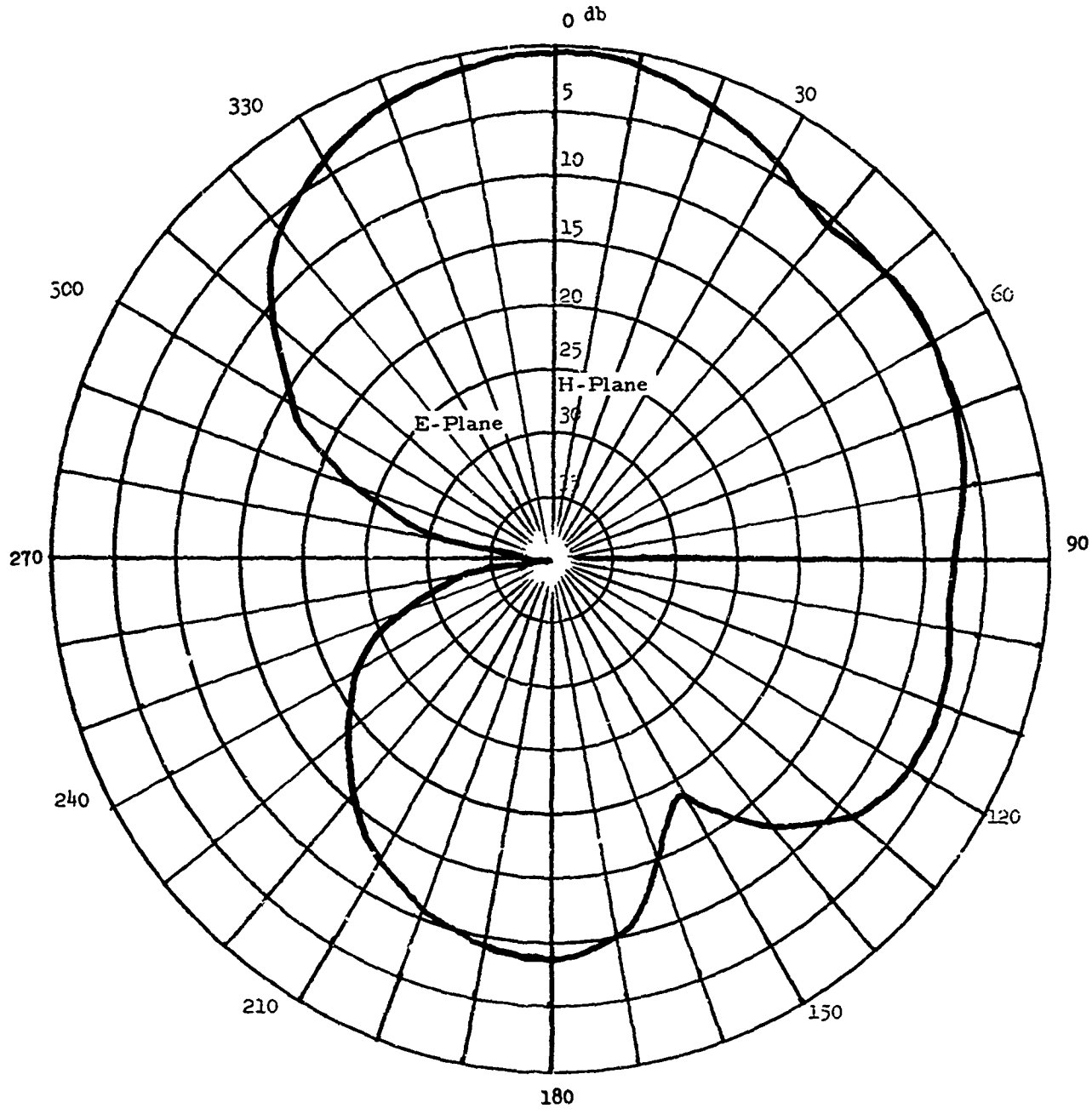

Figure IV C-8 4 Element Array - 0.15 Wavelength Spacing - Gain 8.8 dl

C. (Continued)

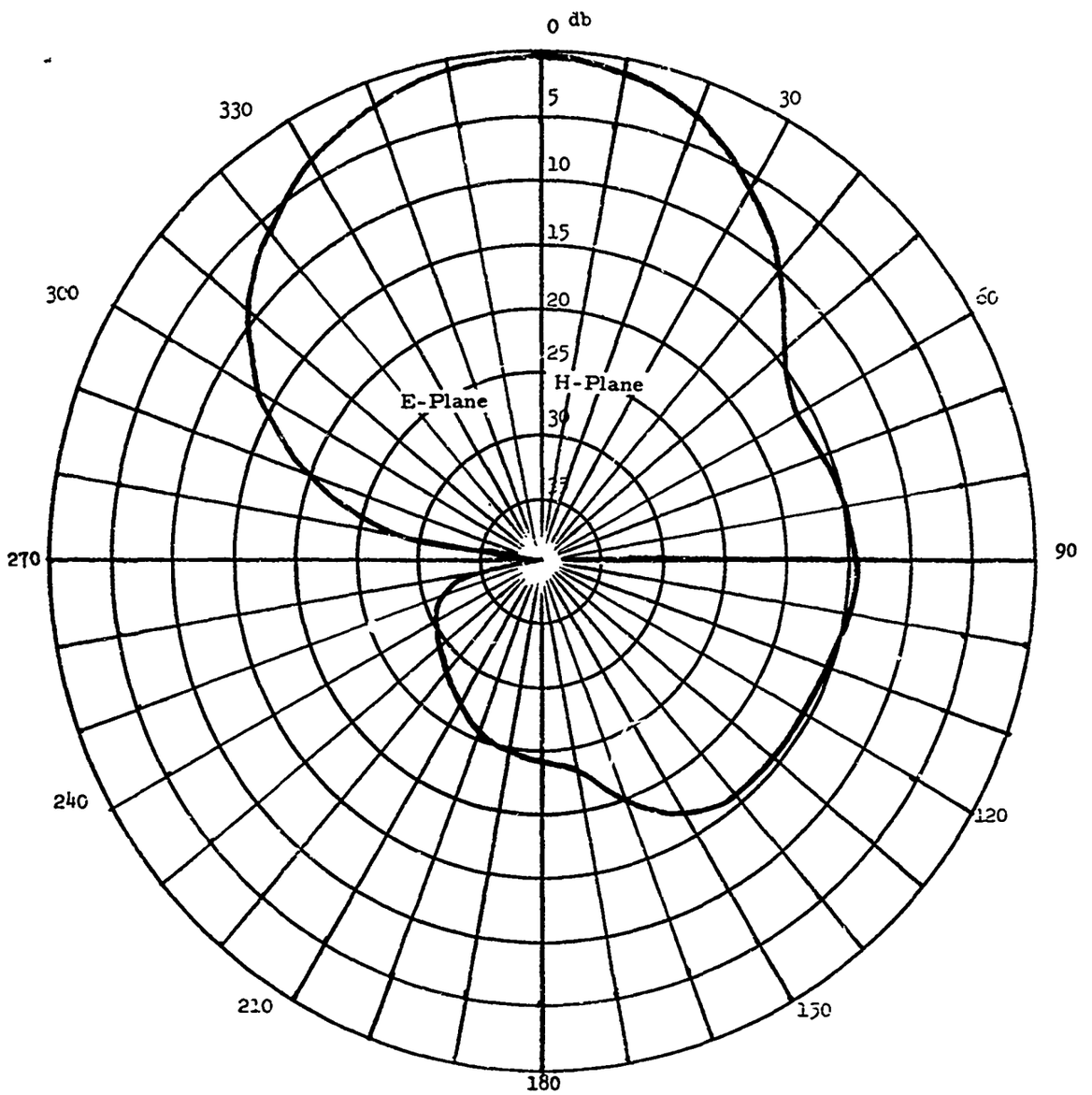

Figure IV C-9 4 Element Array - .25 Wavelength Spacing - Gain 11.1 db

C. (Continued)

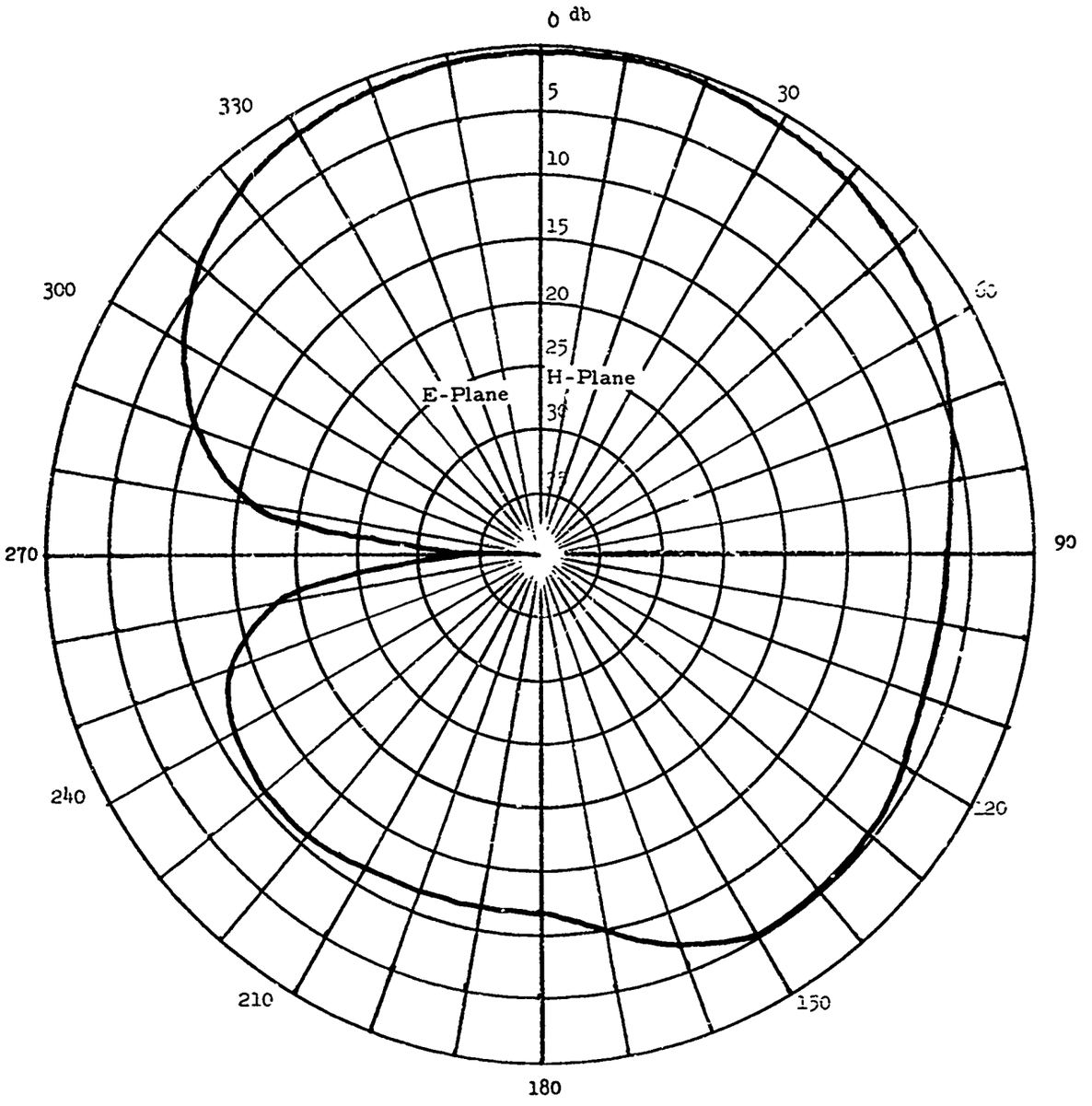

Figure IV C-10 4 Element Array - .5 Wavelength Spacing - Gain 5.8 db

C. (Continued)

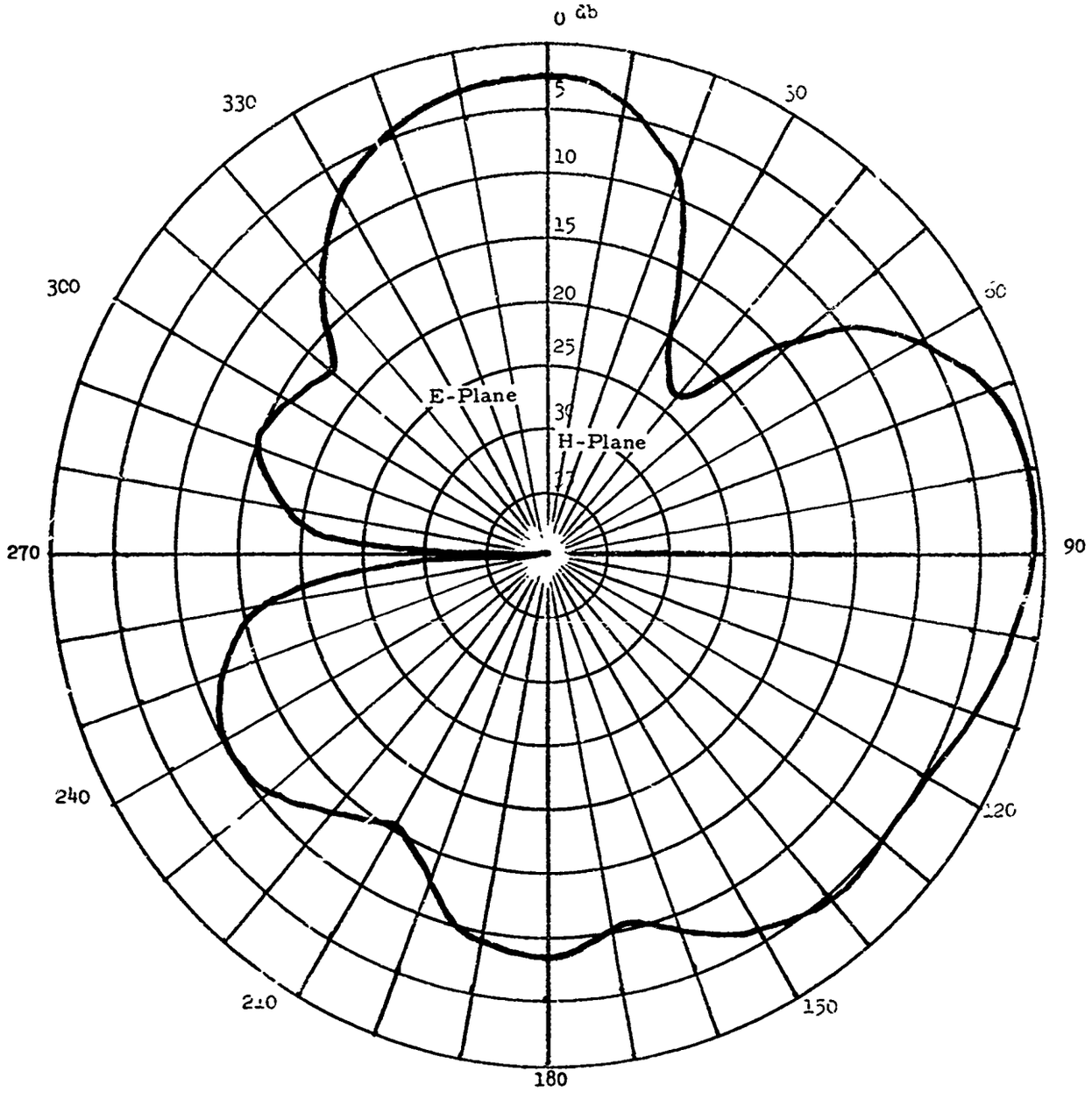

Figure IV C-11 4 Element Array - .75 Wavelength Spacing - Gain 5.5 db

C. (Continued)

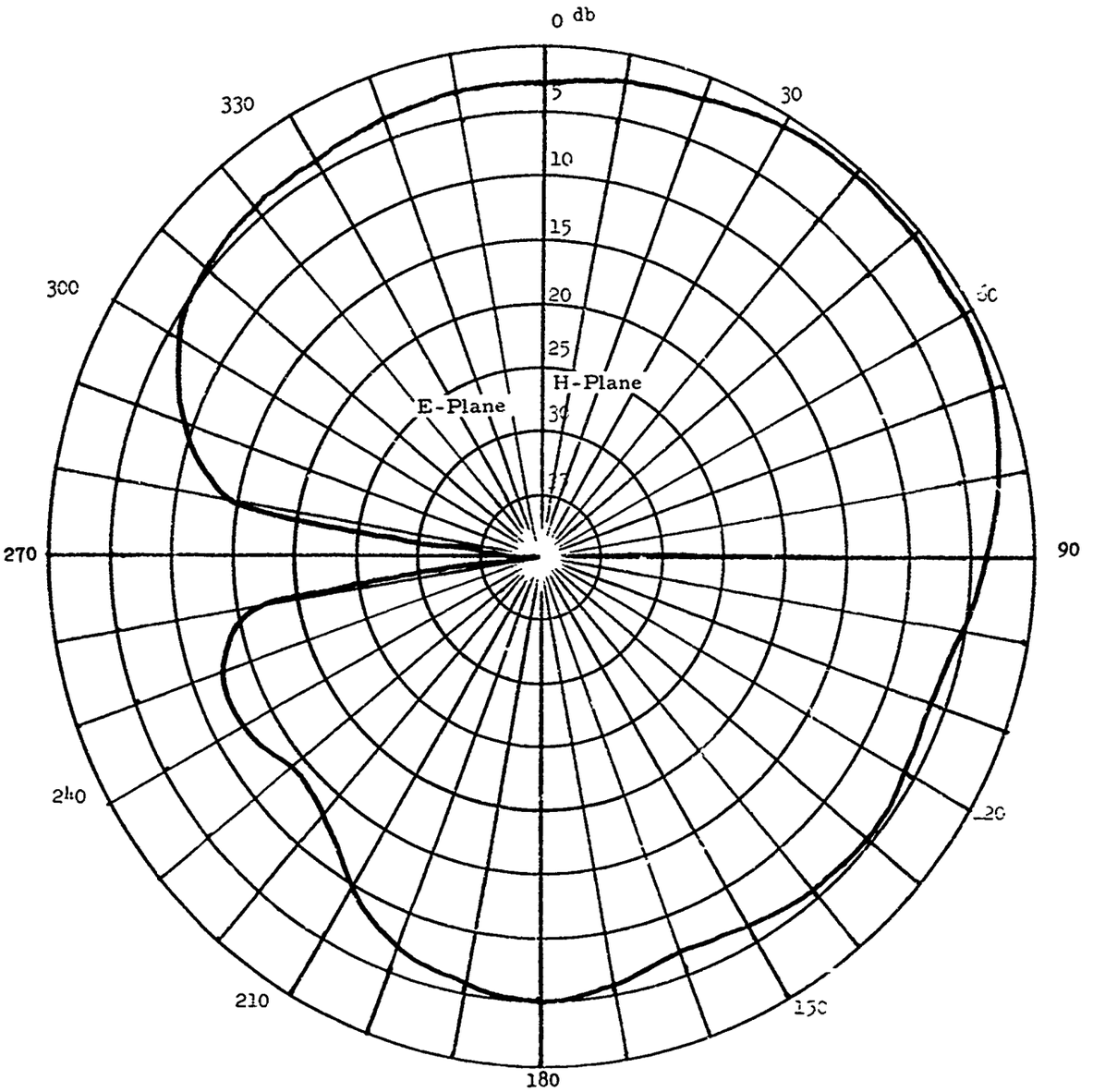

Figure IV C-12 5 Element Array - .5 Wavelength Spacing - Gain 4.5 db

D. HIGH GAIN ELEMENT MEI ARRAYS

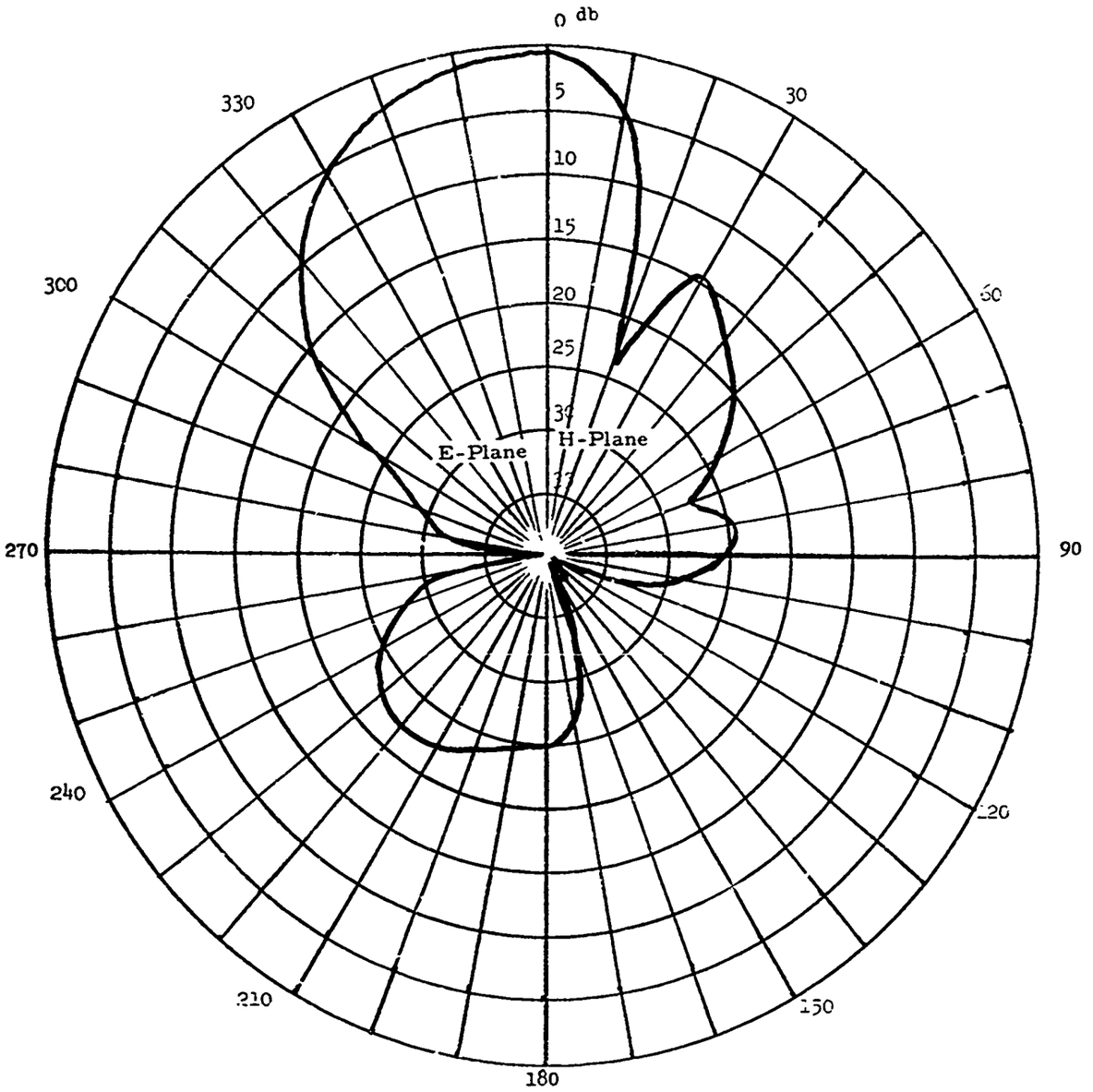

Figure IV D-1 4 Element array - .75 Wavelength Spacing - Gain 16.1 db

D. (Continued)

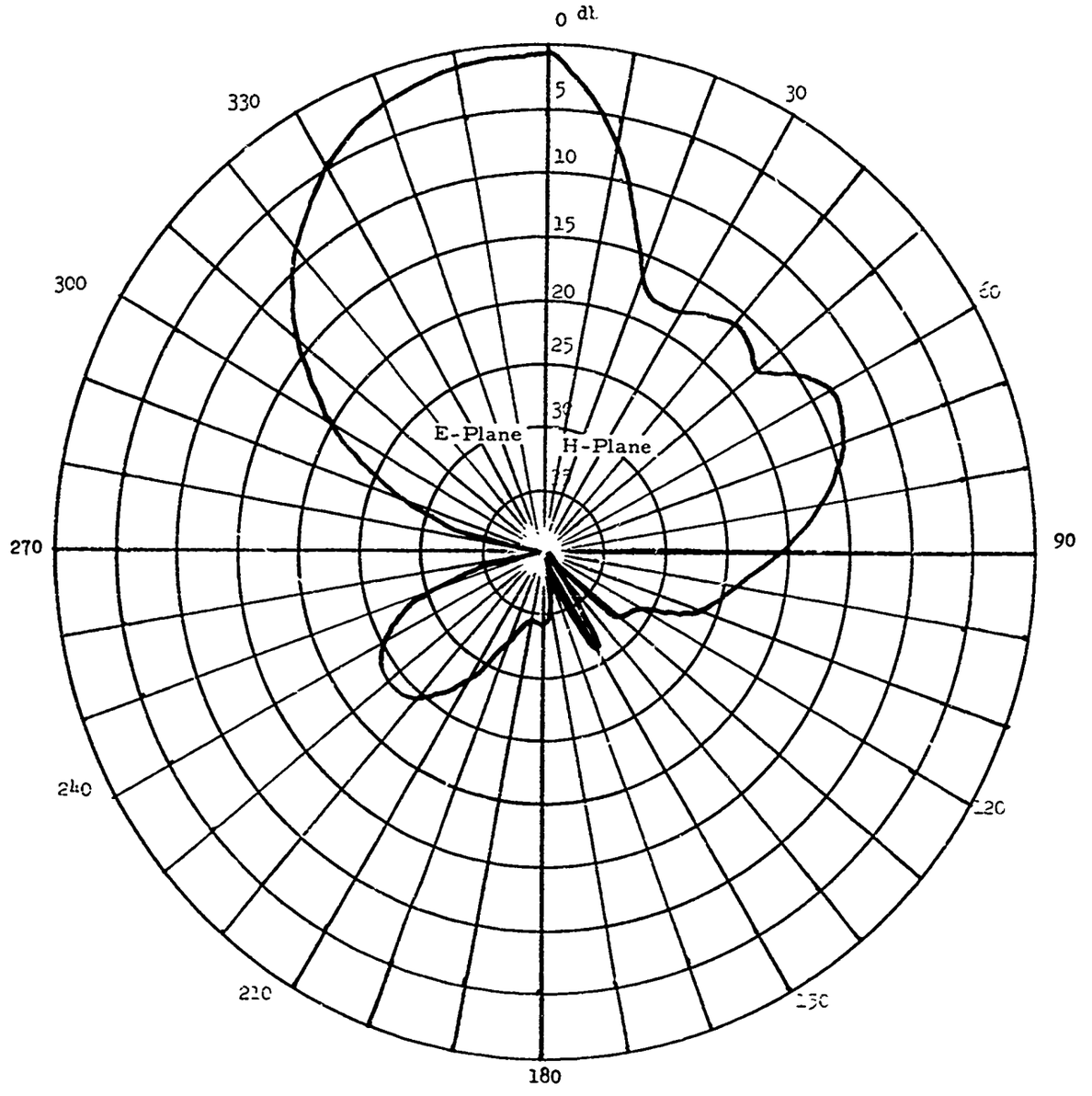

Figure IV D-2 4 Element Array - 1.0 Wavelength Spacing - Gain 16.4 db

D. (Continued)

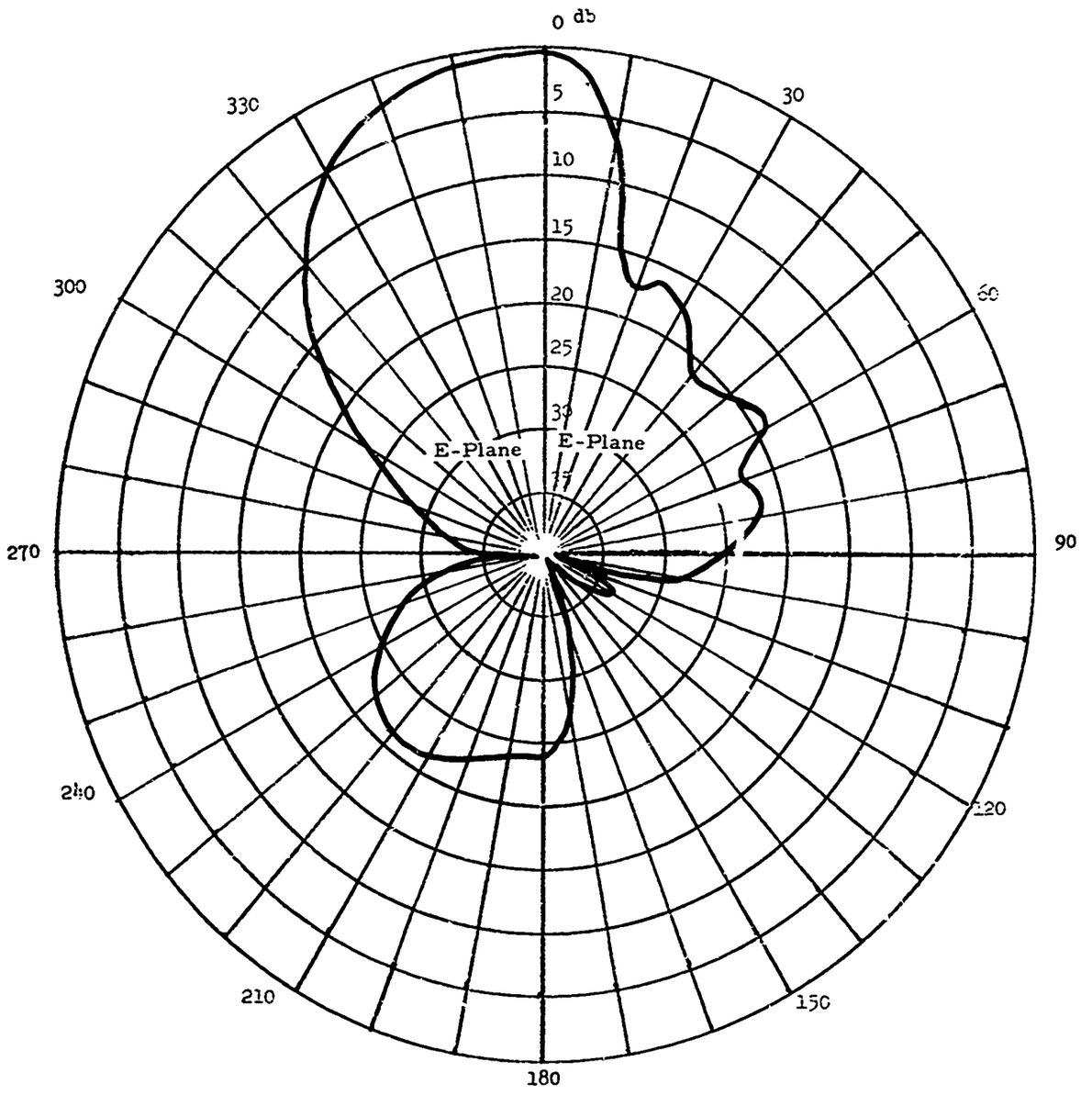

Figure IV D-3 5 Element Array - .75 Wavelength Spacing - Gain 16.9 db

E. MEDIUM GAIN ELEMENT MEI ARRAYS

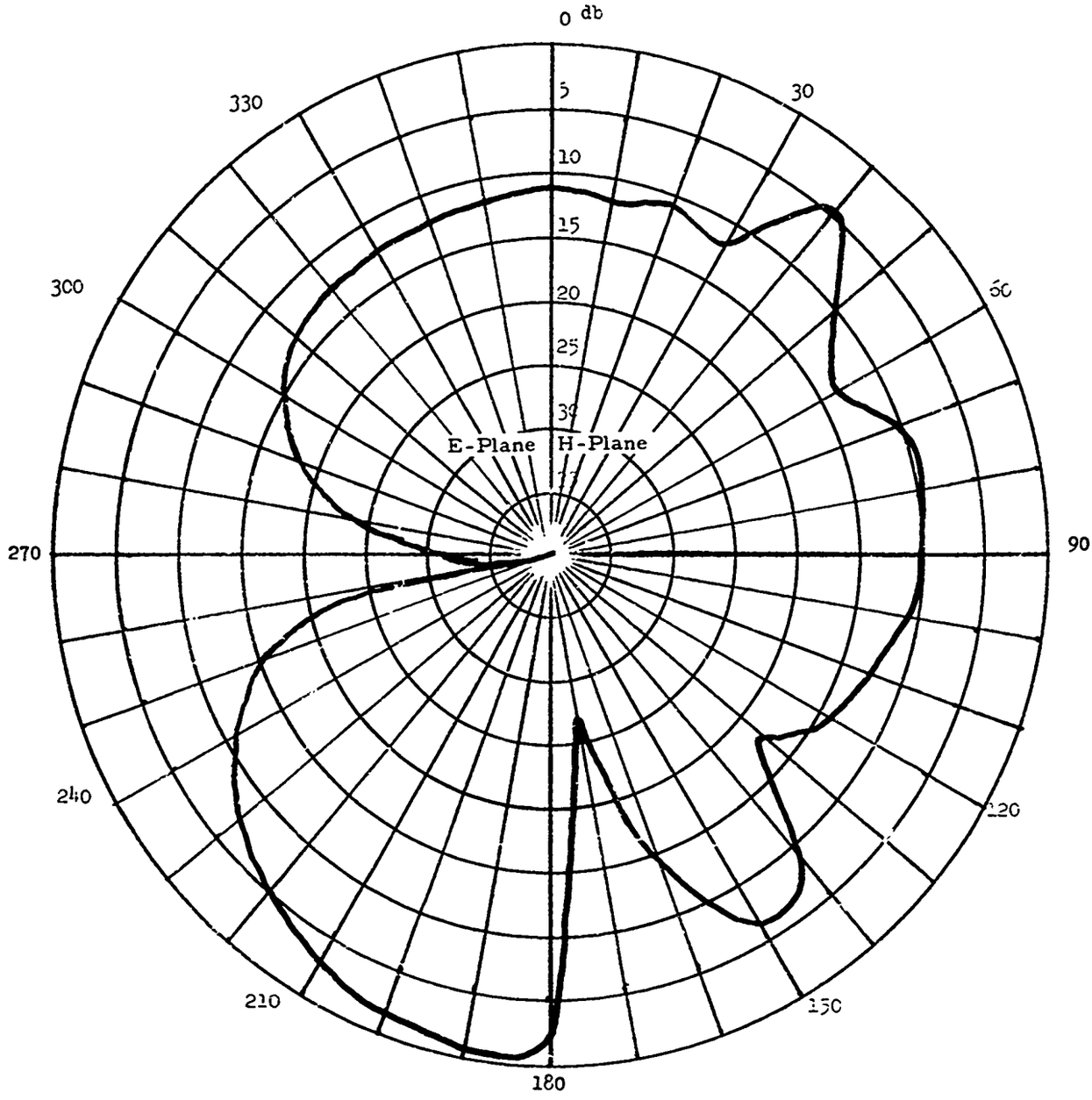

Figure IV E-1 4 Element Array - .5 Wavelength Spacing - Gain 11.3 db

F. HIGH GAIN ELEMENT DUHAMEL ARRAYS OVER REAL EARTH

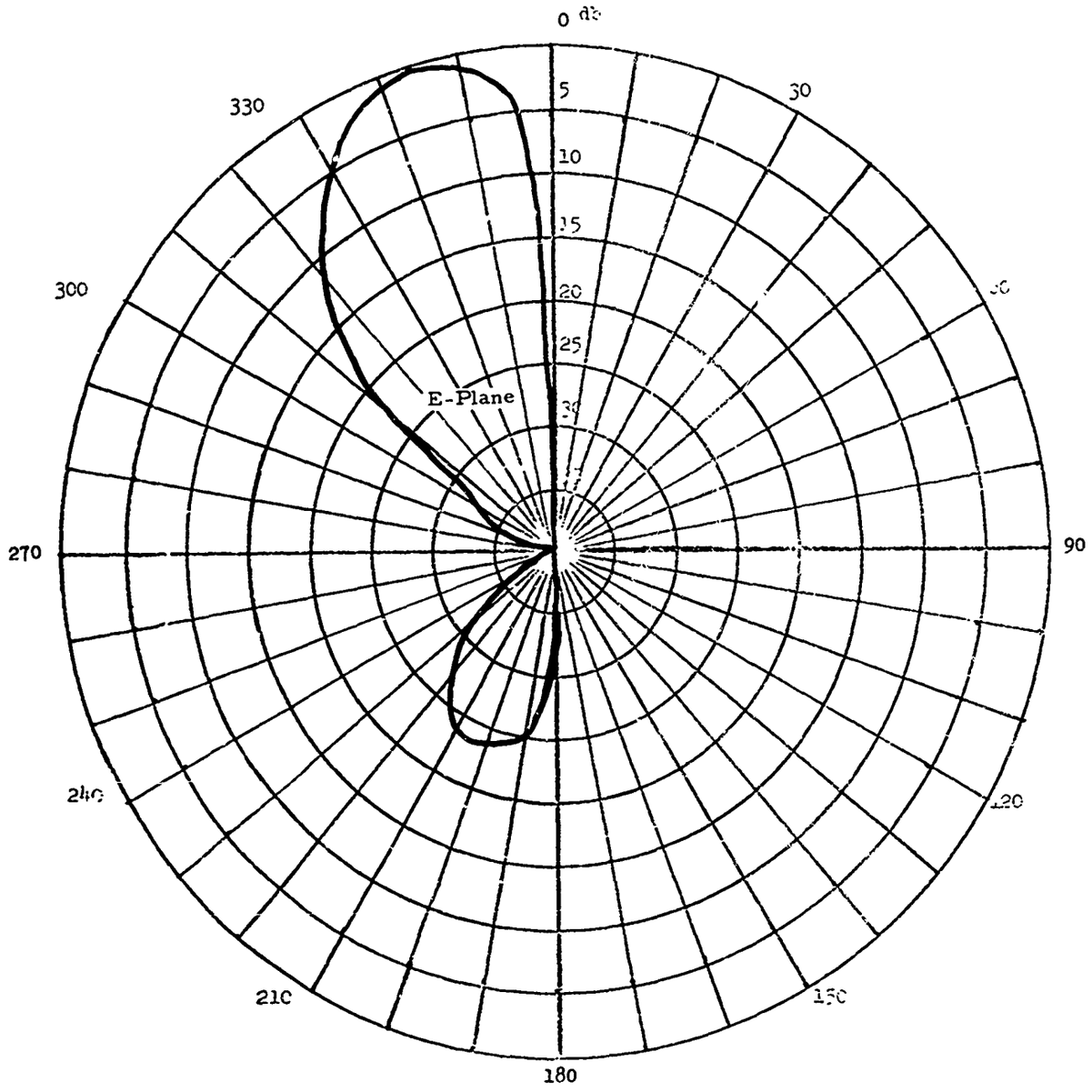

Figure IV F-1 4 Element Array - .75 Wavelength Spacing - Gain 12.6 db

F. (Continued)

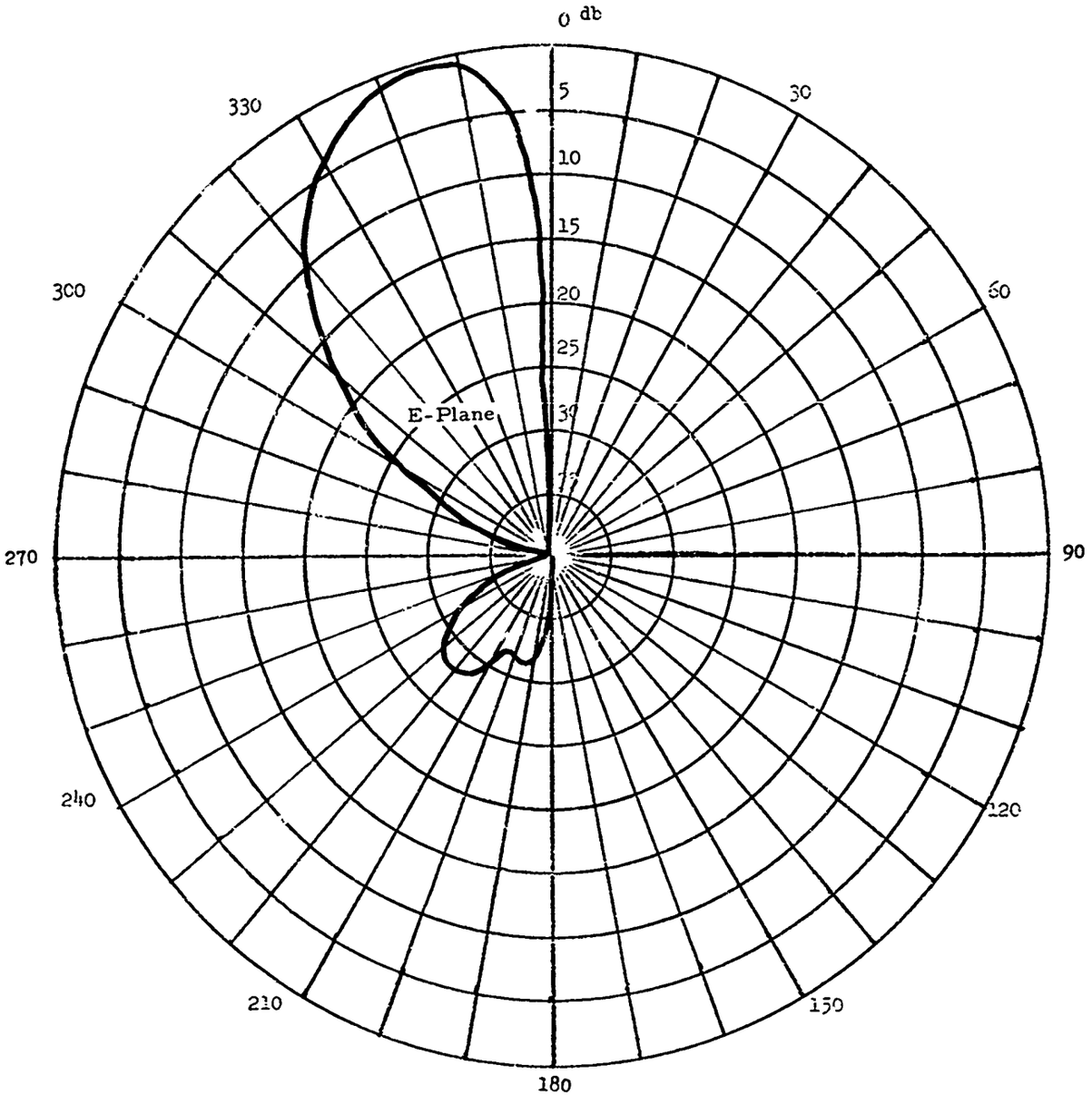

Figure IV F-2 4 Element Array - 1.0 Wavelength Spacing - Gain 12.0 db

V REFERENCES

1. R. W. P. King, The Theory of Linear Antennas with Charts and Tables for Practical Applications, Harvard University Press, Cambridge, Massachusetts (1956).

2. Eward C. Jordan, Electromagnetic Waves and Radiating Systems, p. 415, Prentice-Hall, Inc., Englewood Cliffs, N.J., 1950.

3. J. D. Kraus, Antennas, pp. 279-288, McGraw-Hill, New York (1950).

4. R. L. Bell, C. T. Elfving, and R. E. Franks, "Near-Field Measurements on a Logarithmically Periodic Antenna," IRE Transactions on Antennas and Propagation, pp. 559-567, (November 1960).

5. E. Hallen, "Theoretical Investigations into the Transmitting and Receiving Qualities of Antennas," Nova Acta, Royal Soc. Sciences, (Uppsala) Vol. 11, pp. 1-44 (November, 1938).

6. S. A. Schelkunoff and H. T. Frus, Antenna Theory and Practice, Wiley, New York (1952).

7. S. A. Schelkunoff and C. B. Feldman, "On the Radiation from Antennas," Proc. IRE, Vol. 30, pp. 511-516 (November 1942).

8. L. V. King, "On the Radiation Field of a Perfectly Conducting Base-Insulated Cylindrical Antenna Over a Perfectly Conducting Plane Earth, and the Calculation of Radiation Resistance and Reactance," Phil. Trans. Royal Soc. (London), Vol. 236, pp. 381-422, (November 2, 1937).

9. L. N. Brillouin, Quarterly of Applied Mathematics, Vol. i, No. 3 (October 1943).

10. J. Aharoni, Antennae, An Introduction to Their Theory, Oxford University Press, Oxford, England (1946)

11. R. W. P. King and C. W. Harrison, "The Distribution of Current Along a Symmetrical Center-Driven Antenna," Proc. IRE, pp. 548 (October 1943).

12. F. B. Hildebrand, "Methods of Applied Mathematics," Second Edition, Prentice-Hall, Inc., Englewood Cliffs, New Jersey, pp. 222-283 (1965).

13. J. B. Scarborough, "Numerical Mathematical Analysis", Fifth Edition, pp. 136-174, The John Hopkins Press, Baltimore (1962).

V. (Continued)

14. S. S. Kuo, "Numerical Methods and Computers," pp. 239-245, Addison-Wesley Publishing Company, Reading, Massachusetts (1965).

15. F. B. Hildebrand, Introduction of Numerical Analysis, pp. 312-358, McGraw-Hill, New York (1956).

16. K. L. Nielsen, "Methods in Numerical Analysis," pp. 163-169, Second Edition, The Macmillan Company (1964).

17. Ref. 14 pp. 154-159.

18. K. K. Mei, "On the Integral Equation of Thin Wire Antennas," IEEE Transactions on Antennas and Propagation, Vol. AP-13, pp. 374-378 (May 1965).

19. S. Ramo and J. R. Whinnery, Fields and Waves in Modern Radio, p. 31, Second Edition, John Wiley and Sons, Inc., New York (1953).

20. V. R. Arens, "A Mathematical Model of Vertical Antennas of Finite Length Over an Inhomogeneous Earth," p. 14, Presented at 11th Symposium of the AGARD Electromagnetic Wave Propagation Committee, Leicester, England (July 1966).

UNCLASSIFIED
Security Classification

DOCUMENT CONTROL DATA - R & D

(Security classification of title, body of abstract and indexing annotation must be entered when the overall report is classified)

1 ORIGINATING ACTIVITY (Corporate author) Sylvania Electronic Systems Mountain View, California, 94040	2a. REPORT SECURITY CLASSIFICATION UNCLASSIFIED 2b GROUP

3 REPORT TITLE

HF ANTENNA OPTIMIZATION STUDY

4 DESCRIPTIVE NOTES (Type of report and inclusive dates)

Final Report - Oct 66 to Oct 68

5 AUTHOR(S) (First name, middle initial, last name)

Arens, Virgil R. Embry, Ursel R.
Elfving, Claes T. Johnstone, Donald L.

6 REPORT DATE	7a. TOTAL NO OF PAGES	7b. NO OF REFS
February 1969	144	20

8a CONTRACT OR GRANT NO	9a. ORIGINATOR'S REPORT NUMBER(S)
F30602-67-C-0045 b. PROJECT NO 5582 c. Task No. 558202 d.	9b. OTHER REPORT NO(S) (Any other numbers that may be assigned this report) RADC-TR-68-397

10 DISTRIBUTION STATEMENT

This document is subject to special export controls and each transmittal to foreign governments or foreign nationals or representatives thereto may be made only with prior approval of RADC (EMLI), GAFB, N.Y.

11 SUPPLEMENTARY NOTES	12 SPONSORING MILITARY ACTIVITY
RADC Project Engineer CARMEN S. MALAGISI EMATA/AC 315 330-2443	Rome Air Development Center Techniques Branch (EMAT) Griffiss AFB, NY 13440

13 ABSTRACT

This report presents a summation of ~~the work performed under the Antenna HF Optimization Study~~, a study to determine the optimum log periodic dipole array design for a high gain, low coverage HF antenna over real and/or ground screen covered earth. The major problem encountered is one of determining antenna electrical characteristics accurately in free space and in a real earth environment. The present state of the art in analytical antenna design does not allow the engineer to predict log periodic antenna electrical characteristics, especially over real earth, with sufficient accuracy to be valuable for strict system requirements. To solve this problem, a mathematical model of a log periodic antenna is set up and solved with the use of high speed digital computers. The model used allows one to obtain the current distribution on the antenna knowing only its physical dimensions and something about the conductivity of the material used in its construction. The theoretical model, which treats the antenna as a boundary value problem, automatically includes all the interactions or mutual coupling between elements. From the computed values of the currents on the antenna all electrical characteristics of the antenna, such as radiation patterns, absolute gain, and input impedance are calculated. Theoretical and measured UHF radiation patterns and gains are compared for evaluation of the technique. Free space and real earth calculations are presented and an optimum antenna design is chosen from this information.

DD FORM 1 NOV 65 1473

UNCLASSIFIED
Security Classification

UNCLASSIFIED

Security Classification

14 KEY WORDS	LINK A		LINK B		LINK C	
	ROLE	WT	ROLE	WT	ROLE	WT
Antennas Log Periodic						

UNCLASSIFIED

Security Classification